SUMMARY OF FINAL PROJECT COMPLETION REPORT

UGC-MAJOR RESEARCH PROJECT

(July 2015 – June 2018)

Submitted to

UNIVERSITY GRANTS COMMISSION

BAHADUR SHAH ZAFAR MARG

NEW DELHI – 110 002

Project Title: "*Synthesis, characterization, DNA-binding, cytotoxicity, apoptotic inducing activity and photocleavage studies of Ru(II) Polypyridyl complexes*"

UGC Reference F. No. 43-169/2014(SR) and Dated

Principal Investigator:

Prof. S. Satyanarayana
Department of Chemistry
University college of Science
Osmania University
Hyderabad-500007
Telangana State
India

Table of contents

List of the Figures

increase of CT–DNA concentration. Insert: Plots of [DNA]/(ε_a–ε_f) against [DNA] for the titration of DNA with complex.

Fig 24. The electronic absorption spectrum of complex 7 in Tris buffer upon addition of CT-DNA. Arrow shows the hypochromism upon increasing CT–DNA concentration. Plots of [DNA]/($\varepsilon_a - \varepsilon_f$) vs [DNA] for the titration of DNA with Ru(II) complexes.

Fig 25. Absorption spectra of complex 11 in Tris-HCl buffer upon addition of CT-DNA. Arrow shows hypochromic and bathochromic shifts with increasing concentration of DNA.

Fig 26. Fluorescence spectra of complexes 1-6 in Tris–HCl buffer at 25°C upon addition of CT–DNA, [Ru] = 10 μM, [DNA] = 0–120 μM. The arrow shows the increase in intensity upon increasing CT–DNA concentrations.

Fig 27. The fluorescence spectra of complexes $[Ru(phen)_2debip]^{2+}$ (**7**), $[Ru(bpy)_2debip]^{2+}$ (**8**) and $[Ru(dmb)_2debip]^{2+}$ (9) with addition of CT–DNA, in Tris buffer with increasing concentration of CT-DNA. The arrow shows the fluorescence intensity change upon increase of DNA concentration. Inset: Scatchard plot of r/C_f vs r.

Fig 28. Fluorescence spectra of complex 11 in Tris–HCl buffer upon addition of CT-DNA. Arrow shows the intensity change upon the increase of DNA concentration.

Fig 29. The fluorescence quenching of complex-1 with increasing concentration of $[Fe(CN)_6]^{4-}$. In figure, (a) complex alone, (b) 1:10 and (c) 1:100 ratios of complex and DNA.

Fig 30. Emission quenching of complexes 7, 8 and 9 with $[Fe(CN)_6]^{4-}$ in the absence of DNA (A), presence of DNA 1:30 (B) and 1:200 (C). [Ru] =10 μM, $[Fe(CN)_6]^{4-}$ = 0.1 M.

Fig 31. Emission quenching of complexes 10 (1), 11 (2) and 12 (3) with $[Fe(CN)_6]^{4-}$ in the absence of DNA (a), presence of DNA 1:20 (b) and 1:200 (c).

Fig 32. The DNA molecular light switch *on* and *off* effect of complex-1 showing the change in intensity upon addition of Co^{2+} and EDTA to complex + DNA.

Fig 33. DNA light switch *on* and *off* experiment of complex 7 showing the emission changes where A is emission of complex alone, B is emission of complex with DNA, C is upon addition of Co^{2+} to B (Switch *off*) and D is upon addition of EDTA to C (Switch *on*).

Fig 34. The effect of ethidium bromide (a), complex 1 (b), complex 4 (c), complex 2 (d), complex 5 (e), complex 3 (f) and complex 6 (g) on relative viscosity of CT-DNA.

Fig 35. Effect of increasing amount of Ethidium bromide (A), complex 7 (B), complex 8 (C) and complex 9 (D) on relative viscosity of CT-DNA at 30 ± 0.1 ºC.

Fig 36. Effect of increasing amounts of Ethidium bromide (EtBr) (a), complex 10 (b), complex 11 (c) and complex 12 (d) on the relative viscosity of calf thymus DNA at $30(\pm 0.1)^0$C.

Fig 37. The effect of synthesized complexes 1-3 (**a**) and 4-6 (**b**) with different concentrations (10, 20 and 40μM) on cleavage of pBR322 DNA after irradiation at 365nm for 30 min. **(c)** Photocleavage of pBR322 DNA experiments in the presence of various reactive oxygen species inhibitors, lane-1(Mannitol+complex-1), lane-2(DMSO+complex-1), lane-3(SOD+complex-1) and lane-4(Histidine+complex-1).

Fig 38. i). Photoactivated cleavage of pBR322 DNA in the absence (Control) and presence of different concentrations (20, 40 and 80μM) of complexes **7**, **8** and **9** after irradiation at 365 nm for 30 min. **ii)**. Photoactivated cleavage of pBR322 DNA in the presence of complex **7** and scavengers (10 μM) after irradiation at 365 nm for 30 min.

Fig 39. Agarose gel electrophoresis of pBR322 DNA in absence and in the presence of complexes 10, 11 and 12 at different concentrations (20, 40 and 60 μM).

Fig 40. Cell viability of Hela cell lines in vitro treatment with cisplatin (positive control) and ruthenium complexes **1-6**. Each data point is the mean±standard error obtained from at least three independent experiments. Negative control (untreated cells) considered as 100% of viable cells.

Fig 41. Cell viability of HeLa cell lines in vitro treatment with complexes **7**, **8** and **9**.

Fig 42. a) HeLa cells were treated with complexes 10, 11 and 12 with different concentrations for 48h and untreated cells were used as control and then cell viability was evaluated by MTT assay. b) Cisplatin was used as positive control.

Fig 43. Lipophilicity of complexes 1-6.

Fig 44. The morphological changes of HeLa cells in presence of cisplatin and complexes1-6

Fig 45. Morphological changes occurred in HeLa cells after treatment with complexes 10, 11 and 12 at a concentration of 50 μM for 48h. Cell number reduced after treatment with complexes compared to control cells (untreated).

Fig 46. HeLa cells were treated with complexes 10, 11 and 12 at a concentration of 50 μM for 48h and then induction of apoptosis was determined with Annexin V-FITC/PI dual staining assay.

Fig 47. HeLa cells were treated with Cisplatin, complexes 7, 8 and 9 for 24 hrs, and then analyzed for apoptosis by flow cytometry. ii) Effect of ruthenium complexes 7, 8 and 9, and controls (-ve and +ve (Cisplatin) controls) on the mechanism of HeLa cell death (apoptosis) evaluated by flow cytometry after 24hrs of incubation.

Fig 48. HeLa cells were treated with complexes 10, 11 and 12 at a concentration of 50 μM for 48h. After treatment, distribution of cell cycle phases was quantified by flow cytometric analysis.

Fig 49. The cell cycle distribution of untreated cells (control), Cisplatin, ruthenium complexes 7, 8 and 9 on HeLa cells after incubation for 24 hrs at their IC_{50} value. ii) Bars represent the percentage of cells present in each of the cell cycle stages: G_0/G_1, S and G_2/M.

List of the Tables

A DETAILED REPORT ABOUT RESEARCH WORK DONE

1. Introduction

Transition metal complexes are employed in many fields of drug discovery. Pt-metal complexes are widely used as anti tumour drugs. The first Pt antitumor drug introduced into clinical practice was cisplatin (*cis*-diamminedichloroplatinum(II)), which became the most widely used anticancer drug in the world [1]. However, intrinsic and acquired tumor resistance diminishes the clinical efficacy of cisplatin as well as other platinum drugs. Moreover cisplatin is of high toxicity, leading to side effects that limit the administered dose. These limiting issues have led to an intense effort to design new transition metal-based compounds that are capable of overcoming problems associated with cisplatin while maintaining the same level of activity and broadening the spectrum of the therapeutic effect [2]. In attempts to find a new, metal-based anticancer drug with to cisplatin, several ruthenium complexes have recently been investigated for their anti tumor activity [3, 4]. However, DNA is the primary intracellular target of anticancer drugs due to the interaction between small molecules and DNA, which cause DNA damage in cancer cells, blocking the division of cancer cells and resulting in cell death. This due to their possible application as new therapeutic agents and their photochemical that make them potential probes of DNA structure and conformation [5, 6]. However, attention has mainly focused on symmetric aromatic ligands such as 1, 10-phenanthroline and its derivatives, investigations of complexes with asymmetric ligands as DNA-binding reagents have been relatively few. Therefore, to more clearly evaluate and understand the factors that determine the DNA-binding mode of Ru(II) complexes with different shapes and electronic properties and investigation of the DNA binding behaviors are necessary. Drugs based on ruthenium such as

NAMI-A, and KP1019 are under clinical trials for metastatic and colorectal cancers [7-10]. Ru(II) polypyridyl complexes have the possibility to become anticancer agents, because they are effective against primary tumors and easily absorbed and excreted [11, 12].

We have been synthesized novel ligands 2(2,6-dimethoxy pyridine-3-yl)1H imidazo(4,5-f)[1,10]phenanthroline (DMPIP); Methyl4-(benzoate-3-yl)(1H-imidazo[(4,5-f)[1,10] phenanthroline (MBIP); 2-(4-N,N'-diethylbenzenamine) 1H-imidazo[4,5-f][1,10] phenanthroline (DEBIP); 2-(4-(diethoxymethyl)phenyl)-1H-imidazo[4,5-f][1,10]phenanthroline (DEPIP) Synthesis of 4-bromo-2-(1H-imidazo[4,5-f][1,10]phenanthrolin-2-yl)phenol (PIP-Br) Synthesis of 3-(1H-imidazo[4,5-f][1,10]phenanthrolin-2-yl)-6-isopropyl-4H-chromen-4-one (IPIPC) and their novel Ru(II) polypyridyl complexes with the general formula $[Ru(N\text{-}N)_2(L)]^{2+}$ {N-N = 1,10 phenanthroline (phen), 2,2′-bipyridine (bpy) and 4,4′-dimethyl-2,2′-bipyridine (dmb)}. All complexes have been characterized by analytical and various spectroscopic techniques. We describe the physico-chemical properties of complexes such as stability (in 48 h period) and lipophilicity. The interaction mode of the complexes with calf-thymus DNA (CT-DNA) has been explored by spectrophotometric methods and viscosity measurements. Based on the results of the spectral and viscosity studies, it is observed that all the complexes have preferred intercalative binding with DNA. Photoirradiation of the complexes are found to induce strand cleavage of pBR322 DNA via singlet oxygen mechanism. We studied the DNA molecular light switch *on* and *off* behavior of all the Ru(II) complexes. The antimicrobial activity assays of the complexes provided evidence that they are potential agents against gram positive and gram negative. In vitro cytotoxicity evaluated by MTT assay against Hela cell lines, all complexes show cytotoxicity but less when compared to cisplatin against Hela

cell lines. Live cell imaging and lipophilicity demonstrate that these complexes could cross the cell membrane and accumulating in the nucleus. These results support that the cellular localization of Ru(II) complexes regulated by their lipophilicity could affect the anticancer efficacy and action mechanisms.

2 Materials and Methods

2.1 Physical measurements

NMR spectra were recorded by using a Bruker AS400 spectrometer (DMSO-d_6 as the solvent). The Infrared spectra were recorded on IR Affinity-1 FT-IR Shimadzu spectrophotometer (KBr discs in the range 400–4000 cm^{-1}). Mass spectra (ESI–MS) were recorded on a LQC system (Finnigan MAT) using CH_3OH as mobile phase. Molar conductance was measured in CH_3CN using a Syntronics (India) conductivity meter (model 306). Absorption titrations were explored with an Elico biospectrophotometer, model BL198 (Elico, India) at room temperature. Fluorescence titrations were conducted by an Elico spectrofluorometer model SL174 (Elico, India) at room temperature. Viscosity experiments were carried out with an Ostwald Viscometer. Gel electrophoresis was photographed in a Gel doc system (Alpha InfoTech Corporation). 96-well plates (Orange Scientific), (Thermo Scientific Multi Skan EX Elisa reader) were used for MTT assay. Flow cytometer (Guava Easycyte 8HT (Millipore)) was used to study apoptosis inducing activities and cell cycle analysis.

2.2 Materials

Calf thymus DNA (CT–DNA), Ruthenium trichloride, 1,10–Phenanthroline monohydrate, 2,2'–bipyridine, 4,4'–dimethyl–2,2'–bipyridine, Ethidium bromide, bromophenol blue, MTT [3-(4,5-dimethylthiazol-2-yl)-2,5-diphenyltetrazolium bromide], Cisplatin, RPMI 1640 medium supplemented with 10% (v/v) fetal bovine serum (FBS), Guava cell cycle reagent kit, Guava Nexin reagent are provided by Millipore. DMSO-d_6 and glycerol were purchased from Sigma–Aldrich. Agarose and pBR322 DNA were purchased from Bangalore Genie. The human cancer cell lines were obtained from NCCS (Pune).

All reagents and solvents are available commercially and were used without further purification. Ultra-pure Milli-Q water (18.2 mΩ) was used in all biological experiments. Doubly distilled water used for the preparation of various buffers. Ethanol, Methanol, Diethyl ether, Potassium Ferrocyanide, Acetone, Dichloromethane, Dimethyl sulfoxide (DMSO), NaCl, Na_2HPO_4, NaBr, 2-amino-2-hydroxymethyl-1,3-propanediol (Tris), NaH_2PO_4, Na_2-EDTA, Sulphuric acid, Nitric acid, Glacial acetic acid, Dimethyl formamide, $NaClO_4$, HCl, Phosphoric acid, were purchased from Sd fine-Chem limited. 1,10–phenanthroline–5,6–dione [13], cis–[$Ru(phen)_2Cl_2$] $2H_2O$, cis–[$Ru(bpy)_2Cl_2$] $2H_2O$ and cis–[$Ru(dmb)_2Cl_2$] $2H_2O$, were synthesized [14].

2.3 Synthesis

2.3.1 Synthesis of 2-(2,6-dimethoxypyridin-3-yl)-1H-imidazo[4,5-f][1,10]phenanthroline (DMPIP).

This ligand was synthesized [15] with a mixture of 2,6-dimethoxy pyridine-3-carboxaldehyde (0.5 mM) and 1,10-phenanthroline- 5,6 dione (0.5 mM), ammonium acetate

(50.0 mM) and glacial acetic acid (15mL) were refluxed for 4 hrs. The above solution was cooled to room temperature and diluted with water, drop wise addition of Conc. NH_3 gave a yellow precipitate, which was collected, washed with H_2O and dried. The crude product recrystallized with $C_5H_5N.H_2O$ and dried. Yield: 76%. Analytical data for $C_{20}H_{15}N_5O_2$ Calcd (%): C, 67.22; H, 4.23; N, 19.60. Found: C, 67.12; H, 4.18; N, 19.55. FTIR (KBr, cm^{-1}) 3412 (N-H), 1449(C=C), 2949(OC-H), 3071(C-H), 1605, 1580(C=N),1273(C-O) ^{1}H NMR data (400 MHz, ppm, DMSO-d_6 and TMS): ^{1}H: 9.03(d,2H), 8.55(d,2H), 8.52(d,1H), 7.81(t,2H), 6.62(d,1H), 4.15(-OCH_3), 3.98(-OCH_3). ^{13}C[^{1}H] :163.07, 158.90, 147.81, 147.11, 143.52, 141.61, 135.12, 130.09, 129.55, 125.56, 123.47, 119.29, 102.22, 53.83(-OCH_3), 53.66(-OCH_3).

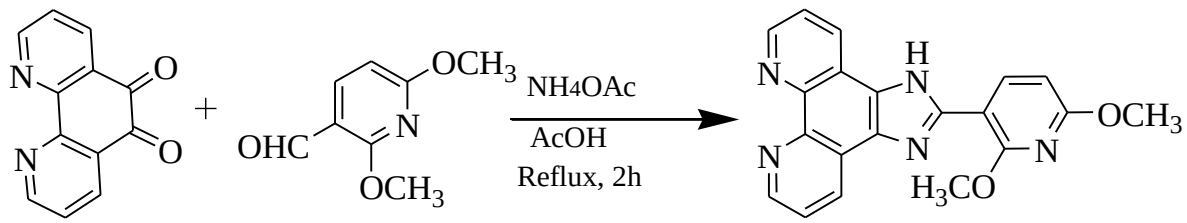

5,6 -phendione

2,6 dimethoxypyridine -3-carboxaldehyde

DMPIP

Scheme 1. Reaction scheme for the preparation of DMPIP

2.3.2 Synthesis of Methyl 4-(1H-imidazo[4,5-f][1,10]phenanthrolin-2-yl)benzoate (MBIP).

This ligand was synthesized by an identical method as described above with a mixture of methyl 4-formyl benzoate (0.5 mM) and 1,10-phenanthroline-5,6-dione (0.5 mM) Yield: 74%. Analytical data for $C_{21}H_{14}N_4O_2$ Calcd (%): C, 71.18; H, 3.98; N, 15.81. Found: C, 71.01; H, 3.63; N, 15.76. FTIR (KBr, cm^{-1}) 3410 (N-H), 1717 (C=O), 1434 (C=C),

1611(C=N), 2952 (OC-H), 3070 (C-H), 1113(C-O), 1278(C-O) ^{1}H NMR data (400 MHz, ppm, DMSO-d_6 and TMS): ^{1}H :8.99(d,2H), 8.8(d,2H), 8.36(d,2H), 8.05(d,2H), 7.77(t,2H), 3.87(s,3H) ^{13}C[^{1}H]: 165.70(C=O), 149.39, 147.68, 143.60, 134.25, 131.56, 129.64, 129.54, 126.07, 123.13, 121.54, 52.11(-OCH_3).

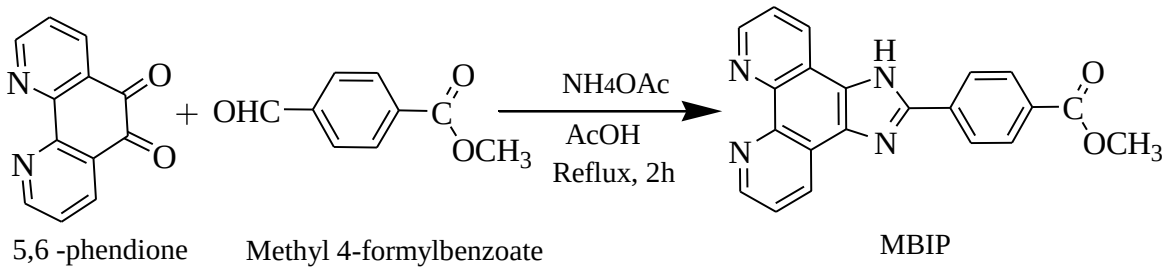

Scheme 2. Reaction scheme for the preparation of **MBIP**

2.3.3 Synthesis of N,N-diethyl-4-(1H-imidazo[4,5-f][1,10]phenanthrolin-2-yl)benzenamine (DEBIP)

This ligand was synthesized by an identical method as described above with a mixture of phen-dione (2.50 mM), N,N'-diethylaminobenzaldehyde (2.50 mM), ammonium acetate (50.0 mM) and glacial acetic acid (15 mL) were refluxed for 4 hrs. Above solution was cooled to room temperature and diluted with water, drop wise addition of Conc NH_3 gave a yellow precipitate, which was collected washed with H_2O and dried. The crude product recrystallized with $C_5H_5N.H_2O$ and dried (yield: 75%). Anal. data for $C_{23}H_{21}N_5$: calc. C, 75.18; H, 5.76; N,19.06; found: C, 75.16; H, 5.74; N, 19.04. ESI–MS Calc: 367; found: 368. IR(KBr, cm^{-1}) 1,620(C=N), 1,528(C=C), 1,231(C−C), 2,816(C−H), 1,271(C−N).

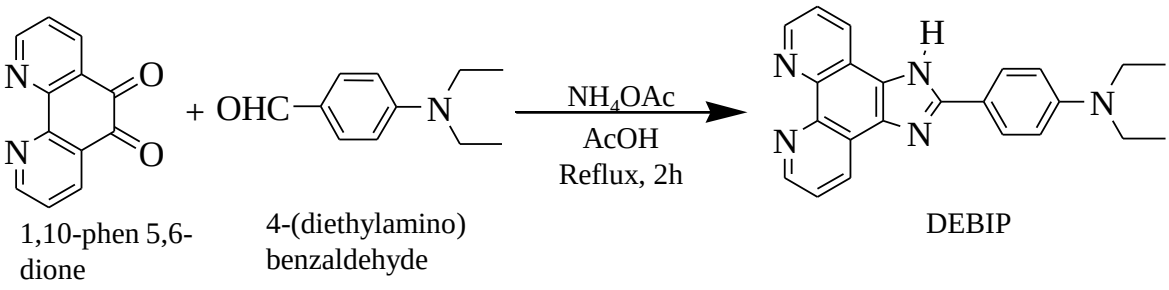

1,10-phen 5,6-dione

4-(diethylamino) benzaldehyde

DEBIP

Scheme 3. Reaction scheme for the preparation of DEBIP

2.3.4 Synthesis of 2-(4-(diethoxymethyl)phenyl)-1H-imidazo[4,5-f][1,10] phenanthroline (DEPIP)

This ligand was synthesized by an identical method as described above with a mixture of a mixture of 4-(diethoxymethyl)benzaldehyde (0.675 g, 3.50 mM), phendione (0.53 g, 2.50 mM), ammonium acetate (3.88 g, 50.0 mM) and glacial acetic acid (15 mL) was refluxed for 4h. The solution was cooled to room temperature and then diluted with distilled water. Drop wise addition of conc. aqueous NH_3 to this solution gave a yellow precipitate at neutralization, the product filtered and washed with water to remove impurities. The obtained product was recrystallized with $C_5H_5N.H_2O$ (yield: 61.4 %). Analytical data for $C_{24}H_{22}N_4O_2$: C, 72.30; H, 5.38; N, 13.61; calculated data: C, 72.34; H, 5.57; N, 14.06. ^{1}H NMR (400 MHz, DMSO-d_6): δ 9.04 (d, 2H, J = 4.0 Hz), 8.90(t, 2H, J = 9.5 Hz), 8.46(d, 2H, J = 8.3 Hz), 8.14(d, 2H, J = 8.2 Hz), 7.72(t, 2H, J = 5.5 Hz), 4.27(q, 4H, J = 7.2 Hz), 1.28(t, 6H, J = 7.0 Hz). ^{13}C[^{1}H] NMR (DMSO-d_6, 100 MHz, d, ppm): 149.32, 148.36, 144.17, 136.60, 135.34, 130.48, 129.13, 127.81, 126.84, 123.63, 114.12, 61.79, 14.33. Ligand mass 398. IR (KBr, cm^{-1}): 3354 (ν, NH), 1697 (ν, CN), 1124 (ν, COC).

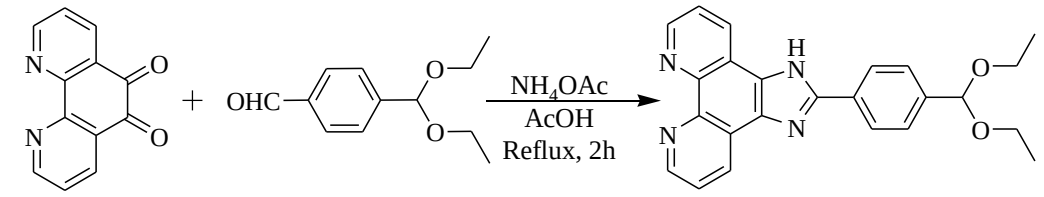

1,10-phen 5,6-dione

4-(diethoxymethyl) benzaldehyde

DEPIP

Scheme 4. Reaction scheme for the preparation of DEPIP

2.3.5 Synthesis of 4-bromo-2-(1H-imidazo[4,5-f][1,10]phenanthrolin-2-yl)phenol (PIP-Br)

This ligand was synthesized by an identical method as described above with a mixture of a mixture of 1,10-phenanthrolin 5,6-dione (2.50 mmol), 5-bromo-2-hydroxybenzaldehyde (3.50 mmol), and ammonium acetate in 10 ml glacial acetic acid were refluxed together for 2 h, and then cooled to room temperature and diluted with water. Drop wise addition of ammonia gave a yellow precipitate which was collected washed with water, purified and dried; yield (72%). Analytical data for $C_{19}H_{11}N_4$ for Anal. Calcd (%) C: 65.81; H: 3.20; N: 16.16; Found C: 65.73; H: 3.12; N: 15.98; LC-MS in DMSO M/Z: 347.5 ^{1}H-NMR (DMSO- d_6, 400 MH_Z, δ ppm): 9.10 (d, 2H), 8.80 (d, 2H), 8.25 (d, 2H), 7.70 (m, 2H), 7.53 (d, 2H), 7.25(s, 1H),7.10 (d,2H), 6.90 (s, 1H), 6.65 (d, 2H). ^{13}C-NMR (100 MHz, DMSO-d_6, δ ppm): 156.36(C-k, 1C), 154.33(C-I, 1C), 152.99(C-a, 2C), 146.72(Cc, 2C), 132.81(C-e, 2C), 131.25(C-m,1C), 129.49 (C-o,1C), 128.29 (C-d,C-n,3C), 125.06 (C-g,1C), 122.84 (C-b, C-f, 3C), 121.85(C-j, 1C), 118.23(C-l, 1C).

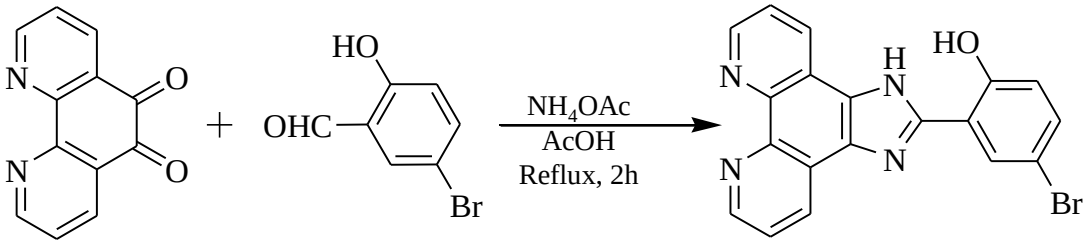

1,10-phen 5,6-dione | 5-bromo-2-hydroxy benzaldehyde | PIP-Br

Scheme 5. Reaction scheme for the preparation of PIP-Br

2.3.6 Synthesis of 3-(1H-imidazo[4,5-f][1,10]phenanthrolin-2-yl)-6-isopropyl-4H-chromen-4-one (IPIPC)

This ligand was synthesized by an identical method as described above with a mixture of a mixture of 1,10-phenanthrolin 5,6-dione (2.50 mmol), 6-isopropyl-4-oxo-4H-chromene-3-carbaldehyde (2.50 mmol), and ammonium acetate in 10 ml glacial acetic acid were refluxed together for 2 h, and then cooled to room temperature and diluted with water. Drop wise addition of ammonia gave a yellow precipitate which was collected washed with water, purified and dried; yield (72%). Analytical data for $C_{25}H_{18}N_4O_2$ for Anal. Calcd (%) C: 73.88, H: 4.46, N: 13.78; Found C: 73.51, H: 4.32, N: 13.64. Mass (m/z): 406. IR (KBr, cm^{-1}): 3579 (N-H), 2963(C-H), 1739 (C=O), 1479 (C=C), 1559 (C=N), 1220 (C-O). ^{1}H-NMR (DMSO- d_6, 400 MH_Z, δ ppm): 9.02 (d, 2H), 8.04 (d, 2H), 7.82 (s, 1H), 7.80 (t, 2H), 7.78 (s, 1H), 7.68 (d, 1H), 7.10 (d, 1H), 3.10 (sept, 1H), 1.29 (d, 6H). ^{13}C-NMR (100 MHz, DMSO-d_6, δ ppm): 23.64 (-CH_3), 32.88(-CH), 174.34 (-C=O), 157.49, 154.00, 147.75, 146.55, 144.18, 143.52, 138.69, 133.49, 129.96, 126.39, 123.17, 123.07, 121.55, 118.64, 117.5.

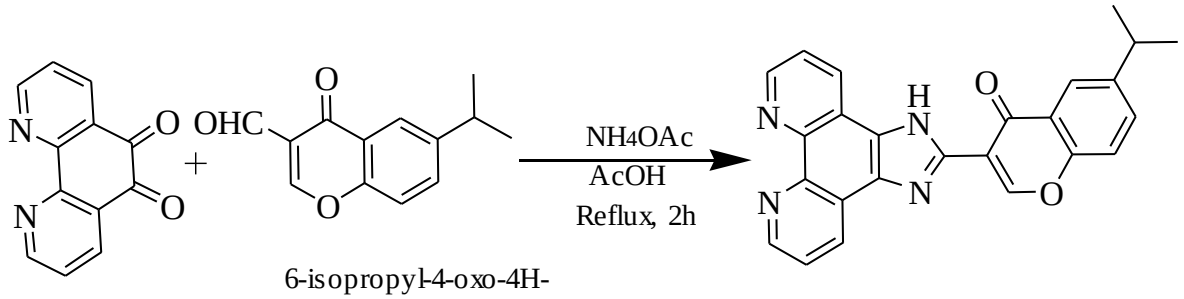

1,10-phen 5,6-dione

6-isopropyl-4-oxo-4H-chromene-3-carbaldehyde

IPIPC

Scheme 6. Reaction scheme for the preparation of IPIPC ligand.

2.4 Synthesis of Ru(II) complexes type $[Ru(N\text{-}N)_2\ L]^{2+}$

General procedure for preparing all the complexes is a mixture of cis-$[Ru(N\text{-}N)_2Cl_2]$ $2H_2O$ (0.5 mM) and L (0.5 mM) was refluxed in 25 mL ethanol and 15 mL water for 8 h under nitrogen atmosphere to give a clear red solution. On cooling, the solution was treated with a saturated aqueous solution of $NaClO_4$ to give a red precipitate. The red solid was collected and washed with a small amount of water, ethanol and ether then dried under vacuum. (Where N-N =1,10 phenanthroline / 2,2$^{'}$ -bipyridine / 4,4$^{'}$-dimethyl-2,2$^{'}$-bipyridine; L = DMPIP, MBIP, DEBIP, DEPIP, PIP-Br and IPIPC).

2.4.1 Synthesis of Ru(II) polypyridyl complexes 1-3

$[Ru(phen)_2(DMPIP)](ClO_4)_2\ 2H_2O$ (1): This complex was synthesized as described above by taking a mixture of $[Ru(phen)_2Cl_2]$ $2H_2O$ (0.5 mM), DMPIP (0.5 mM), yield: 74%. Anal calc for $C_{44}H_{35}Cl_2N_9O_{12}Ru$: Calcd (%): C, 50.15; H, 3.35; N, 11.96. Found: C, 50.11; H, 3.33; N, 11.87. FTIR (KBr, cm^{-1}) 3578(N-H), 3084(OC-H), 2950(C-H), 1276(C-O), 1454(C=C), 1604, 1580(C=N), 622(M-N). ^{1}H NMR data (400 MHz, ppm, DMSO-d_6 and TMS): δ 9.18(d,2H), 8.79(d,4H), 8.53(d,2H), 8.40(s,4H), 8.14(d,4H), 8.10(t,2H), 7.81(t,4H),

7.71(d,1H), 6.68(d,1H), 4.17(s,-OCH_3), 3.99(s,-OCH_3). $^{13}C[^1H]$ NMR data (100 MHz, DMSO-d_6, Major peaks): 163.65, 159.27, 150.18, 149.22, 147.21, 145.24, 142.02, 136.75, 131.64, 130.61, 128.60, 126.31, 126.26, 125.98, 102.53, 54.054(-OCH_3), 53.82(-OCH_3).

[Ru(bpy)$_2$(DMPIP)](ClO$_4$)$_2$ 2H$_2$O (2): This complex was synthesized as described above by taking a mixture of [Ru(bpy)$_2$Cl$_2$] 2H$_2$O (0.5 mM), DMPIP (0.5 mM), yield 71% Anal calc for $C_{40}H_{35}Cl_2N_9O_{12}Ru$: (%): C, 47.77; H, 3.51; N, 12.53. Found: C, 47.61; H, 3.24; N, 12.42. FTIR (KBr, cm^{-1}) 3598(N-H), 2950(C-H), 3078(OC-H), 1607, 1583 (C=N), 1455 (C=C), 1276(C-O), 622(M-N) ^1H NMR data (400 MHz, ppm, DMSO-d_6 and TMS): δ 9.17(d,2H), 9.12(d,4H), 8.88(d,2H), 8.54(d,4H), 8.13(d,1H), 7.91(t,4H), 7.74(t,2H), 7.35(t,4H), 6.63(d,1H), 4.16(s,-OCH_3), 3.99(s,-OCH_3). $^{13}C[^1H]$ NMR data (100 MHz, DMSO-d_6, Major peaks): 163.21, 158.99, 156.75, 147.51, 147.46, 142.19, 136.08, 130.80, 128.60, 124.42, 123.56, 114.02, 104.73, 102.31, 54.03(-OCH_3), 53.71(-OCH_3).

[Ru(dmb)$_2$(DMPIP)] (ClO$_4$)$_2$ 2H$_2$O (3): This complex was synthesized as described above by taking a mixture of [Ru(dmb)$_2$Cl$_2$] 2H$_2$O (0.5 mM), DMPIP (0.5 mM).Yield: 75%. Anal calc for $C_{44}H_{43}Cl_2N_9O_{12}Ru$: (%): C, 49.77; H, 4.08; N, 11.87. Found: C, 49.72; H, 4.05; N, 11.76. FTIR (KBr, cm^{-1}) 3599 (N–H), 3081 (C-H), 1605 (C = N), 1714 (C = O), 1453 (C = C), 622 (M–N). ^1H NMR data (400 MHz, ppm, DMSO-d_6 and TMS): δ 9.20 (d, 2H), 8.73 (d, 4H), 8.52 (S, 4H), 8.07 (d, 2H), 7.91 (d, 1H), 7.40 (t, 2H), 7.16 (d, 4H), 6.67 (S, 1H), 4.00, 4.10 (S, -OCH_3), 2.46 (S, -CH_3). $^{13}C[^1H]$ NMR data (100 MHz, DMSO-d_6, Major peaks): 20.72 (-CH_3), 54.06, 53.83 (-OCH_3), 166.8, 163, 159, 156, 150, 149, 145, 142, 131, 130, 128, 126, 124, 102.

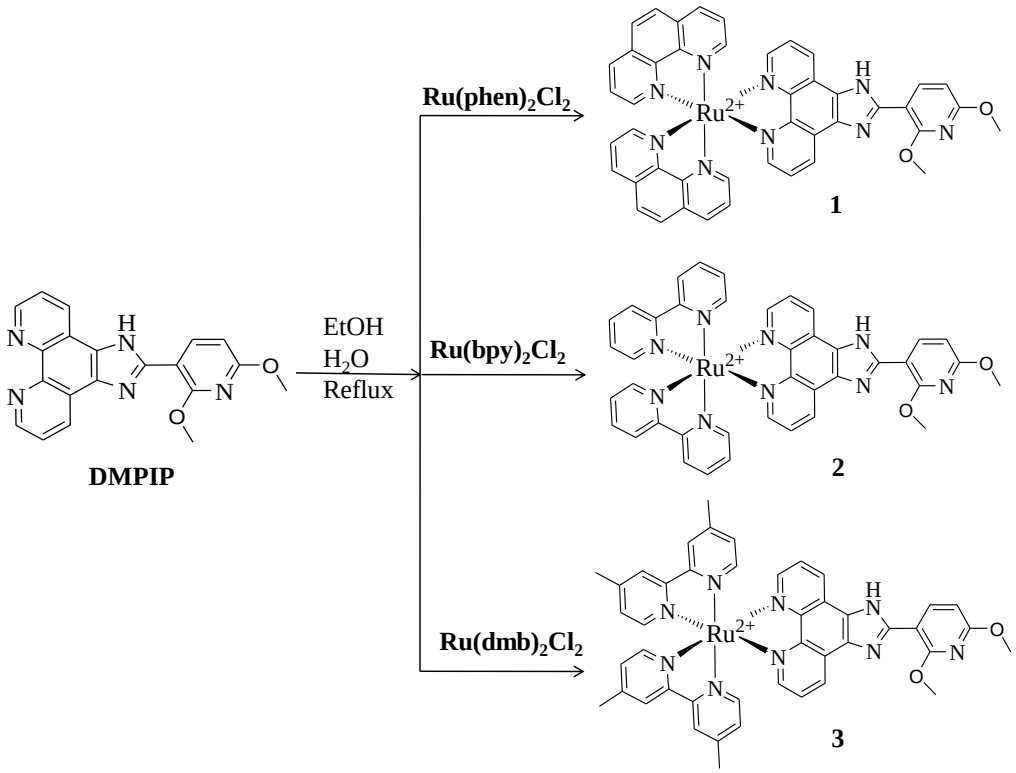

Scheme 7. Synthetic route of Ru(II) polypyridyl complexes **1-3**

2.4.2 Synthesis of Ru(II) polypyridyl complexes 4-6

$[Ru(phen)_2(MBIP)]\ (ClO_4)_2\ 2H_2O$ (4): This complex was synthesized as described above by taking a mixture of $[Ru(phen)_2Cl_2]\ 2H_2O$ (0.5 mM), MBIP (0.5 mM), yield: 71%. Anal calc for $C_{45}H_{34}Cl_2N_8O_{12}Ru$. (%): C, 51.44; H, 3.26; N, 10.66. Found: C, 51.20; H, 3.21; N, 10.59. FTIR (KBr, cm^{-1}) 3598(N-H), 1718(C=O),1429(C=C), 1612(C=N), 1281(C=O), 622(M-N) ^1H NMR data (400 MHz, ppm, DMSO-d_6 and TMS): δ 9.20(d,2H), 9.06(d,4H), 8.80(d,4H), 8.43(d,2H), 8.40(s,4H), 8.21(d,2H), 8.10(d,2H), 7.80(t,4H), 7.60(t,2H), 3.90(s,3H). $^{13}C[^1H]$ NMR data (100 MHz, DMSO-d_6, Major peaks): 165.68(C=O), 152.83,

152.62, 151.15, 150.62, 147.19, 145.70, 136.80, 133.39, 131.47, 130.64, 130.05, 128.61, 128.03, 126.63, 126.63, 127.33, 126.27, 52.34(-OCH_3).

[$Ru(bpy)_2(MBIP)](ClO_4)_2$ $2H_2O$ (5): This complex was synthesized as described above by taking a mixture of [$Ru(bpy)_2Cl_2$] $2H_2O$ (0.5 mM), MBIP (0.5 mM), yield: 72% Anal calc for $C_{41}H_{34}Cl_2N_8O_{12}Ru$ (%): C, 49.11; H, 3.42; N, 11.17. Found: C, 49.02; H, 3.21; N, 11.10. FTIR (KBr, cm^{-1}) 3598 (N-H), 2960(OC-H), 1720(C=O), 3083(C-H), 1611(C=N), 1283(C-O), 1440C=C), 623(M-N). ^{1}H NMR data (400 MHz, ppm, DMSO-d_6 and TMS): δ 9.02(d,2H), 8.93(d,4H), 8.41(d,4H), 8.25(d,2H), 8.17(d,2H), 7.87(t,4H), 7.68(d,2H), 7.59(t,2H), 7.35(t,2H), 3.91(s,3H). ^{13}C[^{1}H] NMR data (100 MHz, DMSO-d_6, Major peaks): 165.78(C=O), 159.13, 151.35, 149.26, 148.07, 143.37, 139.66, 138.91, 133.92, 130.05, 127.85, 126.22, 124.42, 123.68, 123.43, 52.26(-OCH_3).

[$Ru(dmb)_2(MBIP)](ClO_4)_2$ $2H_2O$ (6): This complex was synthesized as described above by taking a mixture of [$Ru(dmb)_2Cl_2$] $2H_2O$ (0.5 mM), MBIP (0.5 mM), yield: 76% Anal calc for $C_{45}H_{42}Cl_2N_8O_{12}Ru$: (%): C, 51.04; H, 4.00; N, 10.58. Found: C, 50.97; H, 3.88; N, 10.21. FTIR (KBr, cm^{-1}). 3598 (N–H), 3079 (C-H), 1721 (C = O), 1618 (C = N), 1436 (C = C), 623 (M–N). ^{1}H NMR data (400 MHz, ppm, DMSO-d_6 and TMS):δ 9.08 (d, 2H), 8.74 (d, 4H), 8.45 (S, 2H), 8.23 (d, 2H), 8.11 (d, 2H), 8.10 (d, 2H), 7.68 (t, 2H), 7.44 (d, 4H), 3.91 (S, -OCH_3), 2.47 (S, -CH_3). ^{13}C[^{1}H] NMR data (100 MHz, DMSO-d_6, Major peaks): 20.72 (CH_3), 52.30 (-OCH_3), 166 (C=O), 156, 150, 149, 145, 133, 131, 130, 128, 126, 124.

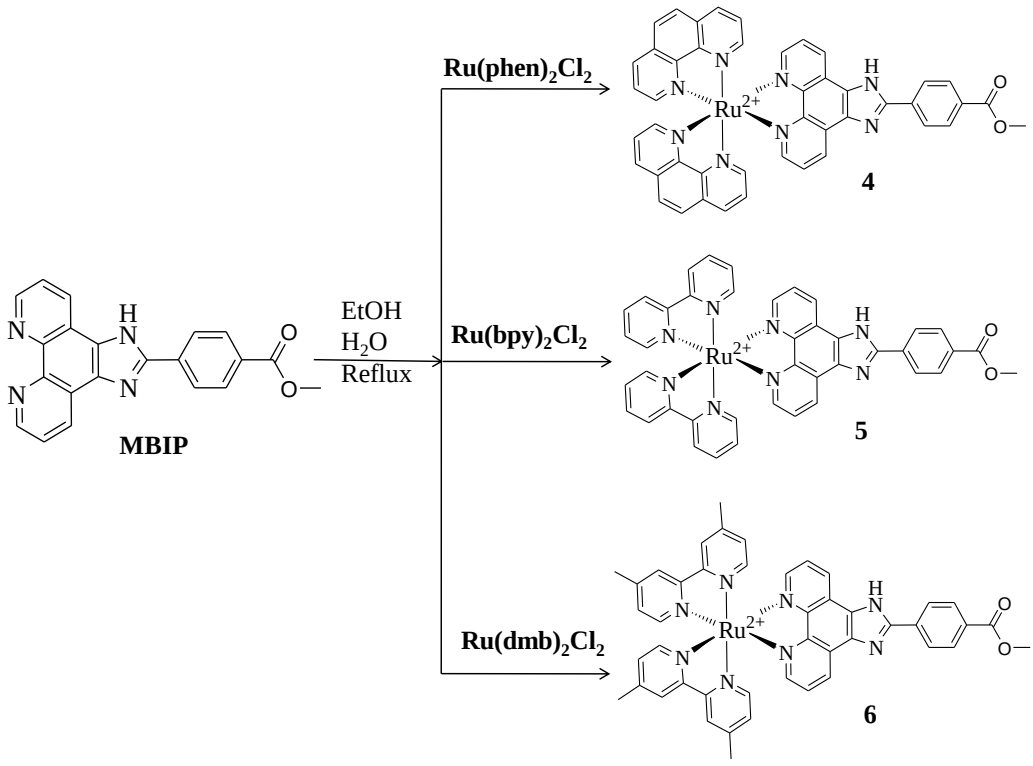

Scheme 8. Synthetic route of Ru(II) polypyridyl complexes **4-6**

2.4.3 Synthesis of Ru(II) polypyridyl complexes 7-9

$[Ru(phen)_2(DEBIP)](ClO_4)_2\ 2H_2O$ (7): This complex was synthesized as described above by taking a mixture of $[Ru(phen)_2Cl_2]\ 2H_2O$ (0.5 mM), DEBIP (0.5 mM), yield: 72%. Anal. data for $RuC_{47}H_{41}N_9Cl_2O_{10}$: cal. C,48.49; H, 3.52; N, 10.83; found: C,48.46; H, 3.51; N, 10.81. ESI–MS: 1063. IR(KBr, cm^{-1}) 1,605(C=N), 1,473(C=C), 1,277(C-C); 2,926(C-H) and 620(Ru–N). ^1H NMR data (400 MHz, ppm, DMSO-d_6 and TMS): δ 9.2 (d, 6H), 8.6 (d, 6H), 8.2 (s, 4H), 8.0 (t, 6H), 7.7 (d, 2H), 6.8(d, 2H), 3.2 (q, 2H, - CH_2), 1.2 (t, 3H, N- CH_3). $^{13}C[^1H]$ NMR data (100 MHz, DMSO-d_6, Major peaks): 156.3, 151.2, 150.6, 142.4, 136.6, 130.1, 122.3, 113.6, 47.5(N-CH_2), 20.1(N-CH_3).

[Ru(bpy)$_2$(DEBIP)](ClO$_4$)$_2$ 2H$_2$O (8): This complex was synthesized as described above by taking a mixture of [Ru(bpy)$_2$Cl$_2$] 2H$_2$O (0.5 mM), DEBIP (0.5 mM), yield: 71%. Anal. data for $RuC_{43}H_{41}N_9Cl_2O_{10}$: calc. C, 46.27; H, 3.67; N, 11.30; found: C, 46.25; H, 3.65; N, 11.29. ESI–MS calc: 1015; found: 1016. IR(KBr, cm^{-1}) 1,606(C=N), 1,473(C=C), 1,277(C-C); 3,081(C-H) and 620(Ru–N). ^{1}H NMR data (400 MHz, ppm, DMSO-d$_6$ and TMS): δ 9.1 (d, 2H), 8.8(d, 4H), 8.7 (d, 4H), 8.2 (d, 2H), 7.9 (t, 4H), 7.0(t, 4H), 6.6 (d, 2H) 6.3 (d, 2H), 3.2 (q, 2H, N- CH$_2$), 1.1(t, 3H, N- CH$_3$). ^{13}C[^{1}H] NMR data (100 MHz, DMSO-d$_6$, Major peaks): 157.4, 150.2, 137.4, 136.5, 127.6, 126.3, 124.6, 121.4, 114.5.47.2(N-CH$_2$), 19.9(N-CH$_3$).

[Ru(dmb)$_2$(DEBIP)](ClO$_4$)$_2$ 2H$_2$O (9): This complex was synthesized as described above by taking a mixture of [Ru(dmb)$_2$Cl$_2$] 2H$_2$O (0.5 mM), DEBIP (0.5 mM) (yield: 70%). Anal. data for- $RuC_{47}H_{49}N_9Cl_2O_{10}$ calc. C, 48.16; H, 4.18; N, 10.76; found: C, 48.15; H, 4.16; N, 10.74. ESI–MS calc: 1071; found: 1072. IR(KBr, cm^{-1}) 1,611(C=N), 1,555(C=C), 1,273(C-C); 3,082(C-H) and 622(Ru–N). ^{1}H NMR data (400 MHz, ppm, DMSO-d$_6$ and TMS): δ 9.1 (s, 4H d), 8.8 (d, 4H), 8.2 (d, 2H), 7.9 (t, 4H), 7.52 (t, 2H), 7.3(t, 4H), 6.8 (d, 2H) 6.7 (d, 2H), 3.3 (q, 4H, N- CH$_2$), 1.3 (t, 6H, N-CH$_3$), 2.5(s, 12H, -CH$_3$). ^{13}C[^{1}H] NMR data (100 MHz, DMSO-d$_6$, Major peaks): 157.9, 150.6, 149.8,147.6, 128.5, 120.4, 114.7, 47.0(N-CH$_2$), 26.4(CH$_3$), 19.8(N-CH$_3$).

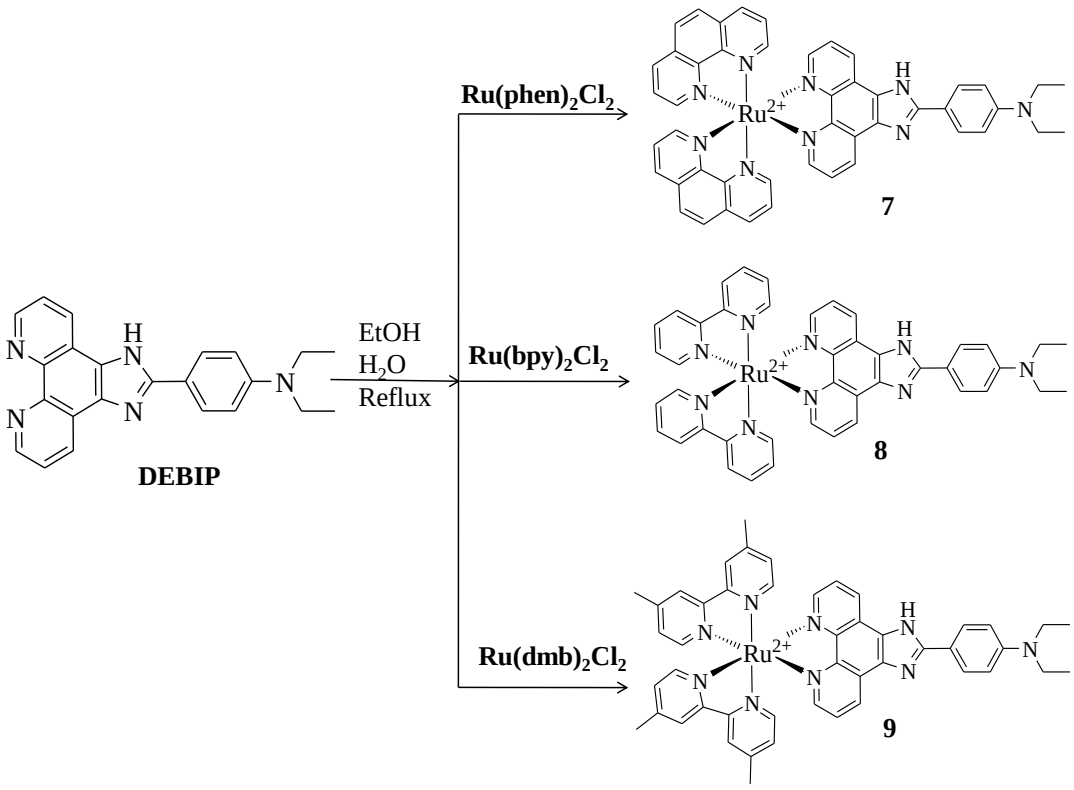

Scheme 9. Synthetic route of Ru(II) polypyridyl complexes **7-9**

2.4.4 Synthesis of Ru(II) polypyridyl complexes 10-12

$[Ru(phen)_2(DEPIP)](ClO_4)_2\ 2H_2O$ (10): This complex was synthesized as described above by taking a mixture of DEPIP (0.3985 g, 1.0 mM), cis-$[Ru(phen)_2Cl_2]\ 2H_2O$ (0.531 g, 1.0 mM) (yield: 81.14%). Analytical data for $RuC_{48}H_{38}C_{l2}N_8O_{10}$: C, 54.14; N, 10.11; H, 3.58; calculated data: C, 54.45; N, 10.58; H, 3.62. ^{1}H NMR (DMSO-d_6, 400 MHz): δ 9.08 (d, 6H, J = 9.2 Hz), 8.78(t, 6H, J = 7.7 Hz), 8.53(s, 4H), 8.41(d, 6H, J = 4.5 Hz), 8.17(d, 2H, J = 7.5 Hz), 8.03(d, 2H, J = 5.0 Hz), 4.28(q, 4H, J=7.0 Hz), 1.27(t, 6H, J = 7.2 Hz). ^{13}C[^{1}H] NMR (DMSO-d_6, 100 MHz, d, ppm): 153.16, 151.75, 147.59, 146.22, 142.24, 137.29, 134.90, 132.23, 130.79, 128.55, 128.96, 127.50, 126.79, 109.72, 62.11, 15.75. ESI mass of is 860. IR (KBr, cm^{-1}): 3390 (ν, NH), 1691 (ν, CN), 1085 (ν, COC) and 628 (ν, RuN).

$[Ru(bpy)_2(DEPIP)](ClO_4)_2\ 2H_2O$ (11): This complex was synthesized as described above by taking a mixture of DEPIP (0.3985 g, 1.0 mM), cis-$Ru(bpy)_2Cl_2]\ 2H_2O$ (0.52 g, 1.0 mM) (yield: 71%). Analytical data for $RuC_{44}H_{38}C_{l2}N_8O_{10}$: C, 52.21; H, 3.72; N, 10.95; calculated data: C, 52.28; H, 3.79; N, 11.09. ^{1}H NMR (DMSO-d_6, 400 MHz): δ 9.08 (d, 2H, J = 7.2 Hz), 8.74(d, 4H, J = 6.5 Hz), 8.53(d, 4H, J = 8.2 Hz), 8.43(d, 2H, J = 8.2 Hz), 8.22(t, 4H, J = 7.7 Hz), 8.09(t, 2H, J = 2.7 Hz), 7.65(t, 4H, J = 9.2 Hz), 7.41(d, 2H, J = 5.2 Hz), 7.16(d, 2H, J = 5.2 Hz), 4.28(q, 4H, J = 7.0 Hz), 1.28(t, 6H, J = 7.0 Hz). ^{13}C[^{1}H] NMR (DMSO-d_6, 100 MHz, d, ppm): 157.24, 152.34, 151.98, 150.64, 145.84, 138.47, 137.35, 134.89, 131.96, 130.83, 128.38, 127.49, 126.95, 124.95, 112.72, 61.79, 14.33. ESI mass is 811. IR (KBr, cm^{-1}): 3390 (ν, NH), 1691 (ν, CN), 1083 (ν, COC) and 628 (ν, RuN).

$[Ru(dmb)_2(DEPIP)](ClO_4)_2\ 2H_2O$ (12): This complex was synthesized as described above by taking a mixture of depip (0.3985 g, 1.0 mM), cis-$[Ru(dmb)_2Cl_2]\ 2H_2O$ (0.576 g, 1.0 mM) (yield: 68%). Analytical data for $RuC_{48}H_{46}C_{l2}N_8O_{10}$: C, 54.02; N, 10.51; H, 4.31; calculated data: C, 54.04; N, 10.50; H, 4.35. ^{1}H NMR (DMSO-d_6, 400 MHz): δ 9.10(d, 2H, J = 8.0 Hz), 8.88(d, 4H, J = 7.0 Hz), 8.52(d, 2H, J = 8.2 Hz), 8.23(s, 4H), 8.09(t, 2H, J = 4.0 Hz), 7.85(d, 4H, J = 5.2 Hz), 7.62(d, 2H, J = 7.0 Hz), 7.35(d, 2H, J = 6.2 Hz), 4.28(q, 4H, J = 7.0 Hz), 2.08(s, 12H), 1.28(t, 6H, J = 7.2 Hz). ^{13}C[^{1}H] NMR (DMSO-d_6, 100 MHz, d, ppm): 167.37, 161.23, 156.77, 151.10, 150.06, 140.94, 138.23, 134.87, 132.15, 131.96, 130.87, 129.11, 127.52, 125.49, 112.87, 61.79, 21.24, 14.34. ESI mass is 868. IR (KBr, cm^{-1}): 3392 (ν, NH), 1699 (ν, CN), 1111 (ν, COC) and 626 (ν, RuN).

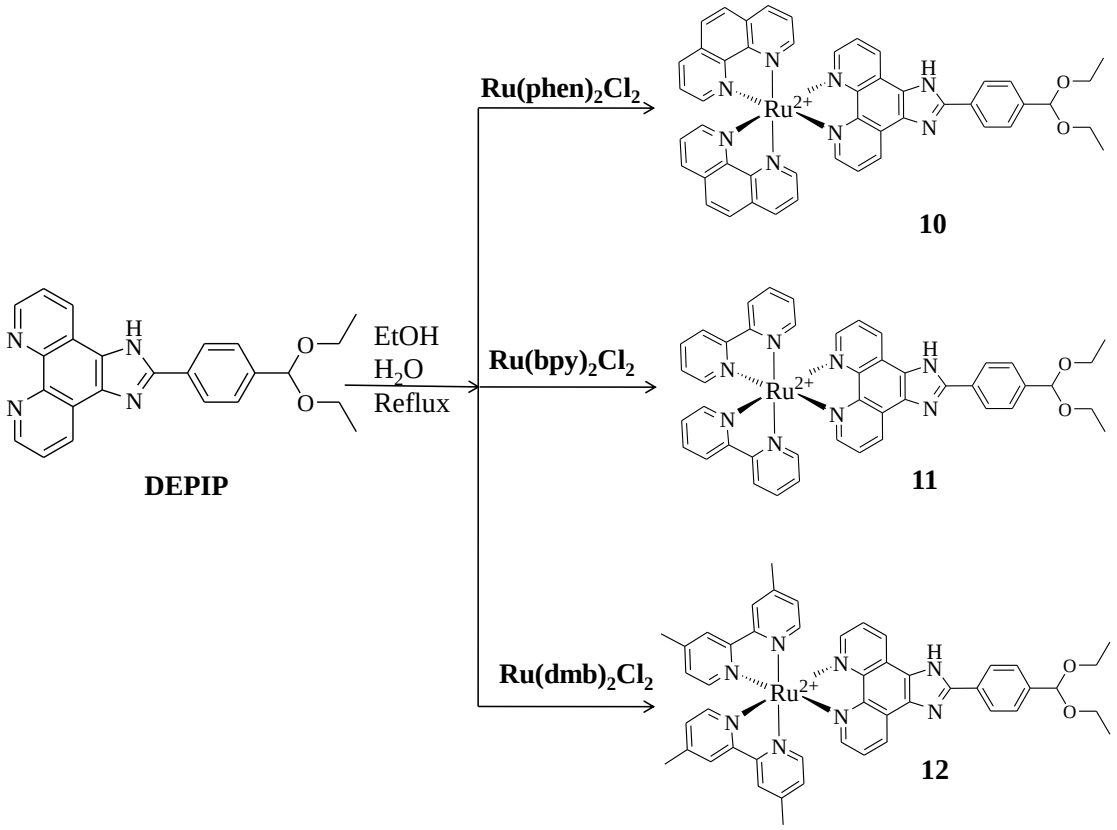

Scheme 10. Synthetic route of Ru(II) polypyridyl complexes **10-12**

2.4.5 Synthesis of Ru(II) polypyridyl complexes 13-15

$[Ru(phen)_2(PIP\text{-}Br)](ClO_4)_2\ 2H_2O$ (13): This complex was synthesized as described above by taking a mixture of a mixture of *cis*-$[Ru(phen)_2(Cl)_2]\cdot 2H_2O$ (0.16 mmol) and PIP-Br (0.16 mmol), yield (69%). Analytical data for $RuC_{43}H_{27}N_9BrCl_2O_{11}$ Calcd. (%) C: 63.83; H: 3.42; N: 13.75. Found: C: 63.90; H: 3.37; N: 13.86. LC-MS in DMSO M/Z: 1071.5. IR: 1484 (C=C), 1627 (C=N), 722 (Ru–N (L)), 627 cm^{-1} (Ru–N(PIP-Cl). ^{1}H-NMR (DMSO- d_6, 400 MH_Z δ ppm): 9.13 (d, 2H), 8.79 (d, 4H), 8.40 (s, 3H), 8.16 (d, 4H), 8.09 (d, 2H), 8.04 (d, 2H),7.70 (t,2H), 7.45 (d, 2H), 7.15 (d, 2H). ^{13}C-NMR (200 MHz, DMSO-d_6, 298 K, δ ppm): 156.51(C-k, 1C), 153.28 (C-i,1C), 151.21(C-e, 2C) 150.86(C-1, C-a, 6C), 147.85(C-5, 4C),

146.17 (C-3,C-c, 6C), 137.27 (C-m,C-4, 5C), 131.61(C-o, 1C), 131.00(C-d, 2C), 128.35(C-6,C-n, 5C) , 127.72 (C-g, 1C), 126.65 (C-f, 1C), 123.64(C-2,C-b, 6C), 119.58(C-l,C-j, 2C).

$[Ru(bpy)_2(PIP\text{-}Br)](ClO_4)_2\ 2H_2O$ (14): This complex was synthesized as described above by taking a mixture of a mixture of *cis*-$[Ru(bpy)_2(Cl)_2]\cdot 2H_2O$ (0.16 mmol) and PIP-Br (0.16 mmol), yield (58%). Analytical data for $RuC_{39}H_{27}N_8BrCl_2O_{11}$: Calcd. (%) C: 63.90; H: 3.37; N: 13.86. Found: C: 63.96; H: 3.35; N: 13.90. LCMS in DMSO M/Z: 1023.5. IR: 1466 (C=C), 1603 (C=N), 768 (Ru–N (L)), 627 cm^{-1} (Ru–N(PIP-Br)). ^{1}H-NMR (DMSO- d_6, 400 MH_Z δ ppm): 9.10 (d, 2H), 8.90 (m, 2H), 8.25 (t, 3H), 8.66 (t, 3H), 8.12 (m, 4H), 8.08 (d, 2H), 7.93(t,2H), 7.65 (t,2H), 7.42 (m, 2H), 7.13 (d, 1H). ^{13}C-NMR (200 MHz, DMSO-d_6, 298K): 157.38(C-5), 157.16(C-k), 156.44(C-i), 151.96(C-a, C-1), 145.81(C-e), 138.45(C-3 , C-c), 131.75(C-m) , 128.16(C-n, C-o C-d), 126.53(C-g,C-4), 124.93(C-b, C-f), 123.69(C-2), 119.64(C-j), 115.61(C-l).

$[Ru(dmb)_2(PIP\text{-}Br)](ClO_4)_2\ 2H_2O$ (15): This complex was synthesized as described above by taking a mixture of a mixture of *cis*-$[Ru(bpy)_2(Cl)_2]\cdot 2H_2O$ (0.16 mmol) and PIP-Br (0.16 mmol), yield: 60%. Analytical data for $RuC_{43}H_{35}N_8BrCl_2O_{11}$: Calcd. (%) C: 63.47; H: 3.99; N: 13.30. Found: C: 63.45; H: 4.15; N: 13.25. LCMS in DMSO M/Z: 1083. IR: 1484 (C=C), 1619 (C=N), 737 (Ru–N (L)), 626 cm^{-1} (Ru–N(pip-Br). ^{1}H-NMR (DMSO- d_6, 400 MH_Z δ ppm): 9.12 (d, 2H), 8.93 (m, 4H), 8.83 (s, 1H), 8.13 (d, 1H), 8.07 (s, 1H), 7.87 (d, 2H), 7.67 (d, 2H), 7.32(d,2H), 6.98 (m,4H), 2.55 (d, 6H), 2.45 (d,6H). ^{13}C-NMR (200 MHz, DMSO-d_6, 298K): 156.91(C-5), 156.50(C-k), 154.53(C-i), 151.13(C-a, C-1), 149.59(C-3), 148.63(C-e),

145.86(C-c), 131.20(C-m), 128.82(C-o), 126.51 (C-n, C-d), 125.65(C-4), 124.20(C-2), 123.77(C-f), 123.53(C-g), 123.43(C-b), 119.47(C-l), 114.77(C-j), 21.05(C-6).

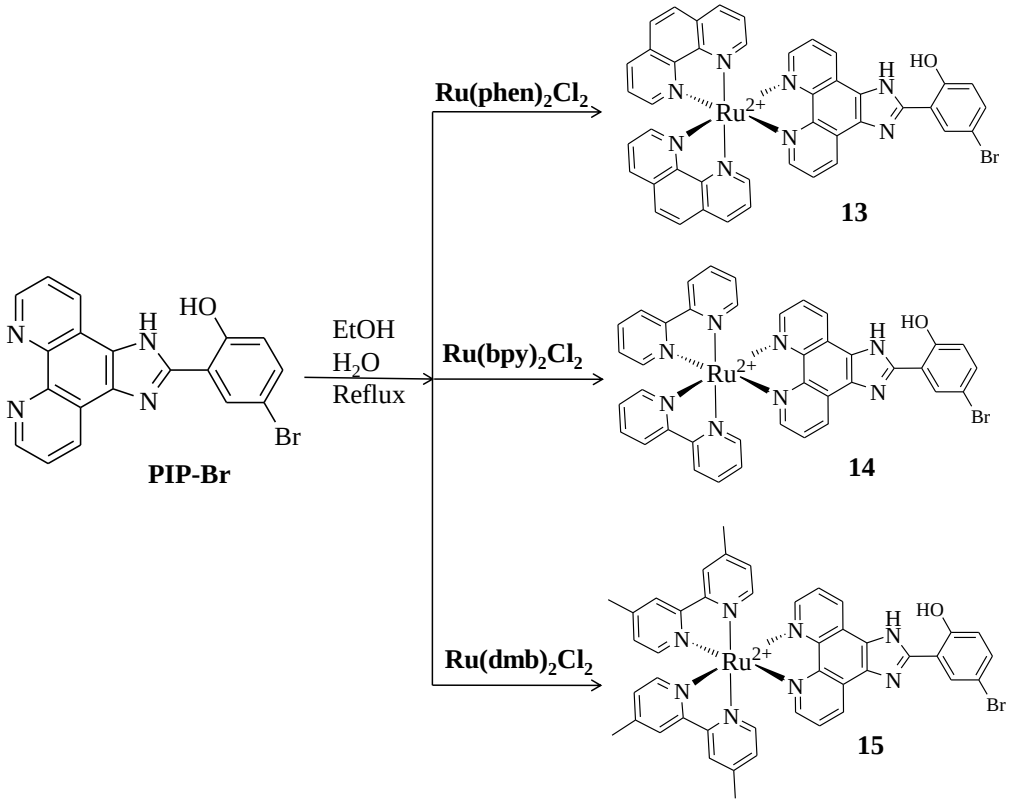

Scheme 11. Synthetic route of Ru(II) polypyridyl complexes **13-15**

2.4.6 Synthesis of Ru(II) polypyridyl complexes 16-18

$[Ru(phen)_2(IPIPC)](ClO_4)_2\ 2H_2O$ (16): This complex was synthesized as described above by taking a mixture of $[Ru(phen)_2Cl_2]\ 2H_2O$ (0.5 mM), IPIPC (0.5 mM), yield: 72%. Anal calc for $C_{49}H_{38}Cl_2N_8O_{12}Ru$: Calcd (%): C: 53.36, H: 3.47, N: 10.16. Found: C: 53.16, H: 3.23, N: 10.01. IR (KBr, cm^{-1}): 3599 (N-H), 2967(C-H), 1722 (C=O), 1428 (C=C), 1578 (C=N), 1225 (C-O), 622 (M-N). ^1H NMR data (400 MHz, ppm, DMSO-d_6 and TMS): δ 9.00 (d, 2H), 8.79 (d, 4H), 8.39 (s, 4H), 8.16 (d, 2H), 8.09 (d, 4H), 8.03 (d, 1H), 7.83 (s, 1H), 7.74

(s, 1H), 7.80 (t, 2H), 7.77 (t, 4H), 7.68 (d, 1H), 3.12 (sept, -CH), 1.29 (d, $-CH_3$). $^{13}C[^1H]$ NMR data (100 MHz, DMSO-d_6, Major peaks): 174.33 (-C=O), 23.66 ($-CH_3$), 32.91 (-CH), 158.21, 154,13, 152.78, 152.59, 147.20, 147.12, 146.88, 146.30, 136.78, 136,75, 133.80, 131.46, 130.22, 128.02, 126.29, 126.26, 123.12, 121.64, 118.80, 117.20.

$[Ru(bpy)_2(IPIPC)](ClO_4)_2$ $2H_2O$ (17): This complex was synthesized as described above by taking a mixture of $[Ru(phen)_2Cl_2]$ $2H_2O$ (0.5 mM), IPIPC (0.5 mM), yield: 69%. Anal calc for $C_{45}H_{38}Cl_2N_8O_{12}Ru$: Calcd (%): C: 51.24, H: 3.63, N: 10.62. Found: C: 51.12, H: 3.41, N: 10.49. FTIR (KBr, cm^{-1}): 3598 (N-H), 2967(C-H), 1738 (C=O), 1447 (C=C), 1618 (C=N), 1225 (C-O), 622 (M-N). ^1H NMR data (400 MHz, ppm, DMSO-d_6 and TMS): δ 9.03 (d, 4H), 8.89 (d, 2H), 8.83 (d, 4H), 8.22 (d, 2H), 8.11 (t, 4H), 7.35 (t, 2H), 7.86 (s, 1H), 7.83 (s, 1H), 7.76 (t, 4H), 7.62 (d, 1H), 7.60 (d, 1H), 3.14 (sept, -CH), 1.30 (d, CH_3). $^{13}C[^1H]$ NMR data (100 MHz, DMSO-d_6, Major peaks): 23.70 ($-CH_3$), 32.93 (-CH), 174.39 (-C=O), 164.32, 157.62, 156.75, 154.10, 151.41, 147.76, 146.68, 144.35, 140.44, 139.29, 138.34, 133.63, 128.61, 124.42, 123.15, 123.12, 121.64, 118.81, 118.77.

$[Ru(dmb)_2(IPIPC)](ClO_4)_2$ $2H_2O$ (18): This complex was synthesized as described above by taking a mixture of $[Ru(phen)_2Cl_2]$ $2H_2O$ (0.5 mM), IPIPC (0.5 mM), yield: 65%. Anal calc for $C_{49}H_{46}Cl_2N_8O_{12}Ru$: Calcd (%): C: 52.98, H: 4.17, N: 10.09. Found: C: 52.71, H: 4.08, N: 10.03. FTIR (KBr, cm^{-1}): 3599 (N-H), 2966(C-H), 1720 (C=O), 1480 (C=C), 1619 (C=N), 1226 (C-O), 622 (M-N). ^1H NMR data (400 MHz, ppm, DMSO-d_6 and TMS): δ 9.20 (d, 2H), 8.73 (d, 4H), 8.12 (d, 4H), 8.07 (d, 2H), 7.41 (t, 2H), 7.67 (d, 4H), 7.79 (s, 1H), 7.77 (s, 1H), 7.16 (d, 1H), 7.86 (d, 1H), 3.15 (sept, -CH), 2.46 (s, $-CH_3$, 12H), 1.30 (d, $-CH_3$, 6H).

$^{13}C[^{1}H]$ NMR data (100 MHz, DMSO-d_6): 20.71 (-4CH_3), 23.68 (-2CH_3), 32.94 (-CH), 174.36 (-C=O), 167.95, 165.93, 158.26, 156.27, 156.12, 154.17, 151.02, 150.74, 149.84, 146.92, 133.83, 131.66, 131.45, 128.60, 128.48, 126.17, 124.97,123.14, 121.66, 118.14, 114.49.

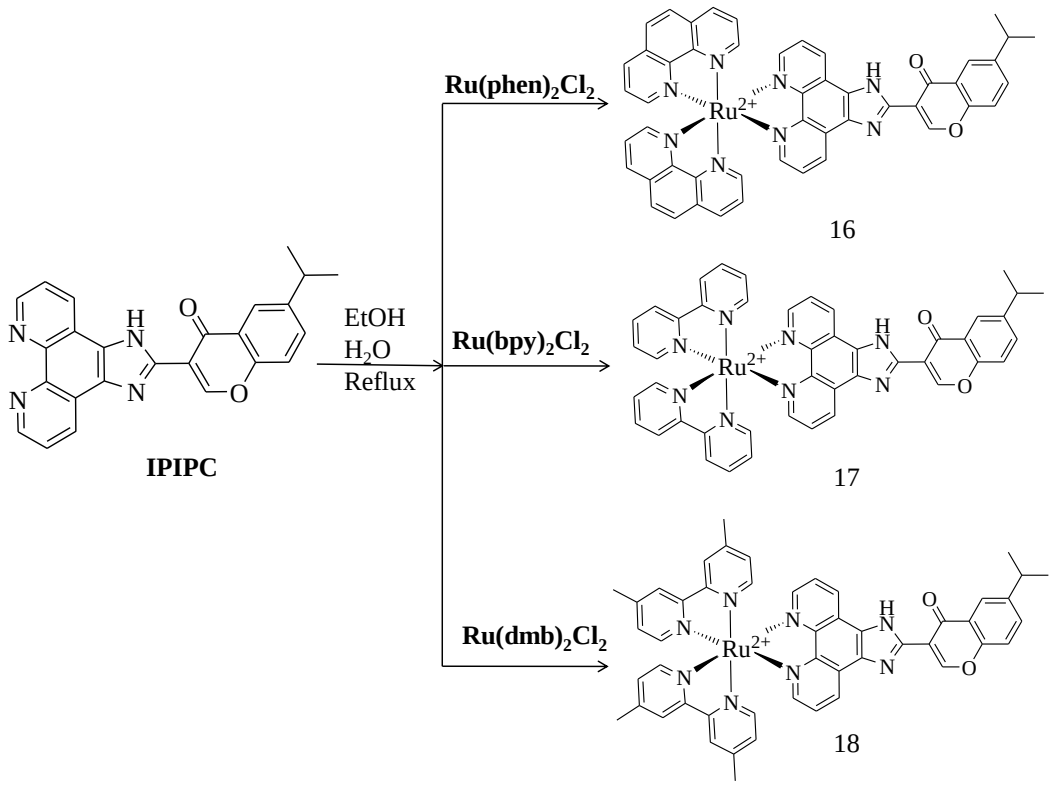

Scheme 12. Synthetic route of Ru(II) polypyridyl complexes **16**-**18**

2.5 DNA Binding Experimental Studies with CT-DNA

2.5.1 UV-Vis absorption Titrations

UV-Vis absorption titrations of the synthesized Ru(II) polypyridyl complexes with CT-DNA were carried out in Tris-buffer at room temperature by adding increasing amounts of DNA to the solution of the complex at a fixed concentration. The Ru(II) complex–DNA

solution was allowed to incubate for 5 min before recording the absorption spectra. The absorption titration process was repeated until there was no change in the spectra, indicating binding saturation had been achieved. To evaluate the binding strength of the Ru(II) complex to DNA, the intrinsic binding constant (K_b) was obtained by monitoring the change in the absorbance at metal–to–ligand charge transfer (MLCT) band. The intrinsic binding constant K_b of the Ru(II) complexes was calculated from the following equation [16]

$$[DNA]/(\varepsilon_a-\varepsilon_f) = [DNA]/(\varepsilon_b-\varepsilon_f) + 1/K_b(\varepsilon_b-\varepsilon_f)$$

where, the apparent extinction coefficient (ε_a) was obtained by calculating A_{obs}/[Ru]. The terms ε_f and ε_b correspond to the extinction coefficients of free (unbound) and the fully bound complex, respectively. [DNA] is the concentration of DNA. From a plot of $[DNA]/(\varepsilon_a-\varepsilon_f)$ against [DNA] will give a slope $1/(\varepsilon_b-\varepsilon_f)$ and an intercept $1/K_b(\varepsilon_b-\varepsilon_f)$, K_b is the ratio of the slope to the intercept.

2.5.2 Fluorescence Titrations

Fluorescence titrations of all the Ru(II) polypyridyl complexes were performed in tris-buffer at room temperature. In this titrations excitation wavelength fixed and the emission range adjusted before recording the spectra. The spectra were recorded by adding increments of the DNA stock solution to a fixed concentration of the complex, followed by thorough mixing. After mixing solutions were allowed to incubate for 5 min before recording the spectra and emission titrations for each sample were repeated at least three times. The fraction of the ligand bound was calculated from the relation $r/C_f = K_b(n - r)$, $C_b = C_t[(F–$

$F_0)/(F_{max}–F_0)]$, $C_f = C_t - C_b$; where, C_t is the total complex concentration, F is the observed fluorescence emission intensity at a given DNA concentration, F_0 is the intensity in the absence of DNA, and F_{max} is when complex is fully bound to DNA. Binding constant (K_b) was obtained from a Scatchard plot of r/C_f against r, where r is the C_b/[DNA] and C_f is the concentration of free complex.

2.5.3 Fluorescence quenching titrations

Fluorescence quenching titrations of the Ru(II) complexes were carried out in tris-buffer at room temperature, in the absence and presence of DNA with varying concentration of $[Fe(CN)_6]^{4-}$ as anion quencher. The Stern-Volmer quenching constant can be determined by using Linear Stern–Volmer equation [17], $I_0/I = 1 + K_{sv}[Q]$, where, I_0 and I are the fluorescence intensities in the absence and presence of quencher respectively, [Q] is the concentration of the quencher $[Fe(CN)_6]^{4-}$. K_{sv} is a linear Stern–Volmer quenching constant. K_{sv} is dependent on the ratio of the bound concentration of Ru(II) complex to the concentration of DNA. In the quenching plot of I_0/I vs [Q] gives the slope as the quenching constant K_{sv}.

2.5.4 DNA Molecular light-switch effect

The DNA molecular light-switch *on* and *off* effect of synthesized Ru(II) polypyridyl complexes were performed in Tris-buffer solution at room temperature by the successive addition of Co^{2+} and EDTA to the DNA bound complex.

2.5.5 Viscosity experiments

Viscosity studies for synthesized Ru(II) polypyridyl complexes were done using an Ostwald viscometer, immersed in a thermostated water bath maintained at a constant temperature 30.0±0.1°C. CT- DNA samples approximately 200 base pairs were prepared by sonicating in order to minimize the complexities arising from DNA flexibility [18, 19]. A fixed volume of the Ru(II) polypyridyl complex solution was added to the solution of DNA. After careful mixing, flow time was measured with a digital stopwatch and each sample was measured three times, and an average flow time was calculated. The data were presented as $(\eta/\eta_0)^{1/3}$ against [complex]/[DNA], where η is the viscosity of DNA in the presence of complex and η_0 is the viscosity of DNA alone.

2.5.6 Photoactivated cleavage of pBR 322 DNA

First Supercoiled pBR322 DNA (100 µM) was treated with different concentrations Ru(II) complex. All the samples were irradiated at room temperature with a UV lamp (365 nm) for 30 minutes. Samples were analyzed by electrophoresis for 2.5 h at 40 V on a 0.8% agarose gel is prepared by dissolving the agarose powder in an appropriate Tris-acetic acid-EDTA buffer (1X TAE buffer). The gel was stained with 1 µg/mL Ethidium bromide is a fluorescent dye and it intercalates between bases of nucleic acids and provides opportunity to detect nucleic acid fragments in gels, and then photographed by illumination with UV light using Gel doc system.

(***CAUTION****: Ethidium bromide is a mutagen and potential carcinogen. Gloves should be worn and care should be taken when handling ethidium bromide solutions. UV light is damaging to eyes and exposed skin. Protective eyewear should be worn at all times while using a UV light source*).

2. 5.7 Antibacterial activity

The Antibacterial Studies were performed by the standard disc diffusion method . The complexes were screened for antibacterial activity against gram positive and gram negative microorganisms. The Mueller Hinton agar was prepared and poured fresh into sterile Petri plates and allowed to dry, and inoculate 0.2 mL of bacterial culture which has 10^6CFU/mL concentrations. Filter paper discs approximately 5mm in diameter were placed in the previously prepared agar plates. The complex was dissolved in DMSO to get a final concentration of 40 µg/mL per disc. Each plate contains standard microorganisms with three different complexes and the agar plates were then incubated at 37ºC. After 24 h of incubation, each plate was examined. The resulting zones of inhibition were uniformly circular with a confluent lawn of growth. The diameters of the zones of complete inhibition were measured (in mm), including the diameter of the disc where the DMSO was used as control.

2.5.8 *In Vitro* Cytotoxicity Studies

The standard 3–(4,5–dimethylthiazole)–2,5–diphenyltetraazolium bromide (MTT) assay procedures were used to assess cell viability [20]. Cells were placed in 96–well microassay culture plates (8×10^3 cells per well) and grown overnight at 37 °C in a 5% CO_2 incubator. The complexes tested were dissolved in DMSO and diluted with RPMI 1640 and then added to the wells to achieve final concentrations ranging from 10^{-6} to 10^{-4} M. Control wells were prepared by addition of culture medium (100 µL). Wells containing culture medium without cells were used as blanks. The plates were incubated at 37 °C in a 5% CO_2 incubator for 48 h. Upon completion of the incubation, stock MTT dye solution (20 µL, 5

mg/mL) was added to each well. After 4h, buffer (100 µL) containing N,N–dimethylformamide (50%) and sodium dodecyl sulfate (20%) was added to solubilize the MTT formazan. The optical density of each well was then measured on a microplate spectrophotometer at a wavelength of 490 nm. The IC_{50} values were determined by plotting the percentage viability against complex concentrations graph and reading off the concentration at which 50% of cells remain viable relative to the control. Each experiment was repeated at least three times to get the mean values. The percentage of cell viability can be measured from the following formula.

$$\% \text{ cell viability (\%MTT reduction)} = \frac{\text{Absorbance of treated cells}}{\text{Absorbance of untreated cells}} \text{ X } 100$$

2.5.9 Apoptosis by Flow Cytometry

For these analyses, HeLa cells were cultured in six-well plates at a density of 1×10^6 cells per well. The cells were incubated at 5% CO_2 and 37 °C with IC_{50} dose of Ru(II) complexes and cisplatin for 24 h and centrifuged at 4 ˚C. Then the cells were washed in 1 mL of Ice cold PBS (phosphate buffered saline) twice for 2 min. The pellets were resuspended in 500 µL of HEPES (4-(2-hydroxyethyl)-1-piperazineethanesulfonic acid) binding buffer and washed at 4 ˚C for 5 min. Resuspended the cells in 70 µL of HEPES binding buffer and add 5 µL of Annexin V, incubate for 15 min at room temperature in the dark. After incubation in dark at room temperature analysis was done by flow cytometer.

2.5.10 Cell cycle analysis by Flow Cytometry

The cells were seeded at a concentration of 1×10^6 cells/mL in a culture dish and washed with PBS. The cells were incubated with IC_{50}value of the Ru(II) complex and cisplatin for 24 h. Control wells were maintained in RPMI-1640 medium supplemented with 10% FBS. Add Buffer I (20mM citrate-Phosphate, 1 mM EDTA, 0.2 Sucrose, 0.1% Triton X-100) 0.5 mL at 4^0C, agitate to suspend and incubate for 10 min. Add Buffer II (10 mM Citrate-Phosphate, 0.1M NaCl) with AO (Acridine Orange) 0.5mL at 4^0C, agitate to suspend. After the treatment cell cycle distribution were determined by flow cytometry.

3. Results and Discussion

3.1 Characterization

3.1.1 NMR spectral studies

The polypyridyl ligands and their Ru(II) complexes 1-18 have been characterized by ^{1}H-NMR and ^{13}C[^{1}H]-NMR spectroscopy. The ^{1}H-NMR spectra of the ligands and their Ru(II) complexes were recorded in DMSO-d_6 solution, using tetramethylsilane (TMS) as internal standard. In the ^{1}H-NMR spectrum of ligands, the aromatic proton region is a set of multiplets in the range of 6.5–8.97 ppm. Upon examination it was found that the proton signal in the spectrum of the complex is shifted downfield compared to the free ligand, suggesting deshielding of the protons due to the coordination with metal ion. The proton resonance of –NH in the imidazole ring of the ligand was not observed, because of the quick exchange of proton between two nitrogens of the imidazole ring, characteristic of an active proton. The ^{13}C[^{1}H]-NMR spectra of the ligands and their Ru(II) complexes were recorded in DMSO-d_6 solution. The spectral data are reported along with their possible assignments in

the second chapter, and all the carbons were found in the expected regions. Comparing the spectra of the free ligand with that of metal complexes shown downfield shift due to the resonance, this indicates clearly that the carbons were affected by coordination. The ^{1}H-NMR and ^{13}C[^{1}H]-NMR spectrum of the DMPIP, MBIP IPIPC ligands and their $[Ru(phen)_2(DMPIP)]^{2+}$ complex, $[Ru(phen)_2(MBIP)]^{2+}$ complex and $[Ru(phen)_2(IPIPC)]^{2+}$ are shown in figures from 1 to 12.

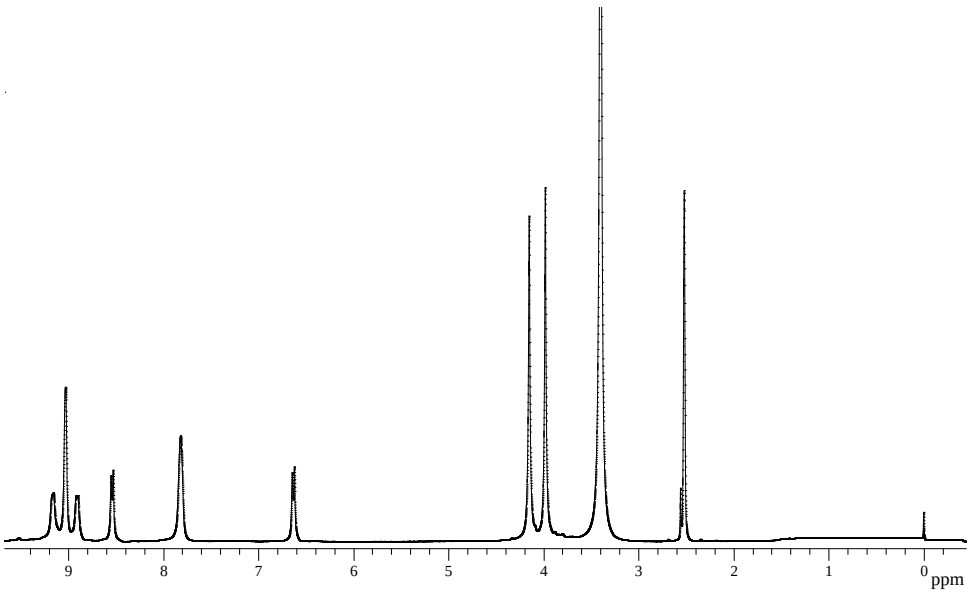

Fig 1. ^{1}H NMR Spectrum of ligand DMPIP.

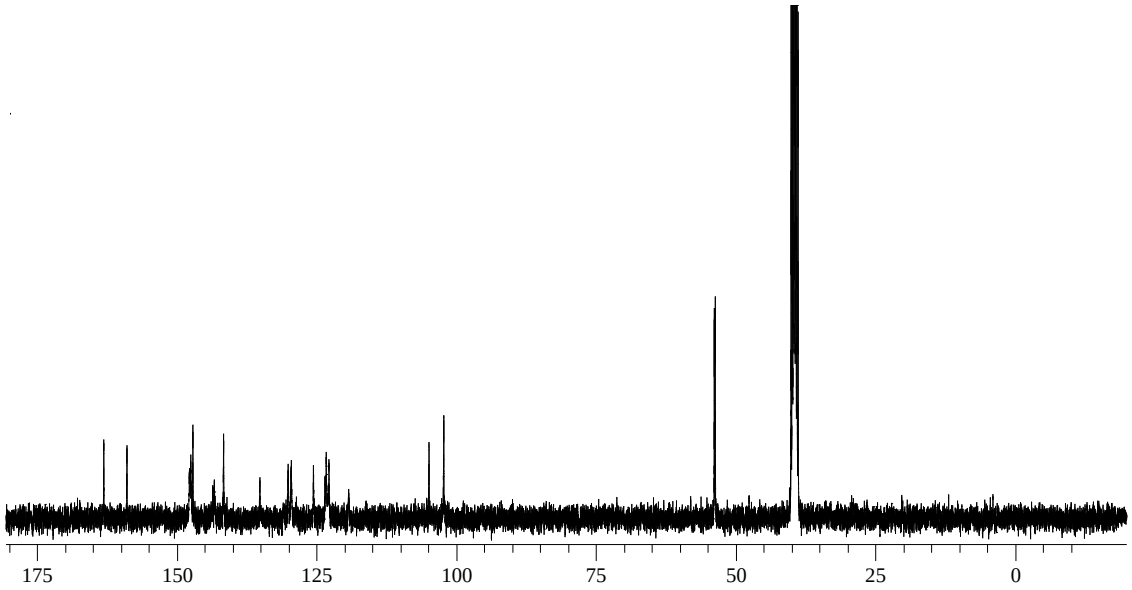

Fig 2. $^{13}C[^{1}H]$ NMR Spectrum of ligand DMPIP.

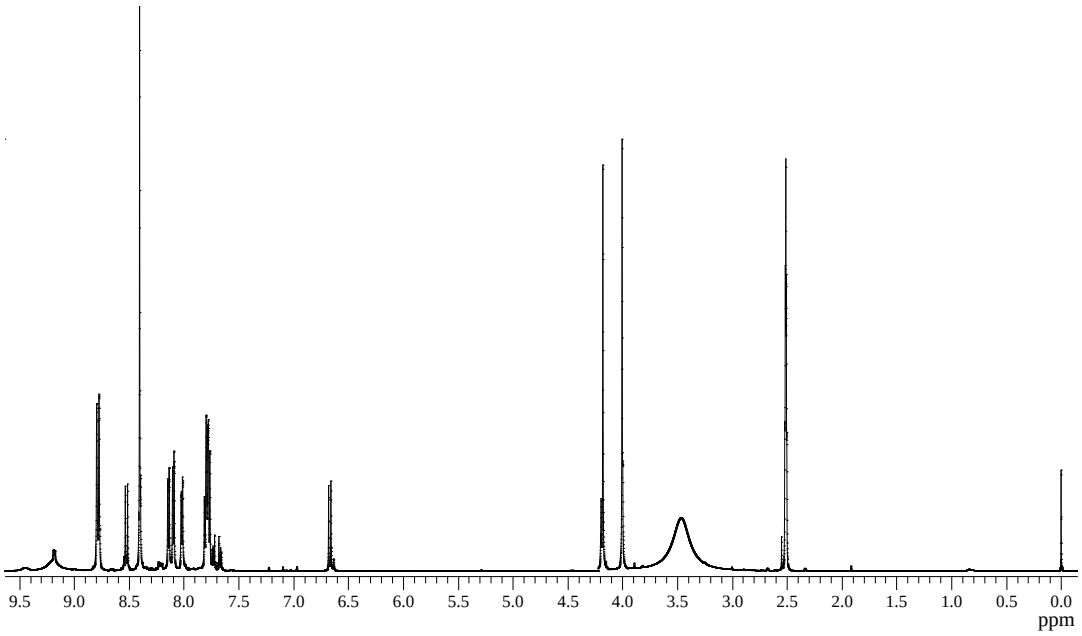

Fig 3. ^{1}H NMR Spectrum of $[Ru(phen)_2(DMPIP)]^{2+}$.

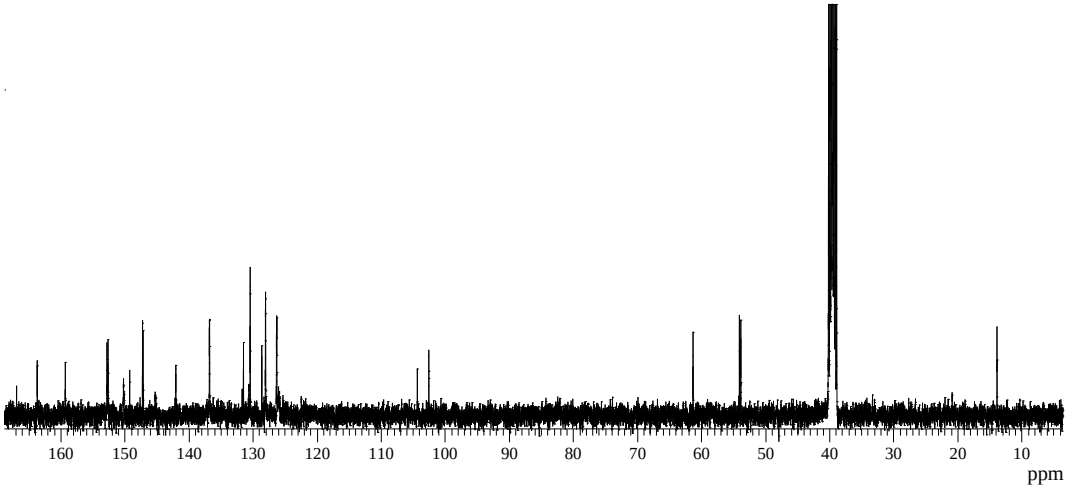

Fig 4. ^{13}C NMR Spectrum of $[Ru(phen)_2(DMPIP)]^{2+}$.

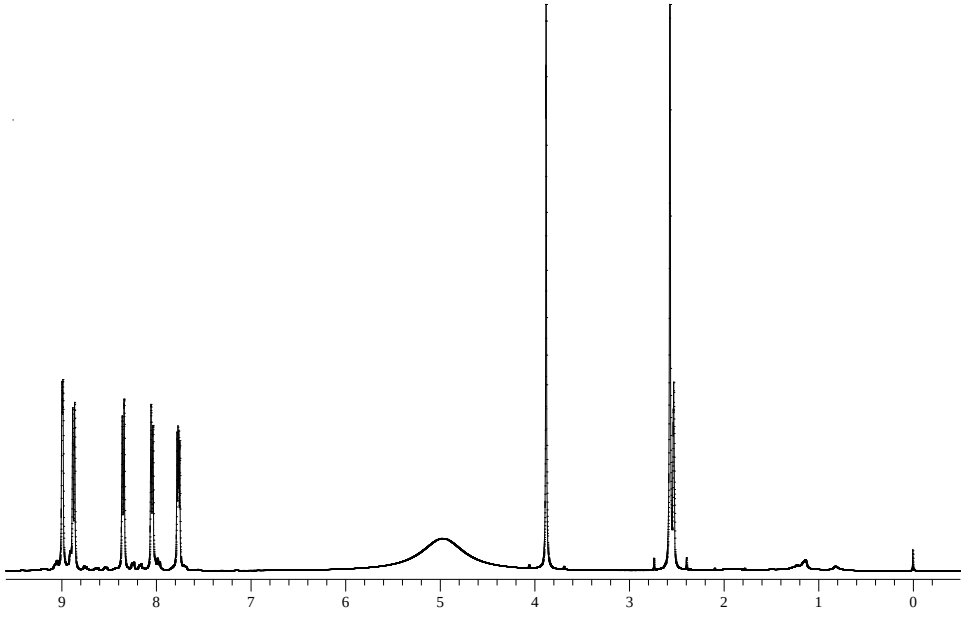

Fig 5. ^{1}H-NMR Spectrum of MBIP ligand.

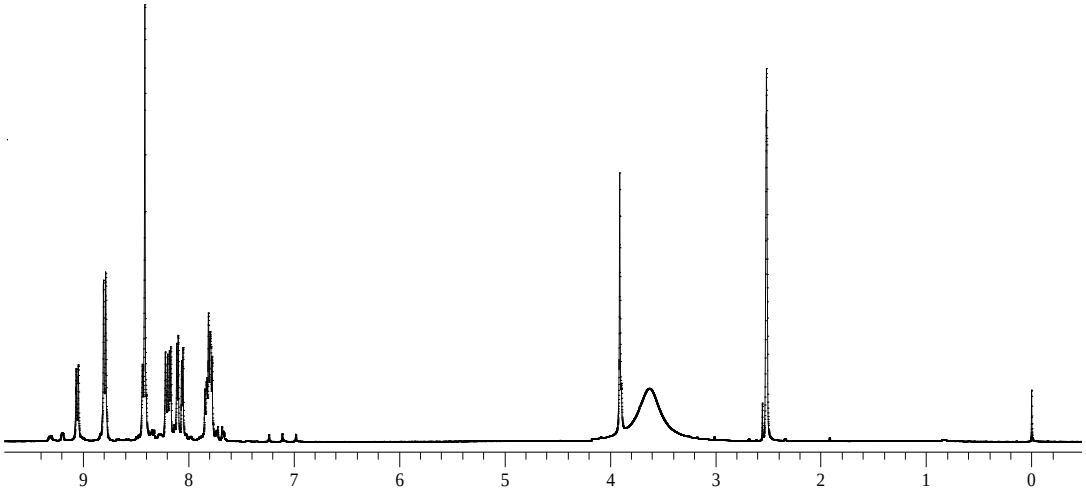

Fig 6. ^{1}H-NMR Spectrum of $[Ru(phen)_2MBIP]^{2+}$ complex.

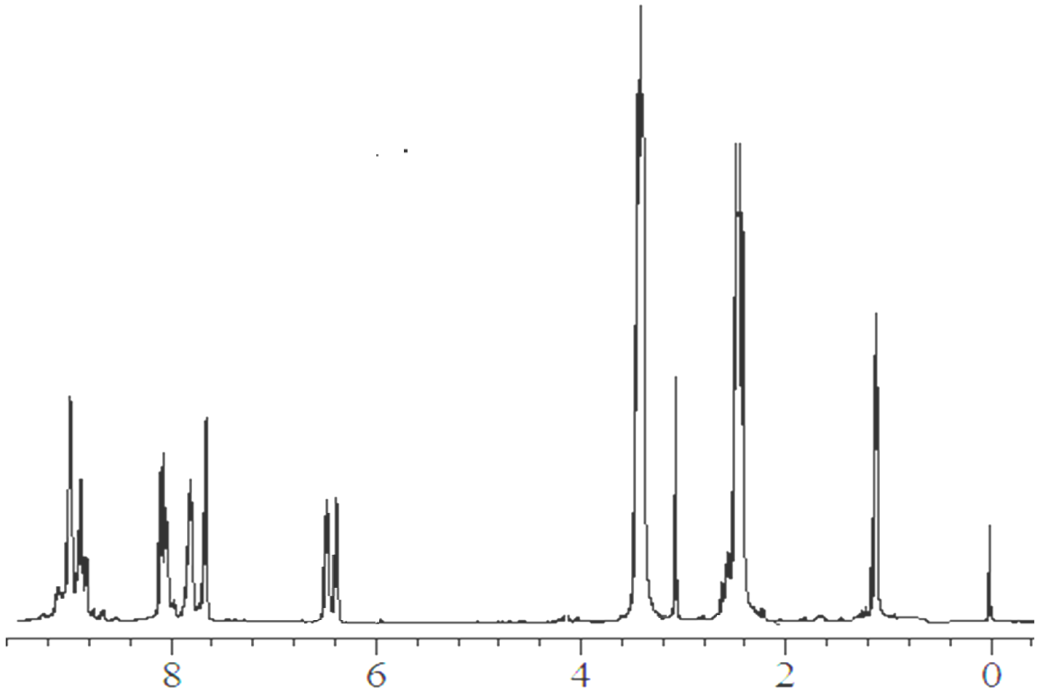

Fig 7. ^{1}H NMR spectrum of DEBIP ligand in dmso-d_6.

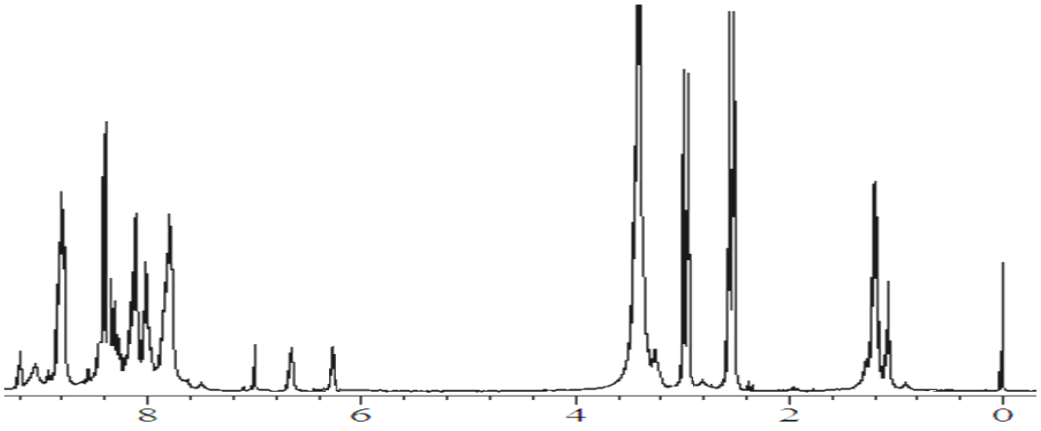

Fig 8. ^{1}H NMR spectrum of $[Ru(bpy)_2DEBIP]^{2+}$ complex in dmso-d_6.

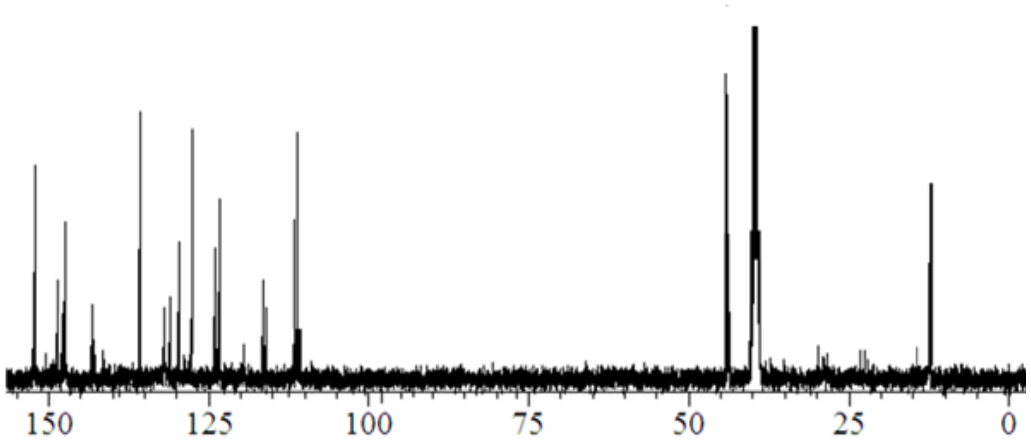

Fig 9. $^{13}C[^{1}H]$ NMR spectrum of DEBIP ligand in dmso-d_6.

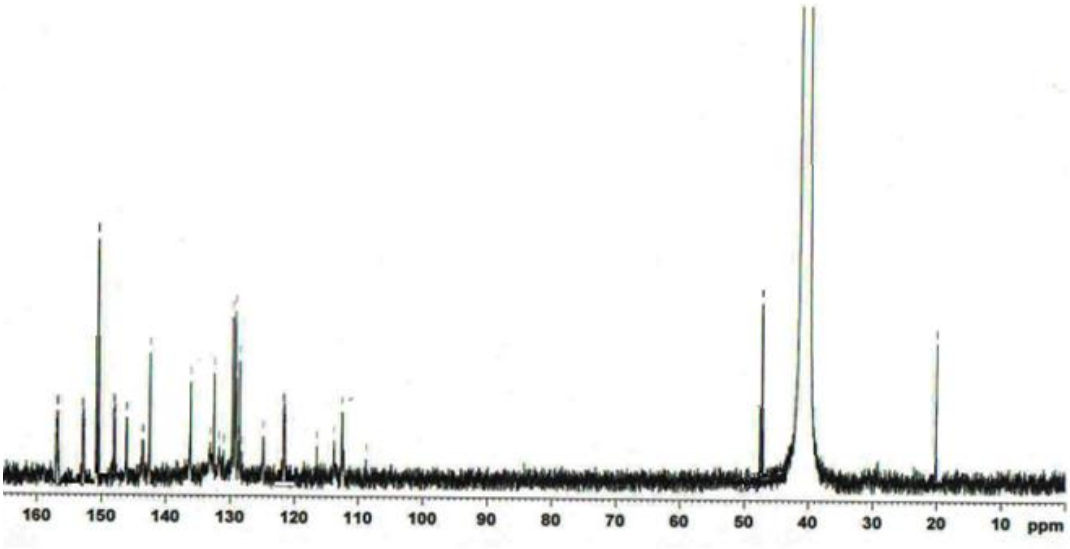

Fig 10. $^{13}C[^{1}H]$ NMR spectrum of $[Ru(phen)_2debip]^{2+}$ complex in dmso-d_6.

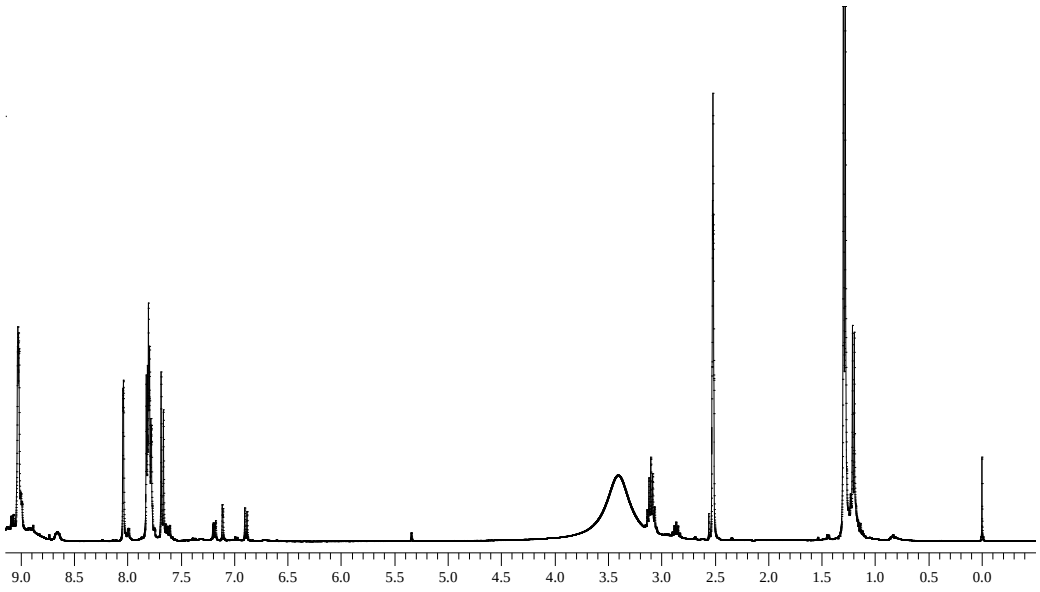

Fig 11. ^{1}H NMR spectrum of IPIPC ligand in dmso-d_6.

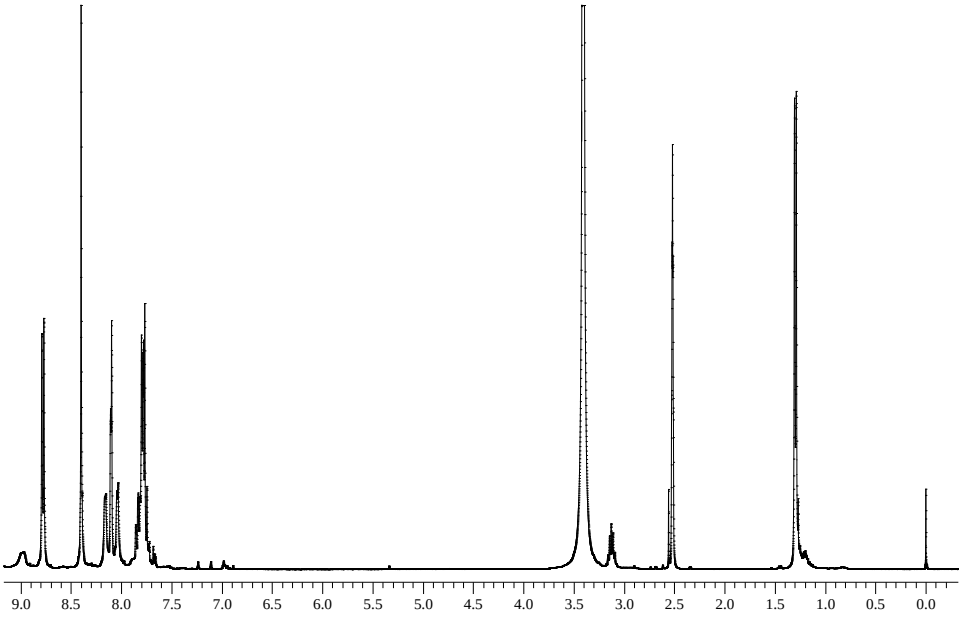

Fig 12. ^{1}H NMR spectrum of $[Ru(phen)_2IPIPC]^{2+}$ complex in dmso-d_6.

3.1.2 Elemental analysis

Elemental analysis provides valuable information regarding for the determination of empirical formulae of the compounds. The ligands and their Ru(II) polypyridyl complexes 1-18 are subjected to elemental analysis and the results of percentage of elements, generally, carbon, hydrogen and nitrogen (C, H and N) with molecular formulae are presented in material and methods. The Analytical data results obtained are in good agreement with those calculated values for the suggested formulae within the limits of experimental errors indicating the purity.

3.1.3 IR spectral studies

The IR spectra provide valuable information regarding the nature of functional group attached to the metal atom. In order to study the binding of the ligand to metal in the

complexes, the IR spectrum of the free ligand was compared with the corresponding metal complexes. The most important IR bands of the ligands and their complexes 1-18 are listed in materials and methods. All synthesized complexes exhibit bands in the region 1568–1528 and 3406–3411 cm^{-1} were assigned to the stretching vibration modes of ν(C=N) and ν(N–H), respectively. Complexes exhibit a band about 3078–3076 cm^{-1}, which is the characteristic absorption of aromatic stretching vibration of ν(C−H). Appearance of the new band in metal complexes around 620-630 cm^{-1}, which is assigned to the metal to nitrogen bond ν(M–N) vibration, and it was absent in free ligand. The IR spectra of the Ru(II) complexes, in comparison with the free ligand, display certain changes, this is confirmed that the formation of coordination bond between the nitrogen atom of polypyridyl ligand and ruthenium metal ion. The IR spectra of the DMPIP, DEBIP, DEPIP ligands and their $[Ru(phen)_2(DMPIP)]^{2+}$, $[Ru(phen)_2DEBIP]^{2+}$ and $[Ru(phen)_2DEPIP]^{2+}$ are given in figures from 13 to 18.

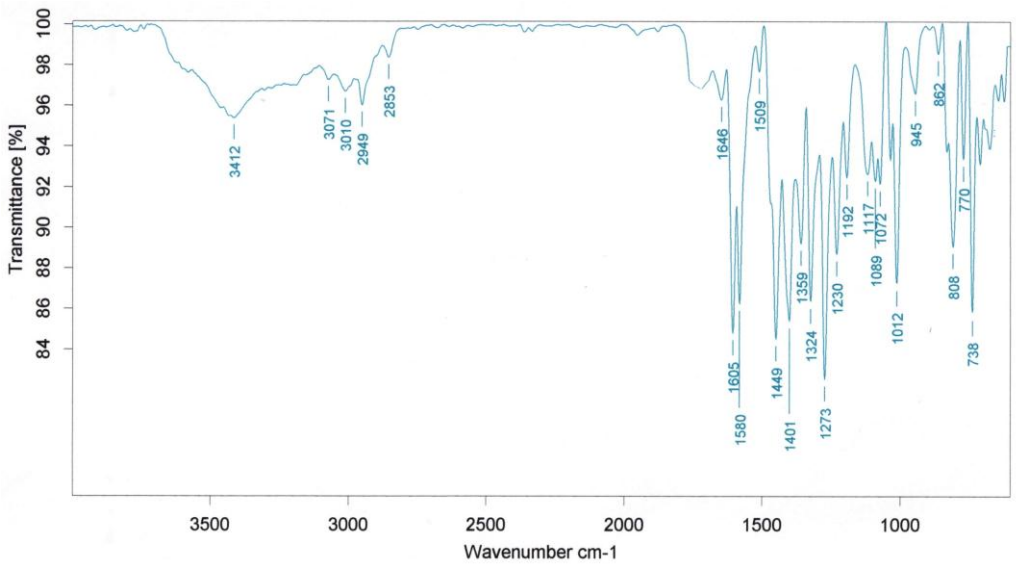

Fig 13. IR Spectrum of ligand DMPIP.

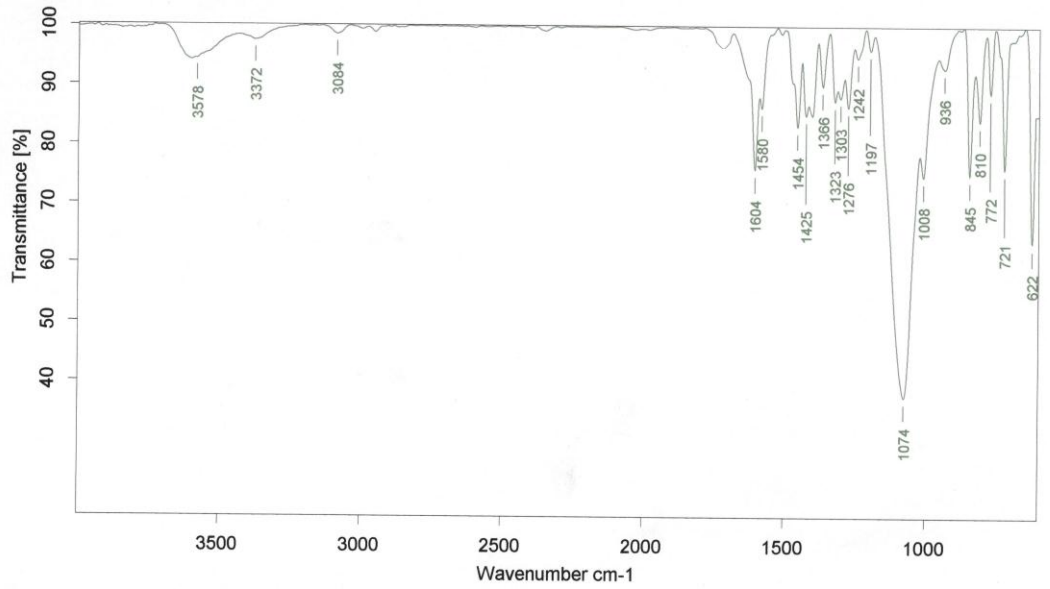

Fig 14. IR Spectrum of $[Ru(phen)_2(DMPIP)]^{2+}$

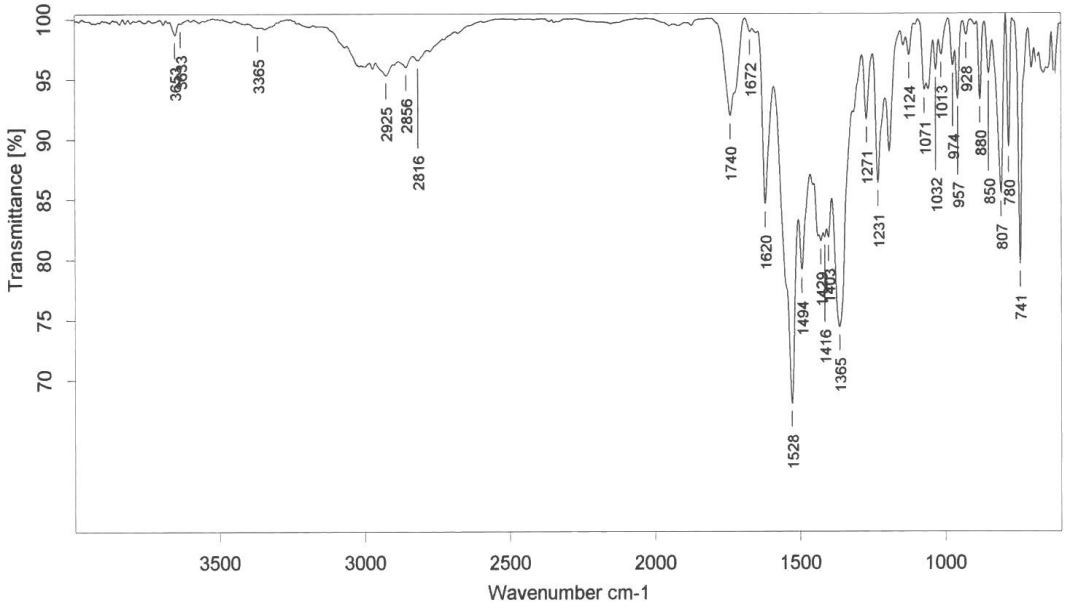

Fig 15. FTIR (KBr, cm^{-1}) spectrum of DEBIP ligand.

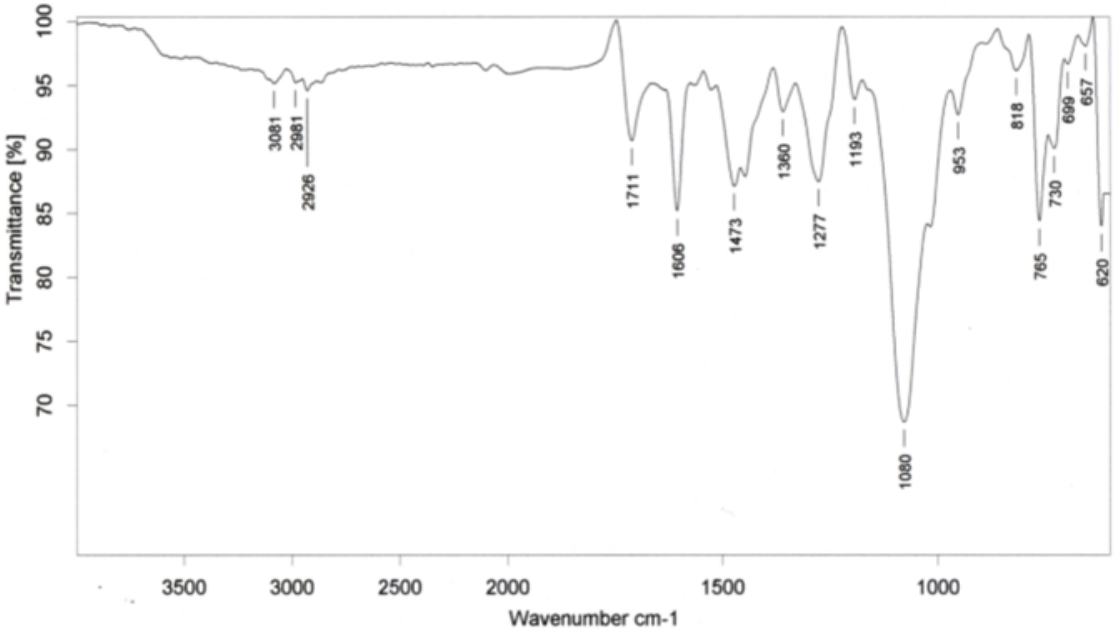

Fig 16. FTIR spectrum of $[Ru(phen)_2DEBIP]^{2+}$ complex.

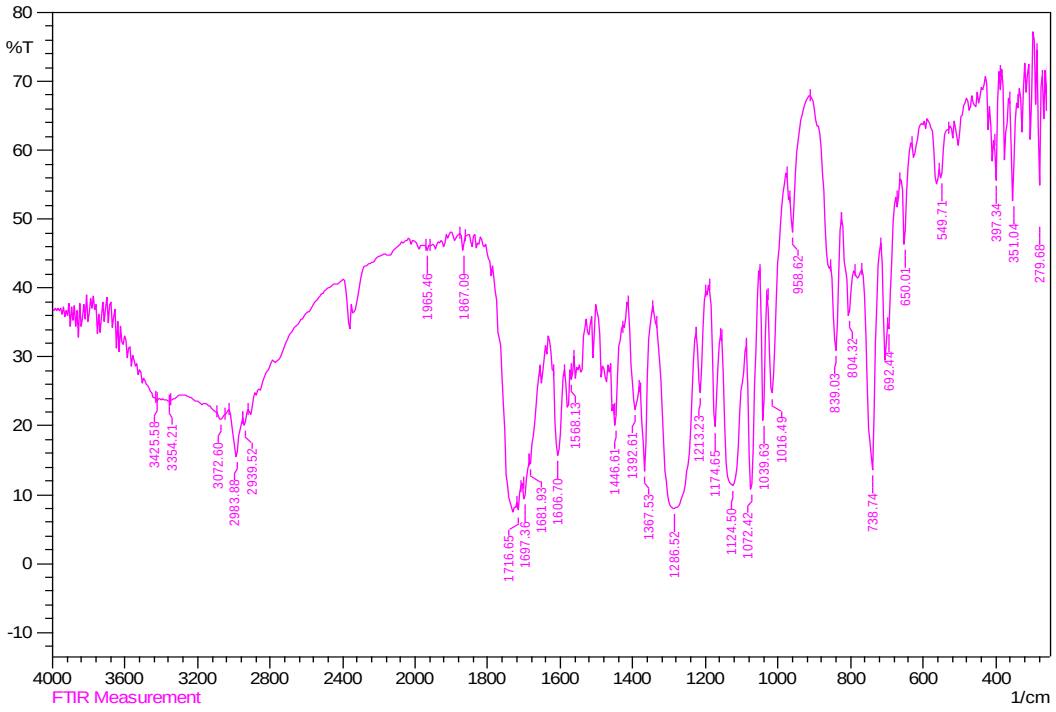

Fig 17. FTIR (KBr, cm^{-1}) spectrum of DEPIP ligand.

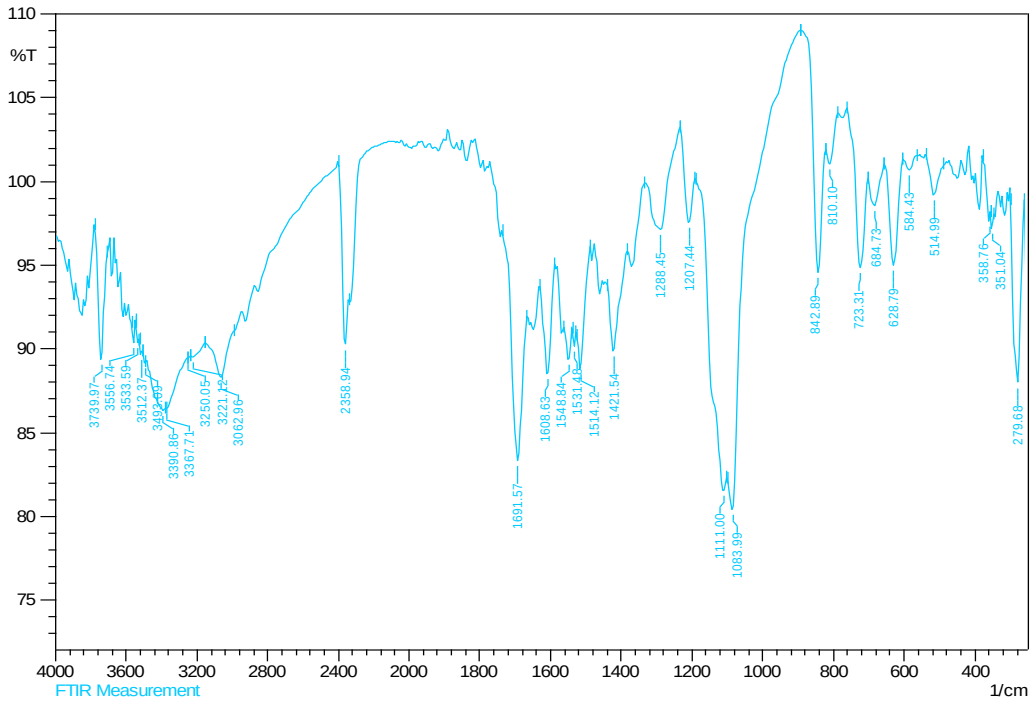

Fig 18. FTIR spectrum of $[Ru(phen)_2DEPIP]^{2+}$ complex.

3.1.5 Mass spectral studies

Mass spectra of the ligands and their synthesized Ru(II) complexes were in good agreement with the expected values and the observed spectral data was depicted in materials and methods. In the mass spectrum of Ru(II) complex, the loss of the $2ClO_4^-$ ions is the dominant ionization process observed and spectrum showed two signals of $[M–2(ClO_4)–H]^+$ and $[M–2(ClO_4)]^{2+}$. It is also supported by the mass spectra of the other complexes, and the determined molecular weights were consistent with corresponding calculated values. The mass spectral data of all synthesized complexes support the structures of mononuclear transition metal complexes. The ESI-MS spectra of free DEBIP, DEPIP ligands and their $[Ru(phen)_2DEBIP]^{2+}$, $[Ru(phen)_2DEPIP]^{2+}$ complex were shown figures from 19 to 22.

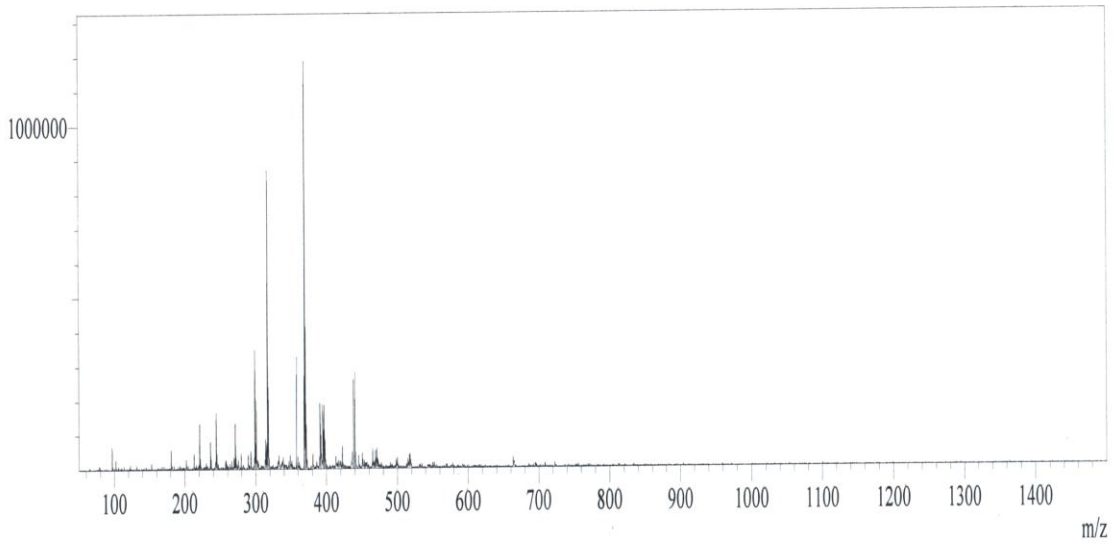

Fig 19. The ESI-MS Spectrum of DEBIP ligand

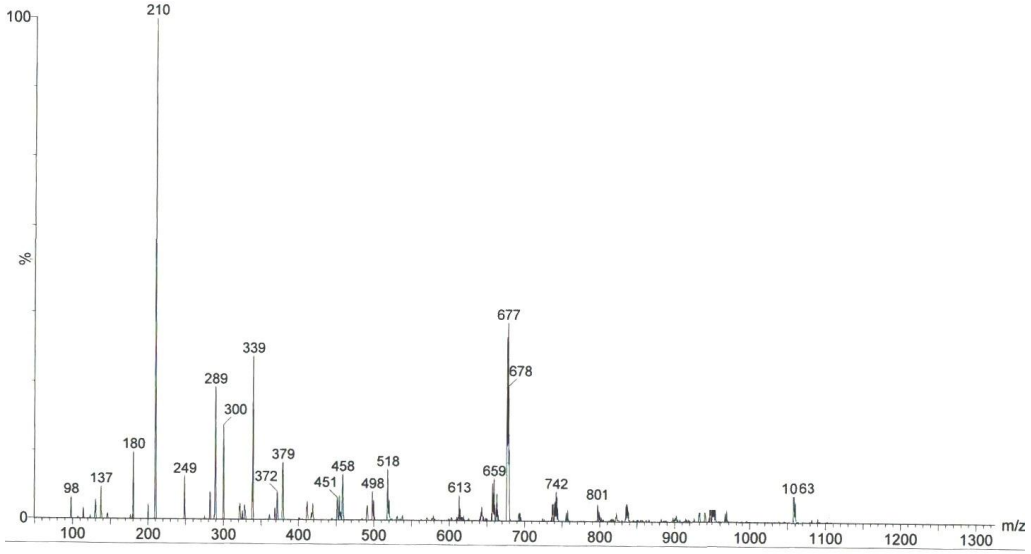

Fig 20. The ESI-MS Spectrum of $[Ru(phen)_2(DEBIP)]^{2+}$

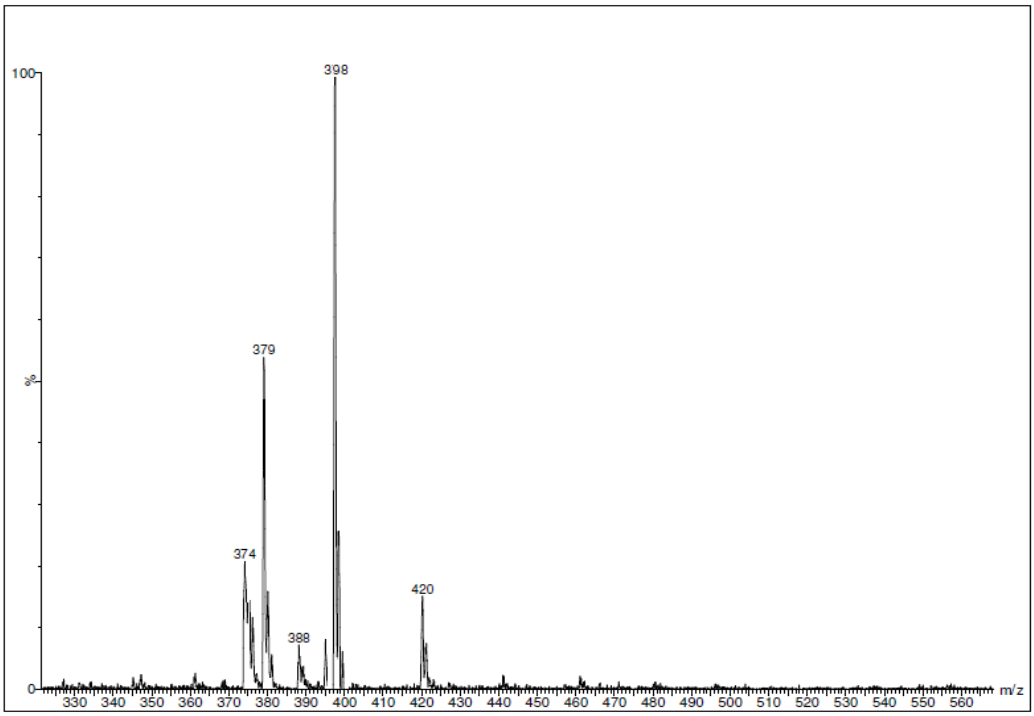

Fig 21. The ESI-MS Spectrum of DEPIP ligand.

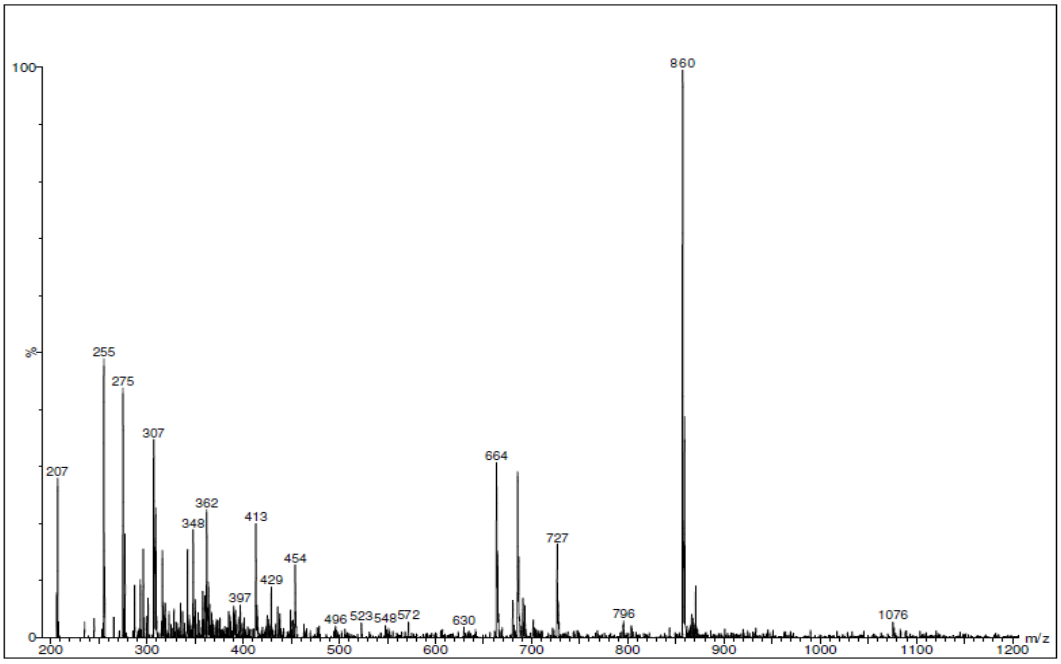

Fig 22. The ESI-MS Spectrum of $[Ru(phen)_2(DEPIP)]^{2+}$

3.2 DNA binding Studies

3.2.1 Absorption titrations

Absorption studies are very important to know the drug-DNA interaction. Complex binding with DNA through intercalation usually results in hypochromism and bathochromism, due to the strong interaction between the aromatic chromophore and the base pairs of DNA. Absorption spectra of Ru(II) complexes shows well resolved bands in the range of 200-600 nm. The bands in UV region are attributed to intra ligand transitions and the lowest energy bands in Visible region at are assigned to the metal–to-ligand charge transfer (MLCT) transitions. The change in the absorbance of the MLCT band with increasing amounts of CT-DNA was used to derive the intrinsic binding constants (K_b). The extent of the hypochromism and red shift is commonly related to the intercalative binding strength. The intrinsic binding constants K_b of complexes indicates that all complexes strongly bind with DNA. The difference in the binding strengths of Ru(II) complexes can be attributed to the difference in steric hindrance and substituent groups of ligands. The intrinsic binding constant K_b for Ru(II) polypyridyl complexes 1–18 tabulated in Table 1. The binding constant K_b of complexes is less than or equal to $[Ru(phen)_2(dppz)]^{2+}$ complex ($>10^6$ M^{-1}). Further studies are needed to elucidate the DNA-binding mode of the complexes. The electronic absorption spectrum of complexes 1-6 shown in Fig 23, complex 7 shown in Fig 24 and complex 11 shown in Fig 25.

Table 1. The UV-Vis absorption binding constants -K_b of all Ru(II) complexes 1–18.

Complex	UV-Vis absorption binding constant K_b (M^{-1})
1	3.3×10^6
2	1.9×10^6
3	1.4×10^6
4	2.5×10^6
5	1.8×10^6
6	1.2×10^6
7	1.9×10^5
8	2.0×10^5
9	3.1×10^5
10	5.0×10^6
11	4.5×10^6
12	4.2×10^6
13	3.0×10^5
14	1.1×10^5
15	1.0×10^5
16	1.0×10^6
17	6.5×10^5
18	5.2×10^5

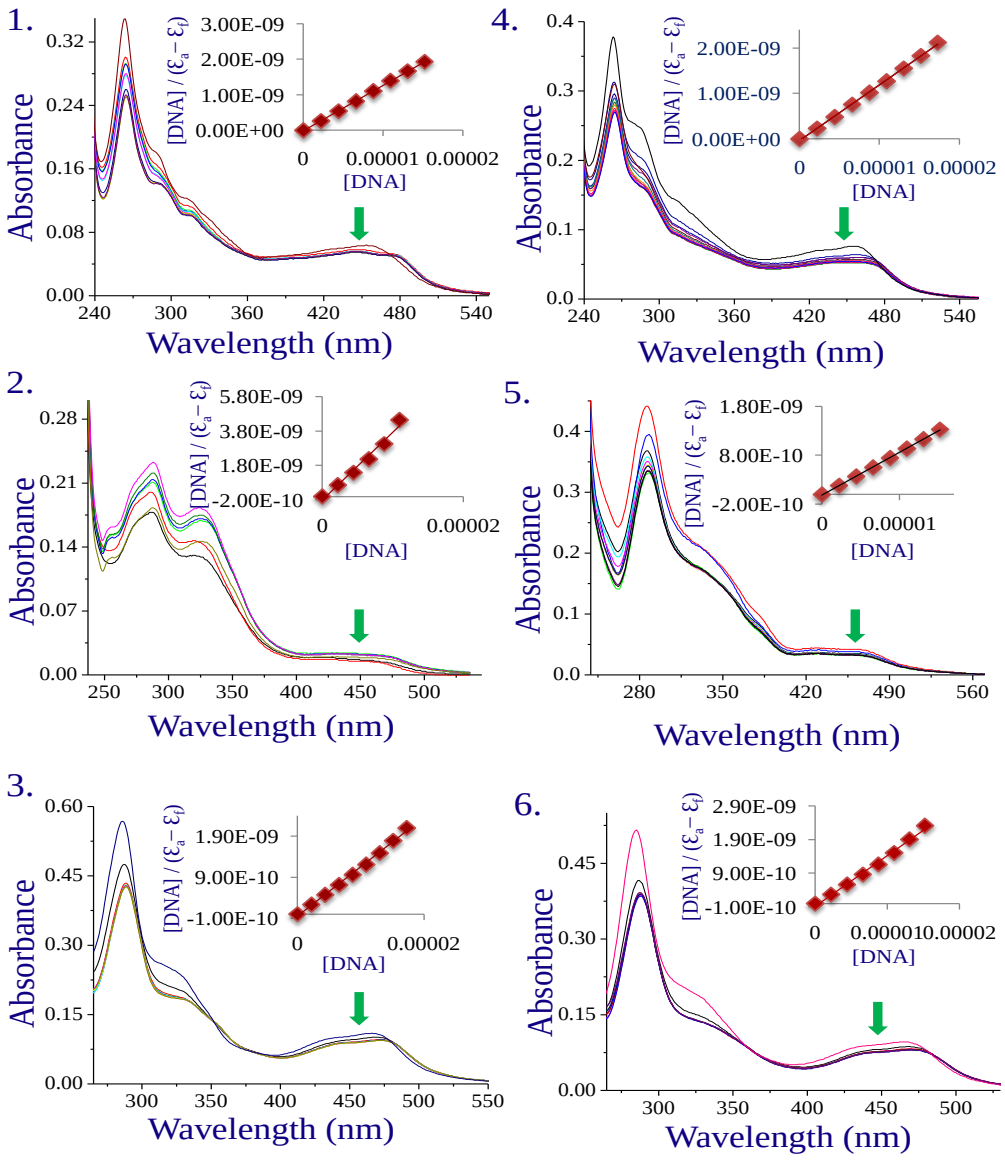

Fig. 23. Absorption spectra of complexes 1-6 in Tris-HCl buffer at 25°C upon addition of CT–DNA, [Ru] = 20 μM, [DNA] = 0–120 μM. The arrow shows the absorbance change upon the increase of CT–DNA concentration. Insert: Plots of [DNA]/(ε_a−ε_f) against [DNA] for the titration of DNA with complex.

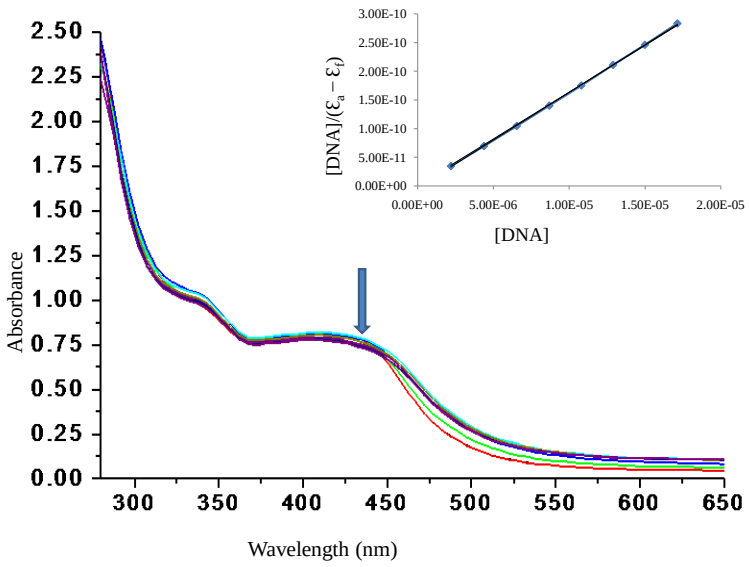

Fig 24. The electronic absorption spectrum of complex 7 in Tris buffer upon addition of CT-DNA. Arrow shows the hypochromism upon increasing CT–DNA concentration. Plots of $[DNA]/(\varepsilon_a - \varepsilon_f)$ vs [DNA] for the titration of DNA with Ru(II) complexes.

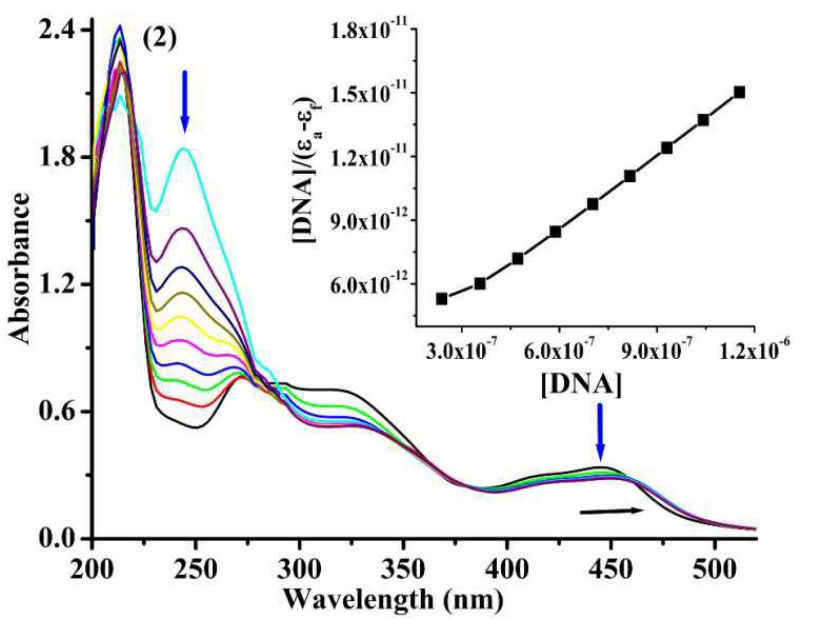

Fig 25. Absorption spectra of complex 11 in Tris-HCl buffer upon addition of CT-DNA. Arrow shows hypochromic and bathochromic shifts with increasing concentration of DNA.

3.2.2 Fluorescence Spectroscopy

Emission spectroscopy is one of the most sensitive ways to analyze metal complex-DNA binding interactions. Upon incremental addition of DNA to each complex, it is observed an enhancement of relative Fluorescence intensity. This enhancement of Fluorescence intensity has confirmed that all complexes are interacting with DNA strongly in between the DNA base pairs and be protected by DNA efficiently. This is due to the hydrophobic environment inside the DNA helix reduces the accessibility of solvent water molecules to the complex and the complex mobility is restricted at the binding site, leading to decrease of the vibrational modes of relaxation and thus higher emission intensity. The calculated binding constants are in the range of 10^6 M^{-1}. These results indicate that the ruthenium complexes exhibit a good binding affinity to CT-DNA. The different DNA-binding affinities of the ruthenium complexes are due to the difference in steric hindrance of the ancillary ligands. The fluorescence binding constant K_b for Ru(II) polypyridyl complexes tabulated in Table 2. The increase in the emission spectra of the complex 1-6 shown in Fig 26, complex 7-9 shown in Fig 27 and complex 11 shown in Fig 28 with increasing CT-DNA concentrations.

3.2.3 Quenching studies

Another common optical method to study the drug-DNA interaction is steady-state emission quenching experiment. This was carried out in Tris –HCl buffer by using a highly negatively anionic quencher potassium ferrocyanide. In this experiments adding varying concentration of quencher solution to the Ru(II) complex solution in presence and absence of DNA. All solutions were allowed to incubate for 5 min before recording the

spectra. Steady state emission quenching experiments of the Ru(II) complexes using $[Fe(CN)_6]^{4-}$ as anionic quencher may provide further information about the differently DNA-bound Ru(II) complexes they do not indicate the binding modes. In the absence of DNA, quenching of the fluorescence intensity of the Ru(II) complex by quencher is strong, whereas in the presence of DNA quenching is weak. This may be explained by repulsion of the highly negative $[Fe(CN)_6]^{4-}$ from the DNA polyanion backbone which hinders access of $[Fe(CN)_6]^{4-}$ to the DNA-bound complexes. The K_{sv} values of all complexes 1–18 are depicted in Table 3. The slope can therefore be taken as a measure of binding affinity. The stern-volmer plots of complex 1 shown in Fig 29, complex 7-9 shown in Fig 30 and complex 10-12 shown in Fig 31.

3.2.4 DNA light–switch *on* and *off* Studies

The DNA molecular "light-switch" studies of Ru(II) complexes were performed in Tris buffer solution by successive addition of Co^{2+} and EDTA to DNA bound complex. Our complexes are exhibiting weak luminescence in the absence of DNA and strong luminescence upon addition of DNA (light switch *on*) in tris buffer. The emission of the complex bound to DNA can be quenched by addition of Co^{2+}, thus turning the light switch off after that the emission can be recovered (light switch *on*) by the addition of EDTA due to the formation of Co^{2+}–EDTA complex. The addition of Co^{2+} (0.03mM) to the complex **1** (0.01mM) bound to DNA (0.2mM) results in loss of luminescence due to the formation of a hetero metallic complex $[Ru(phen)_2(DMPIP)]^{2+}/Co^{2+}$. On adding EDTA to the buffer system containing $[Ru(Phen)_2(DMPIP)]^{2+}/Co^{2+}$ the emission intensity of the complex is recovered again (light switch on) as shown in Fig 32 (complex-1) and 33 (complex-7). This indicates

that the hetero metallic complex becomes free again due to the formation of the Co^{2+}–EDTA complex. Similar emission changes (light switch *on* and *off*) were observed for all complexes under the same conditions. It is worthwhile to note that the DNA light-switch behaviors of transition metal complexes have been identified as a characteristic of the DNA intercalators and regarded as confirmation of DNA intercalation.

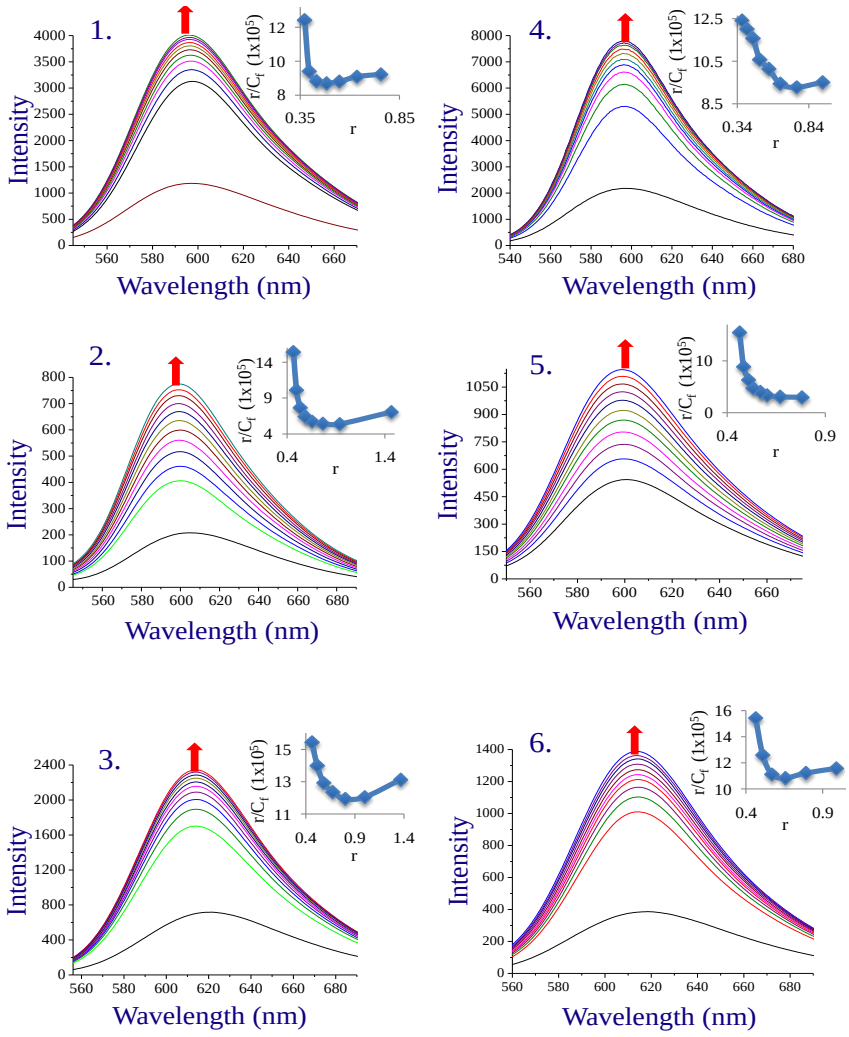

Fig 26. Fluorescence spectra of complexes 1-6 in Tris–HCl buffer at 25°C upon addition of CT–DNA, [Ru] = 10 μM, [DNA] = 0–120 μM. The arrow shows the increase in intensity upon increasing CT–DNA concentrations.

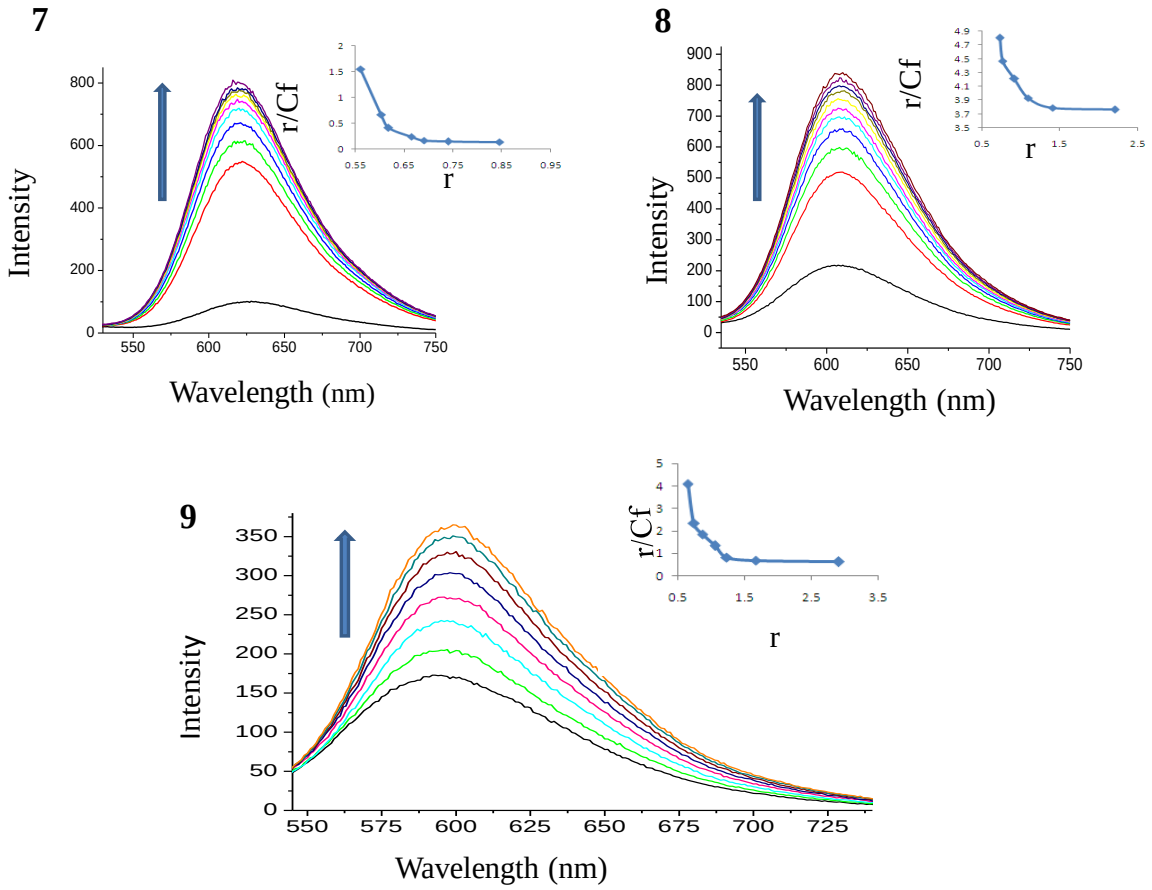

Fig 27. The fluorescence spectra of complexes $[Ru(phen)_2debip]^{2+}$ (**7**), $[Ru(bpy)_2debip]^{2+}$ (**8**) and $[Ru(dmb)_2debip]^{2+}$ (9) with addition of CT–DNA, in Tris buffer with increasing concentration of CT-DNA. The arrow shows the fluorescence intensity change upon increase of DNA concentration. Inset: Scatchard plot of r/C_f vs r.

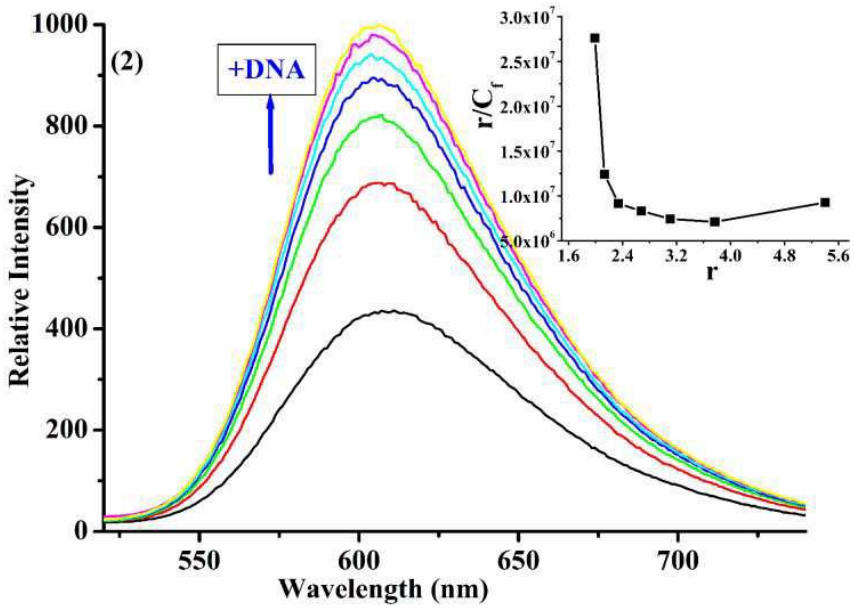

Fig 28. Fluorescence spectra of complex 11 in Tris–HCl buffer upon addition of CT-DNA. Arrow shows the intensity change upon the increase of DNA concentration.

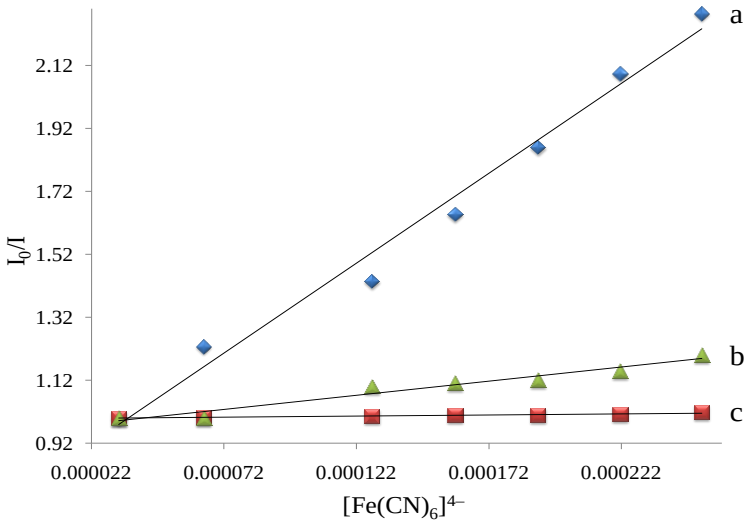

Fig 29. The fluorescence quenching of complex-1 with increasing concentration of $[Fe(CN)_6]^{4-}$. In figure, (a) complex alone, (b) 1:10 and (c) 1:100 ratios of complex and DNA.

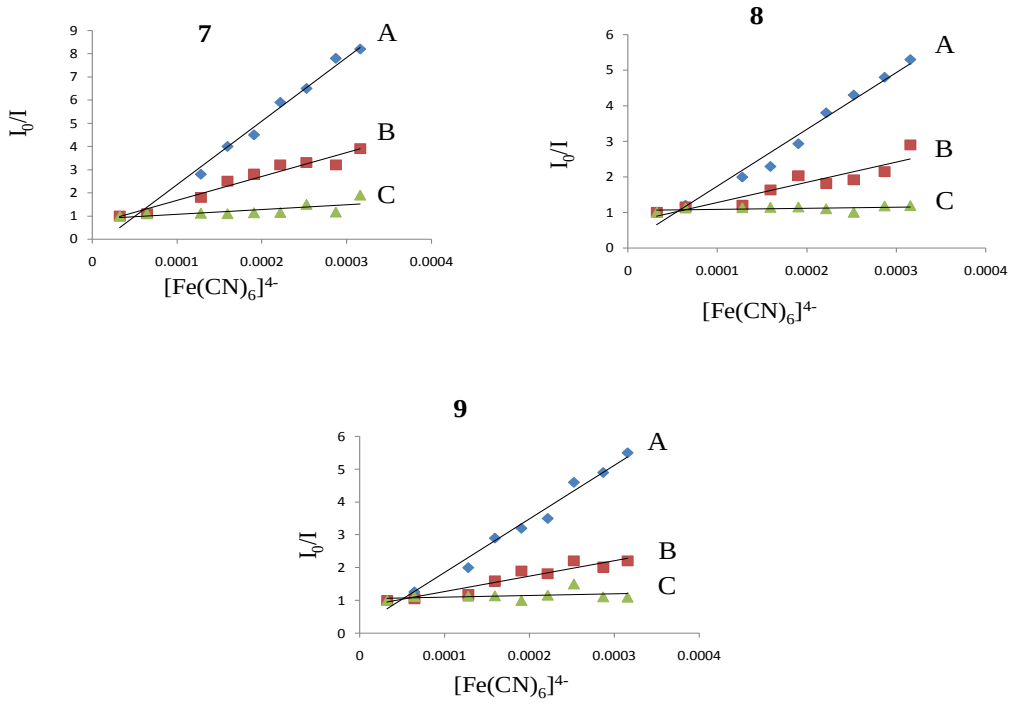

Fig 30. Emission quenching of complexes 7, 8 and 9 with $[Fe(CN)_6]^{4-}$ in the absence of DNA (A), presence of DNA 1:30 (B) and 1:200 (C). [Ru] =10 μM, $[Fe(CN)_6]^{4-}$ = 0.1 M.

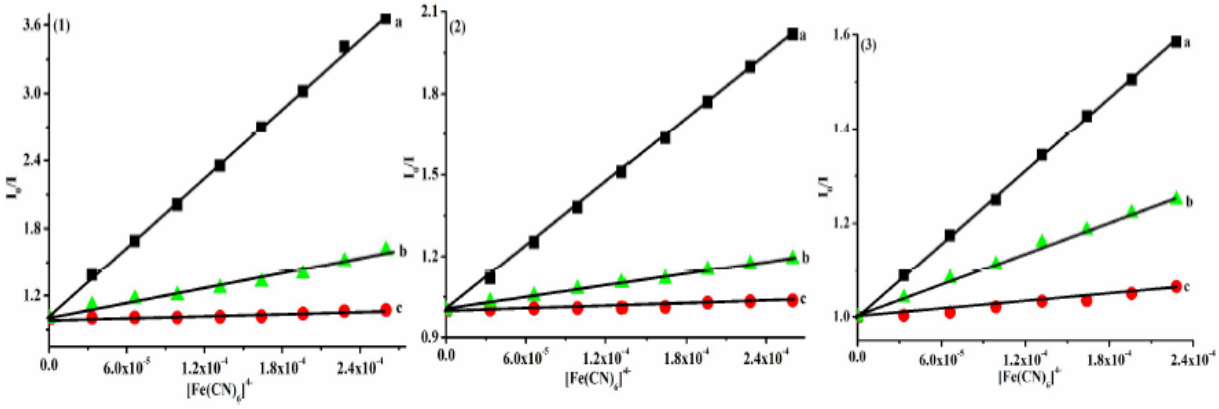

Fig 31. Emission quenching of complexes 10 (1), 11 (2) and 12 (3) with $[Fe(CN)_6]^{4-}$ in the absence of DNA (a), presence of DNA 1:20 (b) and 1:200 (c).

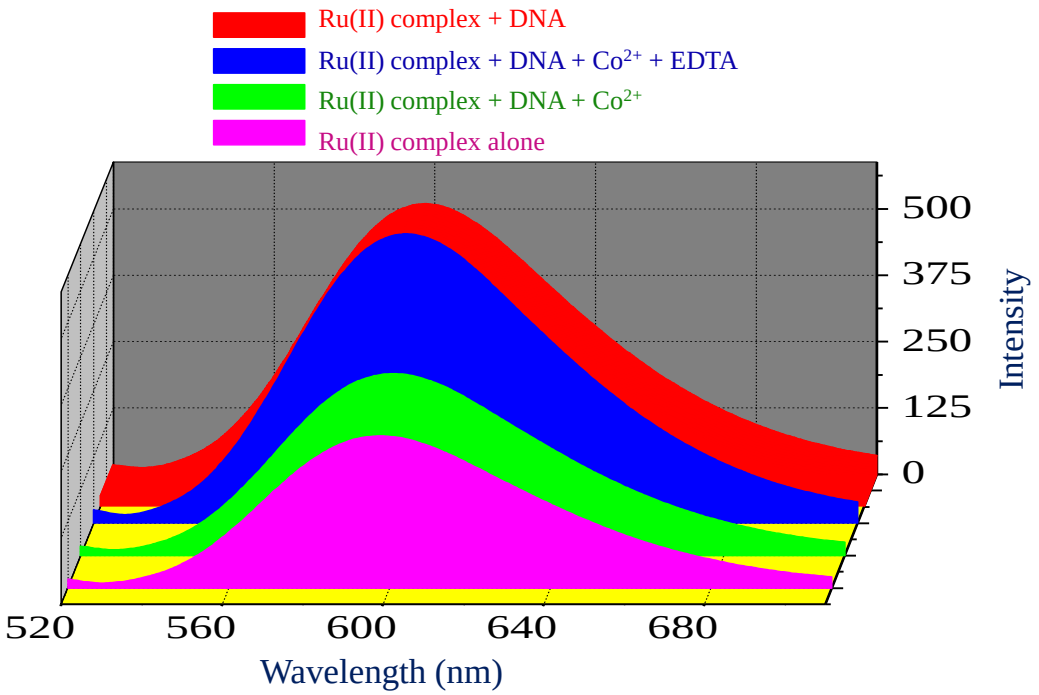

Fig 32. The DNA molecular light switch *on* and *off* effect of complex-1 showing the change in intensity upon addition of Co^{2+} and EDTA to complex + DNA.

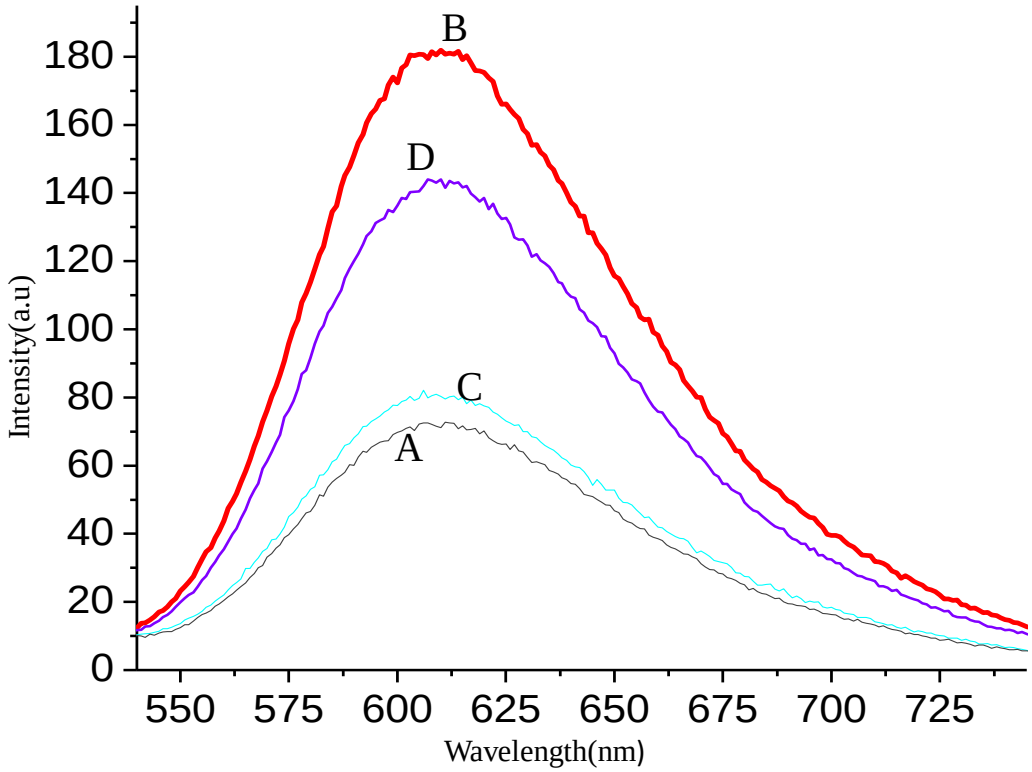

Fig 33. DNA light switch *on* and *off* experiment of complex 7 showing the emission changes where A is emission of complex alone, B is emission of complex with DNA, C is upon addition of Co^{2+} to B (Switch *off*) and D is upon addition of EDTA to C (Switch *on*).

Table 2. The fluorescence binding constants of all Ru(II) complexes 1–18.

Complex	Fluorescence binding constant K_b (M^{-1})
1	2.9×10^6
2	1.8×10^6
3	1.4×10^6
4	2.4×10^6
5	1.6×10^6
6	1.1×10^6
7	3.1×10^5
8	2.0×10^5
9	1.9×10^5
10	6.0×10^6
11	5.0×10^6
12	4.0×10^6
13	1.1×10^6
14	7.5×10^5
15	6.3×10^5
16	2.0×10^6
17	1.5×10^6
18	1.0×10^6

Table 3. The quenching constant $K_{sv}(M^{-1})$ values for complexes 1–18.

Compound	Complex alone K_{sv}	Complex : DNA (1:100) K_{sv}	Complex : DNA (1:200) K_{sv}
1	3571	1514	483
2	2943	1890	1265
3	2689	2282	1341
4	3403	1847	670
5	3015	1850	900
6	2890	2085	780
7	1305	148	34
8	1502	287	88
9	1604	348	98
10	8738	1231	760
11	4071	1419	997
12	2528	1670	1181
13	1583	914	674
14	2911	1351	1093
15	3601	1732	1170
16	3219	2100	924
17	2730	1502	1352
18	3510	1830	1420

3.2.5 Viscosity experiments

Viscosity measurements will give further clarification about mode of interaction between the ruthenium complex and CT–DNA. Optical techniques are widely used to study the binding model for combinations of the ligand, metal complexes and DNA, but give not always sufficient clues to support a binding model. As the concentration of the complexes increases, the relative viscosity of DNA increases, further suggesting that the complexes bind to DNA through an intercalation mode and the difference in the binding strength may be caused by the different ancillary ligands. The increased viscosity, which may depend on the DNA-binding mode and affinity. Fig 34 shows the extent of increase in viscosity, which may depend on the DNA binding affinity, follows the order of EtBr>1>4>2>5>3>6. The effect of increasing amount complexes 7-9 shown in Fig 35 and complexes 10-12 shown in Fig 36 on relative viscosity of CT-DNA.

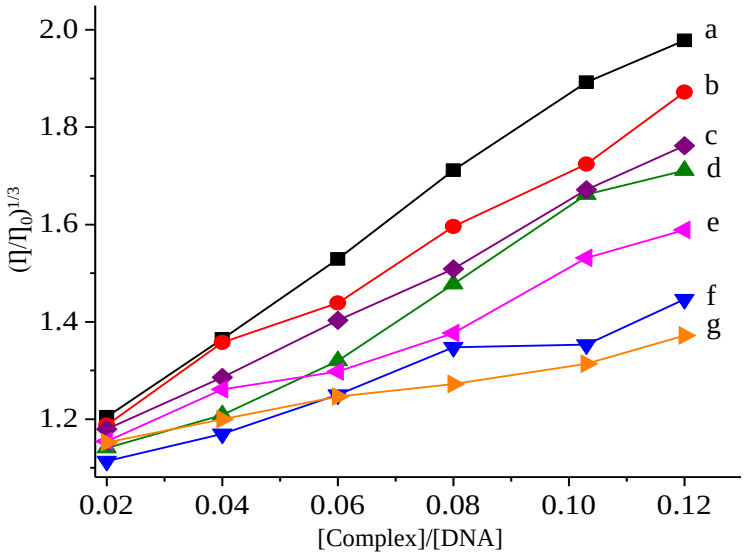

Fig 34. The effect of ethidium bromide (a), complex 1 (b), complex 4 (c), complex 2 (d), complex 5 (e), complex 3 (f) and complex 6 (g) on relative viscosity of CT-DNA.

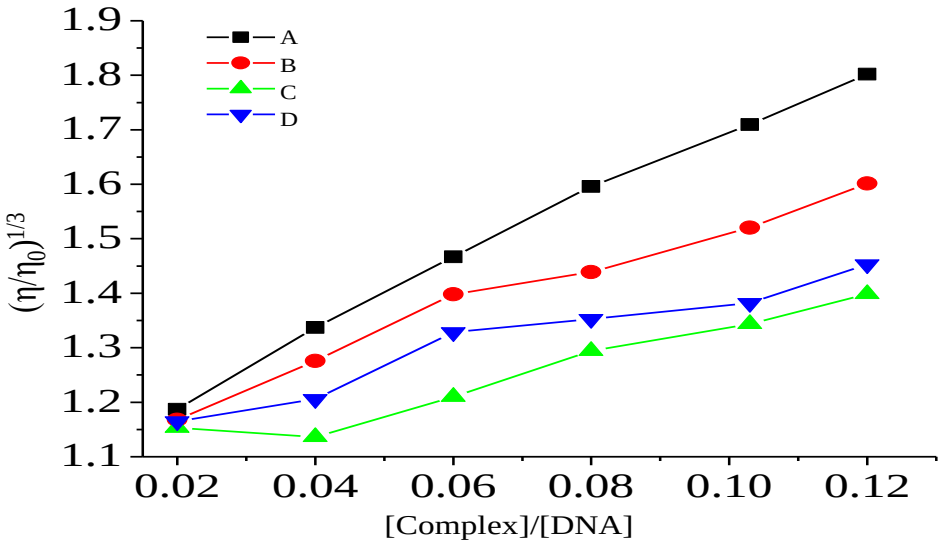

Fig 35. Effect of increasing amount of Ethidium bromide (A), complex 7 (B), complex 8 (C) and complex 9 (D) on relative viscosity of CT-DNA at 30 ± 0.1 ºC.

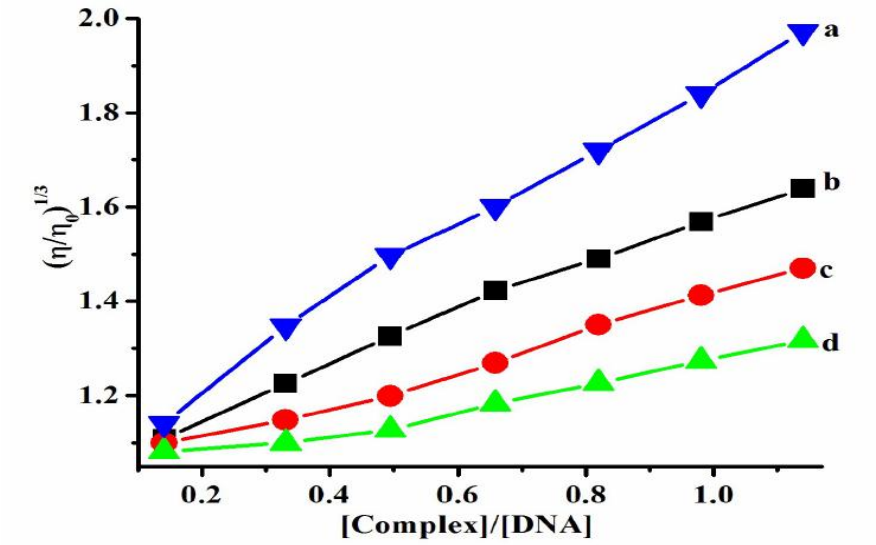

Fig 36. Effect of increasing amounts of Ethidium bromide (EtBr) (a), complex 10 (b), complex 11 (c) and complex 12 (d) on the relative viscosity of calf thymus DNA at $30(\pm 0.1)^0$C.

3.3 Photo activated DNA cleavage studies

The ability of the Ru(II) polypyridyl complexes 1-18 to cleave DNA upon irradiation was determined by gel electrophoresis under physiological conditions with supercoiled pBR322 DNA. No DNA cleavage was observed for control in which complex was absent. With the increasing concentration of complexes the amount of form I is decreased whereas that of form II is increased. The cleavage effect was found to be concentration dependent. All complexes exhibit efficient DNA photo cleavage activity. Fig 37(a, b) shows gel electrophoresis separation of pBR322 DNA after incubation with each of Ru(II) complexes 1-6. Fig 38 (i) shows gel electrophoresis separation of pBR322 DNA with each of Ru(II) complexes 7-9. Fig 39 shows gel electrophoresis separation of pBR322 DNA with each of Ru(II) complexes 10-12. Further, we investigated the DNA photocleavage of the Ru(II) complexes in the presence of singlet oxygen ($^1O_2$) scavenger (Histidine), hydroxyl radical ($OH^{\cdot}$) scavenger (Mannitol and DMSO) and superoxide anion radical (O^{2-}) quencher (SOD) to know about photocleavage mechanism process. The results indicates that, In the presence of Histidine the photocleavage of pBR322 DNA was absent or very less compared to complex with DNA (absence of Histidine), but the cleavage was observed in the presence of Mannitol, DMSO and SOD. The photocleavage of the Ru(II) complex 1 Fig 37(c) and complex 7 Fig 38(ii) in the presence of scavengers. This is suggesting that the singlet oxygen is responsible for the cleavage of pBR322 DNA.

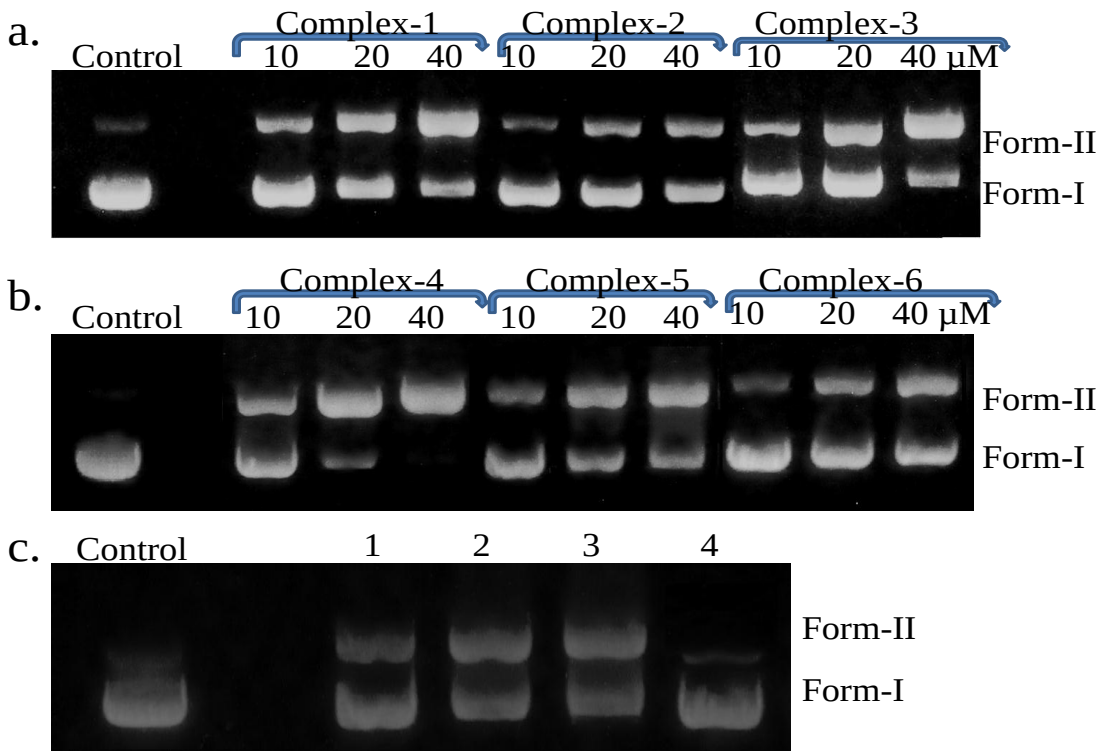

Fig 37. The effect of synthesized complexes 1-3 (**a**) and 4-6 (**b**) with different concentrations (10, 20 and 40µM) on cleavage of pBR322 DNA after irradiation at 365nm for 30 min. **(c)** Photocleavage of pBR322 DNA experiments in the presence of various reactive oxygen species inhibitors, lane-1(Mannitol+complex-1), lane-2(DMSO+complex-1), lane-3(SOD+complex-1) and lane-4(Histidine+complex-1).

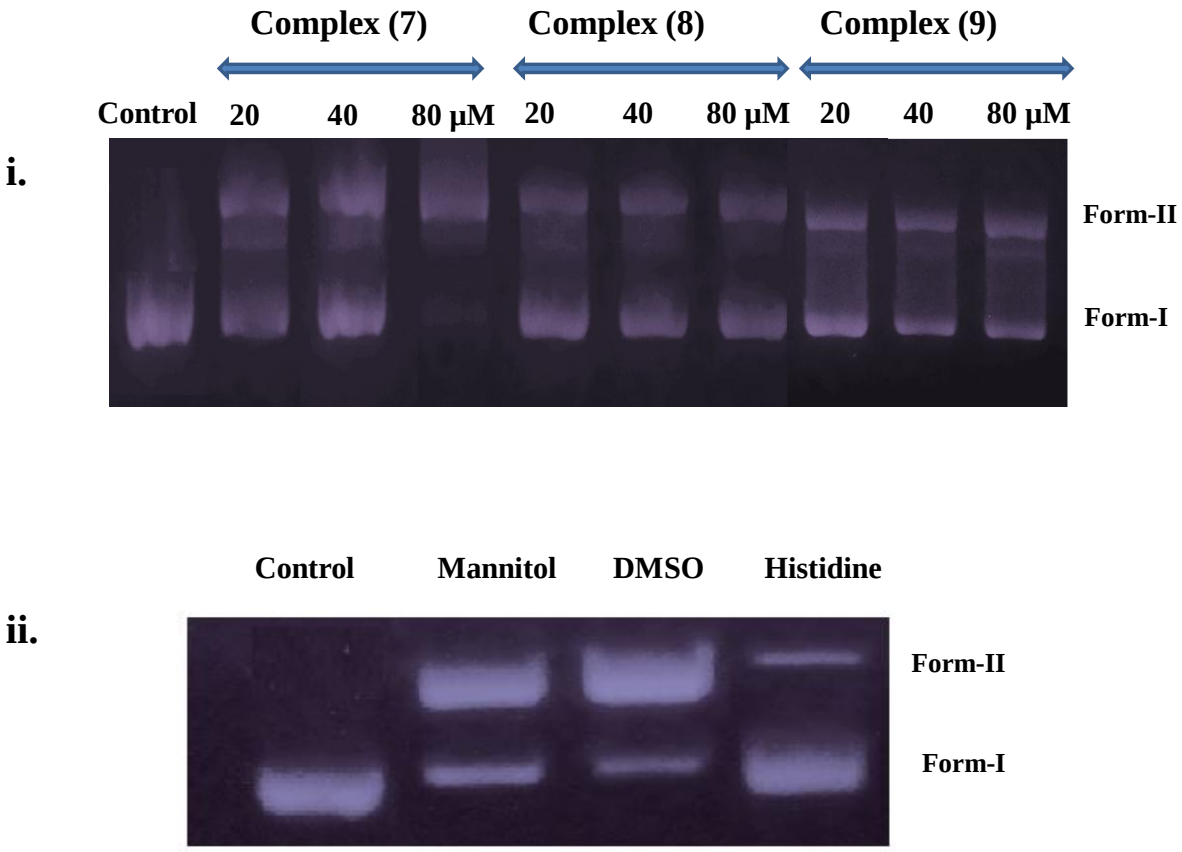

Fig 38. i). Photoactivated cleavage of pBR322 DNA in the absence (Control) and presence of different concentrations (20, 40 and 80µM) of complexes **7**, **8** and **9** after irradiation at 365 nm for 30 min. **ii)**. Photoactivated cleavage of pBR322 DNA in the presence of complex **7** and scavengers (10 µM) after irradiation at 365 nm for 30 min.

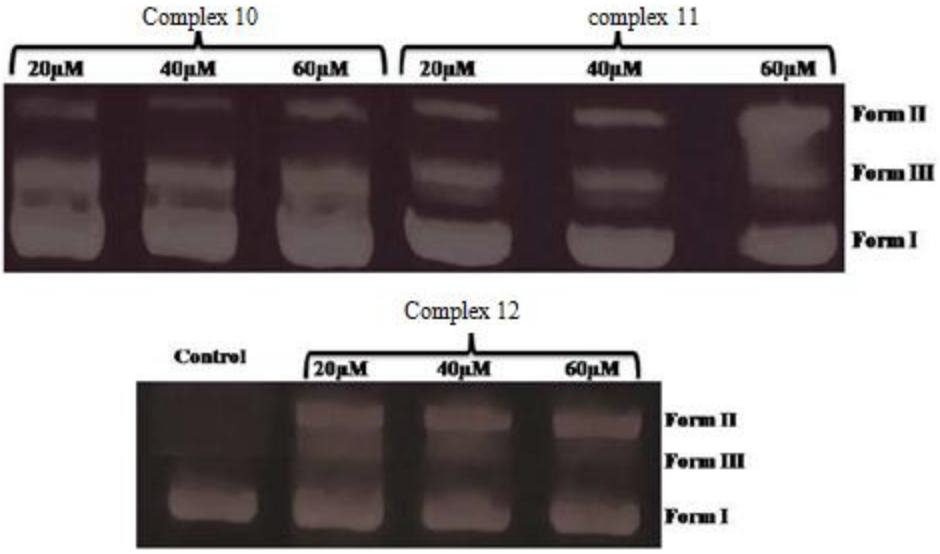

Fig 39. Agarose gel electrophoresis of pBR322 DNA in absence and in the presence of complexes 10, 11 and 12 at different concentrations (20, 40 and 60 µM).

3.4 Antibacterial Activity

In vitro antibacterial activity of the ligands and their Ru(II) complexes were performed on Gram-negative and Gram-positive bacteria's as model organisms by the paper disc method using nutrient agar medium. The results were also compared with the results for the standard antibacterial drug ampicillin at the same concentrations. DMSO control showed a negligible activity as compared with the metal complexes. The experimental results of the compounds were compared against DMSO as the control and are expressed as inhibition zone diameter (in mm). From the results obtained, it has been found that both the ruthenium complexes exhibit good antibacterial activity but greater than that of the corresponding free ligand. The antimicrobial activity increased as the concentration of the complex increased.

The zone of inhibition values of all complexes was comparable with standard compound ampicillin as shown in Table 4.

Table 4. Antimicrobial activity of ligands and their complexes 1-18, and the zones of inhibition were measured in mm.

complex	E. coli	S. Aereus	B. subtilis	M. luteus	B. megatherium
1	10	12	8	10	11
2	9	11	8	13	10
3	10	14	11	14	13
4	15	16	9	16	15
5	7	10	7	12	10
6	8	13	12	14	14
7	12	14	11	13	12
8	11	10	10	12	10
9	12	13	12	12	13
10	13	13	12	14	12
11	11	12	10	11	11
12	14	13	13	14	13
13	13	15	13	12	11
14	10	11	10	10	09
15	12	13	10	13	12
16	11	12	14	12	13
17	10	11	11	09	10
18	13	13	13	11	12
Ampicillin	21	22	24	26	28
DMSO	0	0	0	0	0

3.5 *In Vitro* Cytotoxicity Assay

The *in vitro* cytotoxicity of Ru(II) complexes was assessed using MTT reduction method and in this study cisplatin was used as a positive control. The cytotoxicity of the complexes tested in this work can also be compared by means of the IC_{50} values. The corresponding IC_{50} values of the complexes 1–18 against HeLa cell lines were calculated by plotting the percentage of cell viability against the concentration of the complexes and are depicted in Table 5. The IC_{50} values of all complexes were lower than cisplatin, which indicates that the complexes 1–18 exhibited lower cytotoxicity than cisplatin under identical conditions. The cytotoxicity of complexes was found to be concentration dependent. The cytotoxicity of the Ru(II) complex is higher than that of the free ligand, which can be explained by the fact that the hydrophobicity of the complex is greater than that of the ligand. IC_{50} values for the free ligands were obtained greater than 200μM. The results indicated that the complexes with planar aromatic polypyridyl rings appeared to have more cytotoxicity. The antitumor activity of the complex may be related to the specific molecular shape of the complex and the chemical structure and nature of the ligand. Fig 40 showed that the cell viability of HeLa cell lines decreases with increase in concentration of Ru(II) complexes 1–6. Cell viability of HeLa cell lines in vitro treatment with complexes 7, 8 and 9 are shown in Fig 41 and complexes 10, 11 and 12 are shown in Fig 42.

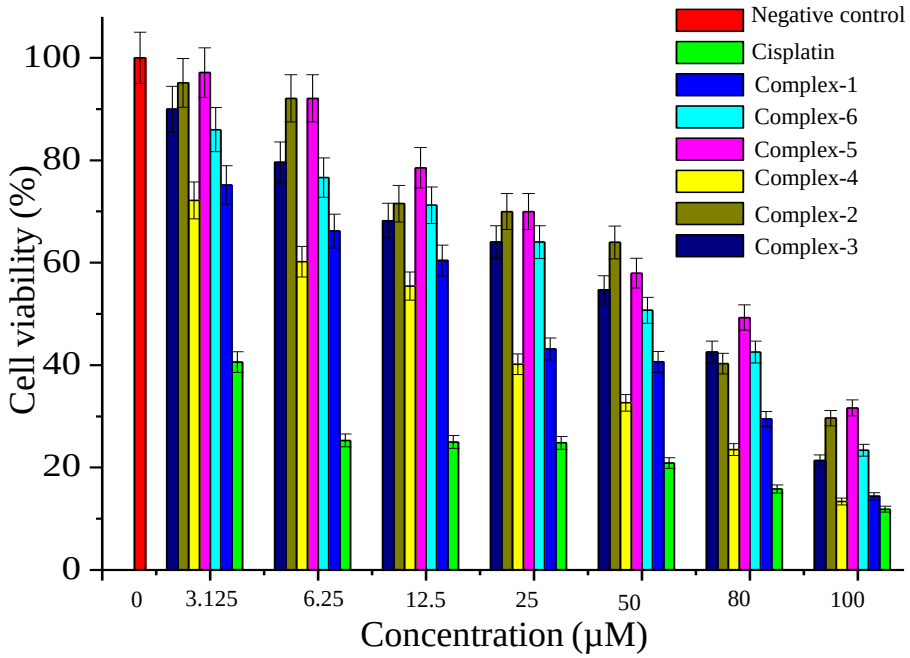

Fig 40. Cell viability of Hela cell lines in vitro treatment with cisplatin (positive control) and ruthenium complexes **1-6**. Each data point is the mean±standard error obtained from at least three independent experiments. Negative control (untreated cells) considered as 100% of viable cells.

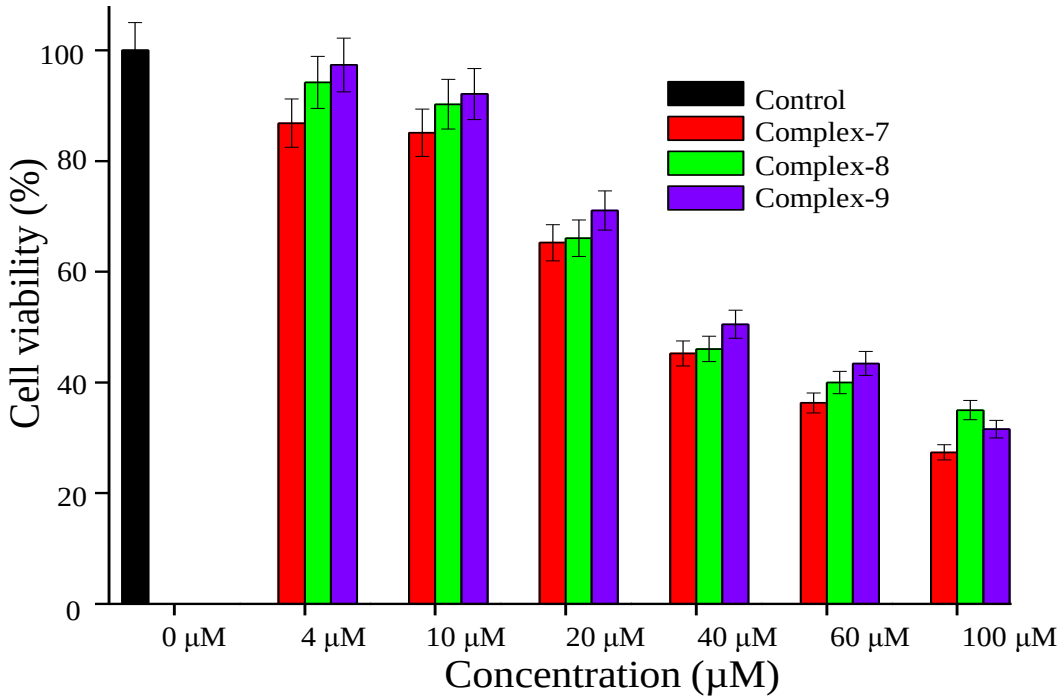

Fig 41. Cell viability of HeLa cell lines in vitro treatment with complexes **7**, **8** and **9**.

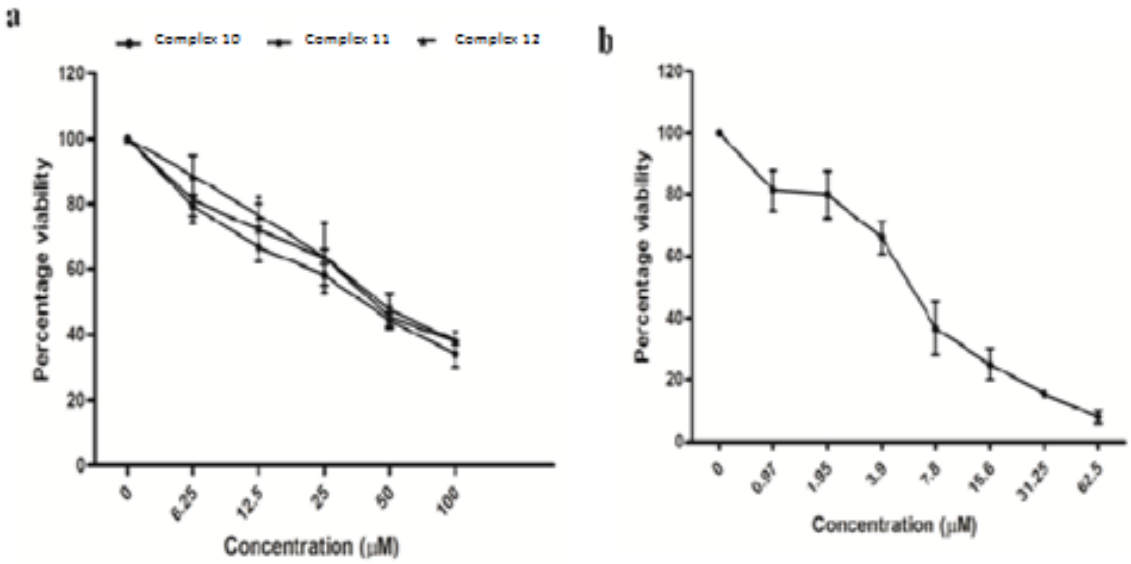

Fig 42. a) HeLa cells were treated with complexes 10, 11 and 12 with different concentrations for 48h and untreated cells were used as control and then cell viability was evaluated by MTT assay. b) Cisplatin was used as positive control.

Table 5. Cytotoxic effects of Ruthenium polypyridyl complexes 1-18 on HeLa cell lines.

Complexes	**IC_{50} (μM)**
1	45.8
2	68.2
3	65.3
4	35.6
5	62.1
6	58.9
7	45.7
8	48.2
9	57.1
10	39.0
11	44.3
12	49.0
13	52.5
14	63.0
15	59.8
16	42.6
17	46.1
18	39.9
Cisplatin	09.32

3.6 Lipophilicity Assay

Log $P_{o/w}$ is the partition coefficient between octanol and water which is determined using the flask-shaking method. UV–visible calibration curve was prepared in the range 10–100 μM in n-octanol with 2% of dimethyl sulfoxide for solubilization of the complexes. The determination was carried out at pH 7.4 in a mixture of equal volumes of water and n-octanol with 2% of dimethyl sulfoxide and continuous shaking for 18 h at room temperature. The concentration of complex in n-octanol was measured spectrophotometrically in order to determine values of P = $[compound]_{(in\ octanol)}$ / $[compound]_{(in\ water).}$ Experiments were carried out three times. Lipophilicity of complexes increases cytotoxicity also increases. The log *p* values measured by the direct shake-flask method for all synthesized complexes were in the range from 0.17 - 0.95. All the Ru(II) complexes showed a log *P* value > 0, pointing out a great affinity to lipophilic system, this is essential for biological applications. Graphical representation of lipophilicity of complexes shown in Fig 43.

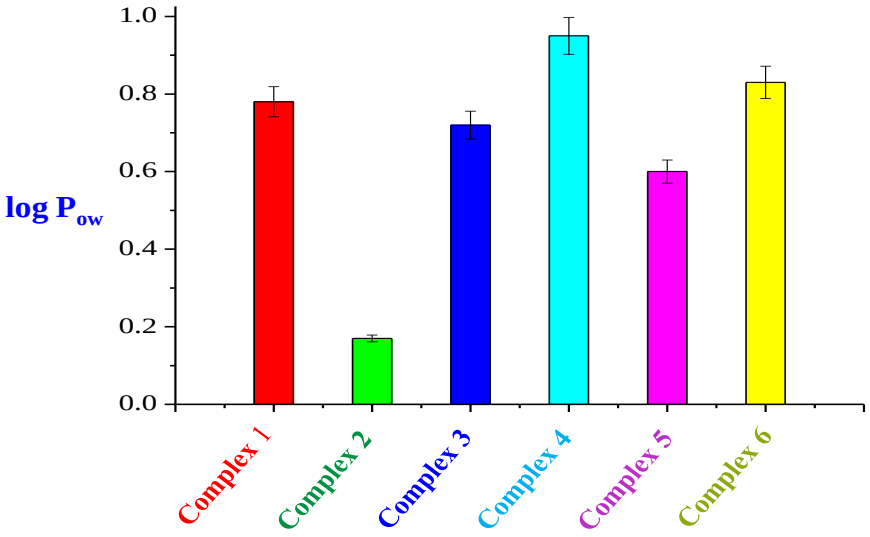

Fig 43. Lipophilicity of complexes 1-6.

3.7 Confocal Microscopy

HeLa cells were cultured on cover slips (Corning; 22mm × 50 mm) until they reached 70% confluency. The cells were incubated with complexes at 10 μM concentrations for 2 h, then washed with PBS and photographed with a Leica TCS SP5 Confocal microscope. The Confocal microscope was equipped with an Ar–Kr laser, which was used to excite Ru(II) complexes. Confocal microscopy imaging was conducted on one set without any staining and one set was stained with DAPI (nuclear stain; 0.1 mg/mL) to identify localization of the complexes and any nuclear disintegration. The morphological changes of HeLa cells in the absence and presence of Ru(II) complexes are shown in Fig 44. The cellular uptake of complexes were studied using confocal microscopy. After 2 h of incubation of HeLa cells with complexes gradually penetrated into the cytoplasm and accumulated in the nucleus and morphological changes are observed. These results suggest that the complexes can be up taken from HeLa cells and also can accumulate in the cell nuclei. From the morphological changes we can conclude that among all the complexes, the complex 4 exhibited the high capacity for fast crossing of the cell membrane and less capacity than cisplatin. We observed that the cell viability falling with increasing complex lipophilicity.

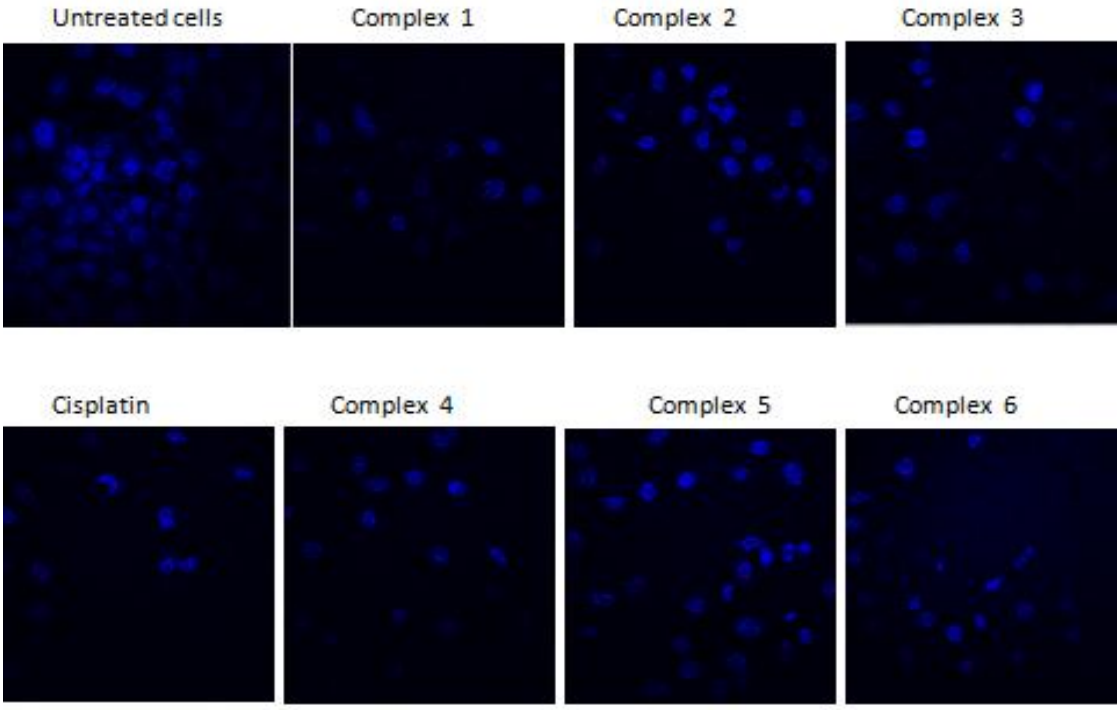

Fig 44. The morphological changes of HeLa cells in presence of cisplatin and complexes1-6

3.8 Morphological Observation

HeLa cells on treatment with complexes 1, 2 and 3 for 48h, showed significant decrease in cell number when compared to untreated cells. Cell number was decreased drastically as shown in Fig 45.

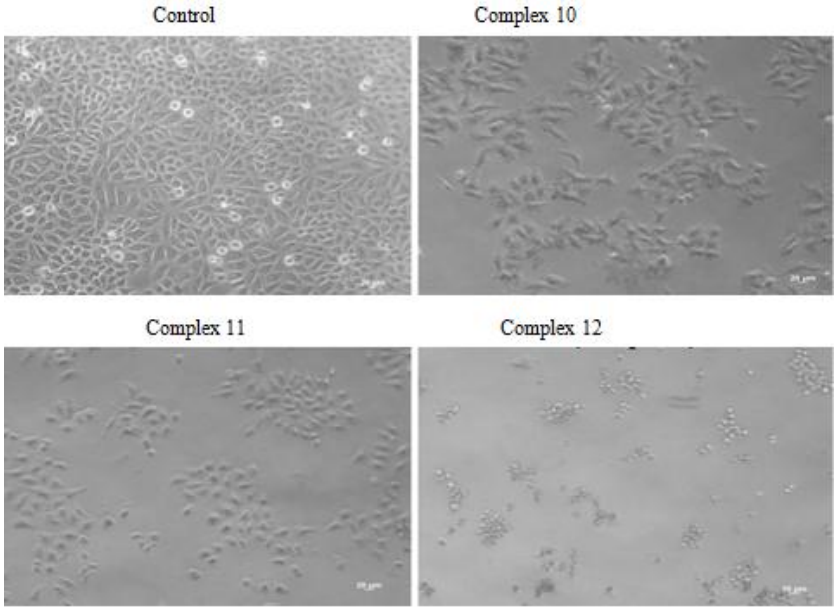

Fig 45. Morphological changes occurred in HeLa cells after treatment with complexes 10, 11 and 12 at a concentration of 50 μM for 48h. Cell number reduced after treatment with complexes compared to control cells (untreated).

3.9 Apoptosis assay

The apoptosis of Ru(II) complexes 10, 11 and 12 against HeLa cell lines, Annexin V FITC/ Propidium Iodide (PI) staining and flow cytometric analysis was performed. The inner leaflet of plasma membrane of cells contains phosphatidyl serine (PS). One of the early events of apoptosis is the translocation of PS from inner leaflet of plasma membrane to the outer leaflet. This event exposes the PS to outer cellular environment which can be detected by FITC labeled Annexin V which has high affinity to phosphatidylserine. The upper left quadrant, Q4 represents dead cells; with positive to PI and Annexin V negative (Annexin V− and PI+). The upper right quadrant Q3 shows the late apoptotic cells (Annexin V+ and PI+). The lower left quadrant, Q1 shows only viable cells (Annexin V and PI negative). The lower right quadrant,Q2 shows early apoptotic cells (Annexin V+ and PI−) as shown in Fig 46.

Treatment of HeLa cells with all the three complexes shows that all these complexes induce apoptosis. HeLa cells treated with complex 10 show 62% of cells in late apoptotic stage. Whereas complex 11 treatments show late apoptotic population of about 47% and 21 % of cell population were still undergoing early stages of apoptosis. The cells treated with complex 12 show 60% of the cells in early apoptosis and 10% of the cells in late apoptosis. From the results, it is evident that treatment with the complexes induces apoptosis.

Induction of apoptosis is one of the considerations in drug development; most of the anticancer drugs in current use have been shown to induce apoptosis in susceptible cells. Annexin V is a recombinant phosphatidylserine-binding protein that interacts strongly and specifically with phosphatidylserine residues and can be used for the detection of apoptosis. The percentage of the Annexin V positive (apoptosis) cells were determined and investigated by flow cytometry, after treatment with complexes 7-9 at their IC_{50} value for a period of 24 hrs. The percentage of Annexin V positive cells 42.02%, 23.09% and 17.2% for complexes 7, 8 and 9, respecively. DNA distribution histograms of HeLa cells in the absence and presence of complexes 7, 8 and 9 after 24 hrs incubation. The percentage of Annexin V positive cells was compared with Cisplatin (positive control), and there was a clear correlation of these complexes with the activity of Cisplatin as shown in shows in Fig 47.

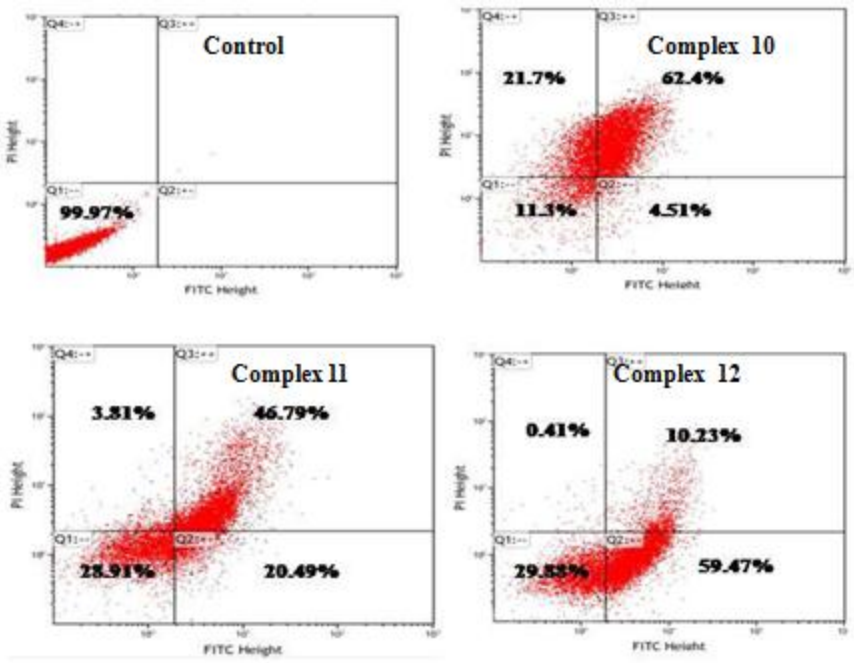

Fig 46. HeLa cells were treated with complexes 10, 11 and 12 at a concentration of 50 μM for 48h and then induction of apoptosis was determined with Annexin V-FITC/PI dual staining assay.

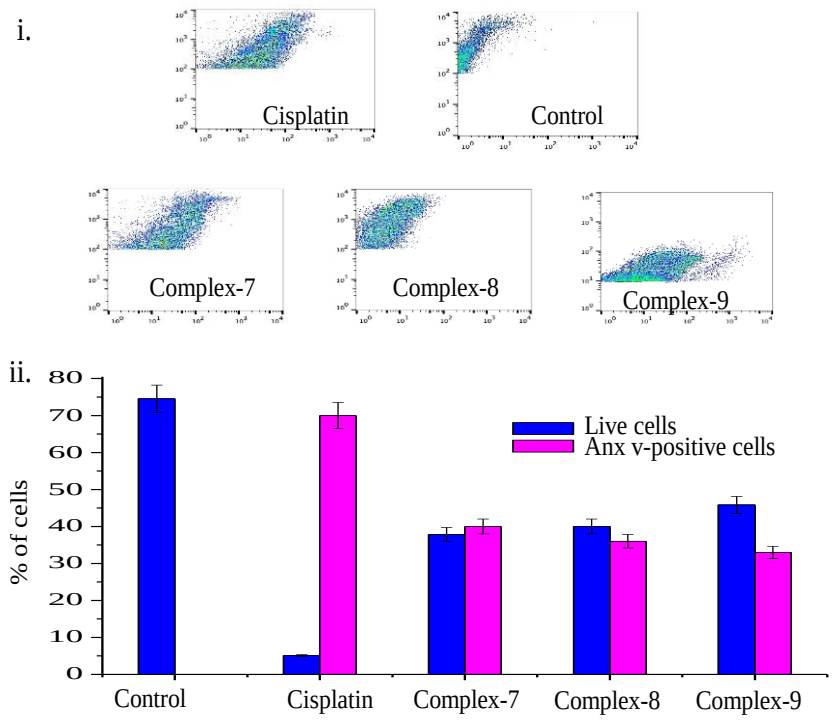

Fig 47. HeLa cells were treated with Cisplatin, complexes 7, 8 and 9 for 24 hrs, and then analyzed for apoptosis by flow cytometry. ii) Effect of ruthenium complexes 7, 8 and 9, and controls (-ve and +ve (Cisplatin) controls) on the mechanism of HeLa cell death (apoptosis) evaluated by flow cytometry after 24hrs of incubation.

3.10 Cell cycle arrest

HeLa cells treated with complex 10-12 showed a distinct G_2/M arrest at 24 h; an increase in cell population of Sub G_1 and S phase arrest was observed when treated for 48h. Results indicated that all complexes showed an increase in percentage of the Sub G1 population in a time dependent manner as shown in the Fig 48 and suggest that all three complexes are effective in causing cell death. The effect of ruthenium complexes 7-9 against cell cycle of HeLa cells was investigated by flow cytometry for 24 hrs. Fig 49 showed that the cell cycle distribution after treating HeLa cells with complexes 7-9 at their IC_{50} value.

The percentage of cells at the G_0/G_1 phase increased from 12.3% in the control to 30.7%, 31.2% and 30.8% after treatment with Ru(II) complexes 7-9. These results indicate that complexes induce the cell cycle arrest in G_0/G_1 phase.

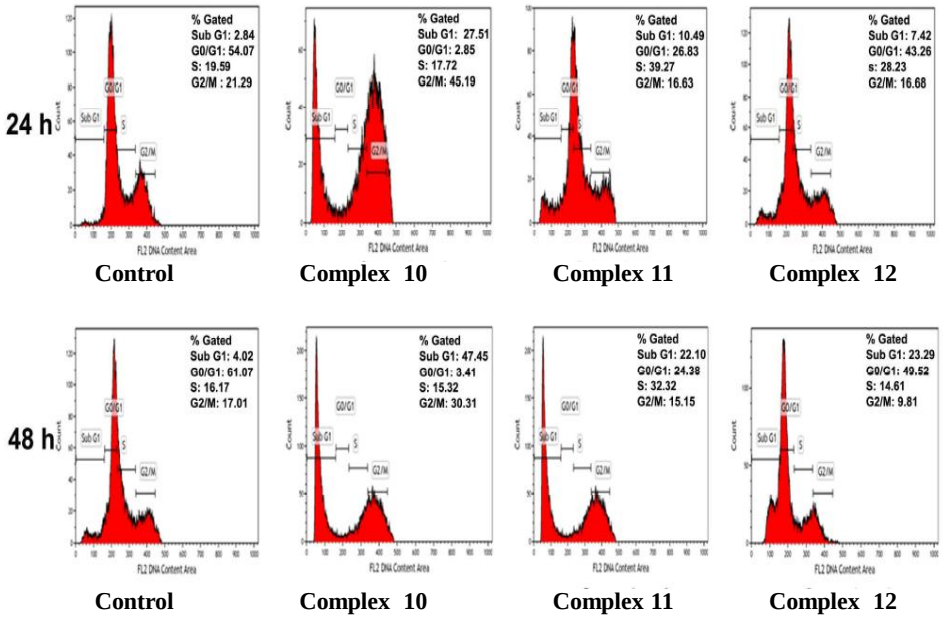

Fig 48. HeLa cells were treated with complexes 10, 11 and 12 at a concentration of 50 μM for 48h. After treatment, distribution of cell cycle phases was quantified by flow cytometric analysis.

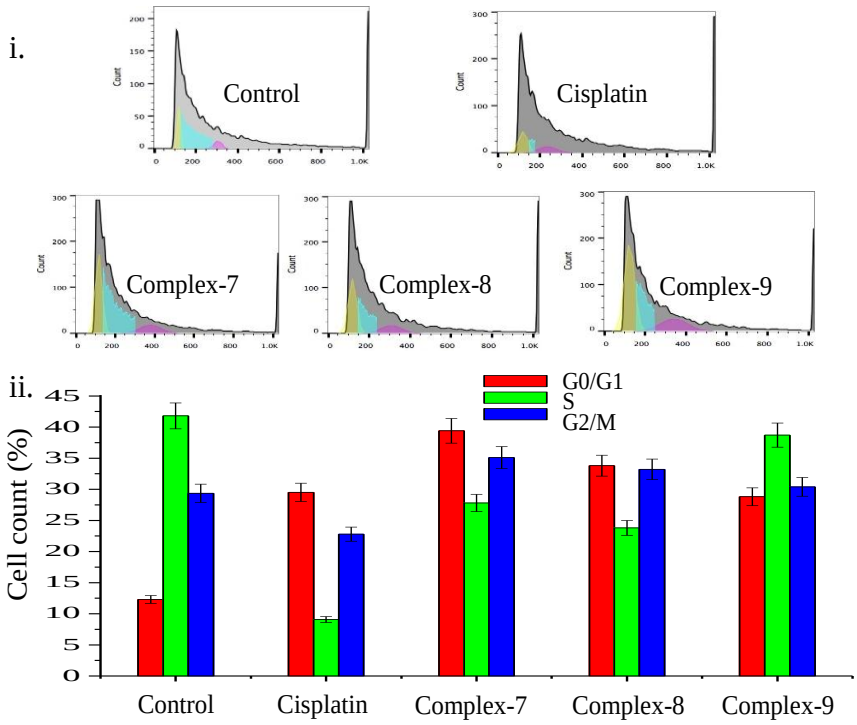

Fig 49. The cell cycle distribution of untreated cells (control), Cisplatin, ruthenium complexes 7, 8 and 9 on HeLa cells after incubation for 24 hrs at their IC_{50} value. ii) Bars represent the percentage of cells present in each of the cell cycle stages: G_0/G_1, S and G_2/M.

4.0 Conclusion

In summary six novel biologically active Ru(II) polypyridyl complexes have been synthesized and characterized by elemental analysis. The complexes were stable in aqueous solutions and observed no changes in the UV-Vis spectra. The log *p* values measured by the direct shake-flask method range from 0.17 - 0.95. The in vitro DNA binding studies of Ru(II) complexes revealed that an intercalative interaction between Ru(II) and CT-DNA, all complexes shows the more DNA -binding affinity. These results suggest that both ancillary ligand and intercalative ligand influence the binding of these complexes to DNA. The DNA -binding affinity of the complexes is not consistent with their cytotoxicity against the tumor

cell lines. All complexes exhibited the DNA molecular “light switch” properties. The agarose gel electrophoresis study shows that novel Ru(II) complexes encourage the oxidative cleavage of pBR322 DNA. Based on the binding and cleaving results Ru(II) complexes not only can bind to DNA through an intercalation binding mode with high CT DNA-binding affinities but also possess a well DNA-cleaving capacity. Antibacterial studies revealed that all complexes show a intense antibacterial activity against both Gram +ve and Gram -ve bacteria. All the complexes exhibiting good cytotoxicity and a favorable lipophilicity is the ability to cell death. The lack of correlation between DNA binding affinity and cytotoxicity suggests that multiple targets and multiple mechanisms involve in the anticancer process of the compounds. This work explains the importance of complexation, stability and the results, further understanding the DNA binding and provide great encouragement to pursue the investigations toward the use of Ru(II) complexes in cellular imaging research.

5.0. References

1. Umar Ndagi, Ndumiso Mhlongo, Mahmoud E Soliman, Drug Des Devel Ther. 2017; 11: 599–616.

2. Pieter C. A. Bruijnincx, Peter J. Sadler, Curr Opin Chem Biol. 2008 Apr; 12(2): 197–206.

3. Yulin Yang, Guojian Liao, Chen Fu, *Review*, Polymers 2018, 10, 650; doi:10.3390/polym10060650.

4. Nafees Muhammad, Zijian Guo, Curr Opin Chem Biol. 2014, 19:144–153.

5. Ana-Maria Florea, Dietrich Büsselberg, Cancers, 2011, 3: 1351–1371.

6. XingKe, LisongShen, Frontiers in Laboratory Medicine, 2017, 1: 69-75.

7. Emmanuel S. Antonarakis, Ashkan, Cancer Chemother Pharmacol. 2010, 66(1): 1–9.

8. Alessio, E., Mestroni, G., Bergamo, A. & Sava, G. Ruthenium antimetastatic agents. Curr Top Med Chem. 20044, 1525–1535.

9. Sava G, Alessio E, Bergamo A, Mestroni G (1999) Sulfoxide ruthenium complexes. Top Biol Inorg Chem 1: 143–169.

10. Pieper T, Borsky K, Keppler B (1999) Non-platinum antitumor compounds. Top Biol Inorg Chem 1:171–199.

11. Heinemann F, Karges J, Gasser G, Acc Chem Res. 2017, 50: 2727-2736.

12. Fergus E. Poynton, Sandra A. Bright, Salvador Blasco, D. Clive Williams, John M. Kellyc, Thorfinnur Gunnlaugsson, Chem. Soc. Rev., 2017, 46: 7706-7756.

13. Yamada M, Tanaka Y, Yoshimato Y, Kuroda S, Shimao I (1992) Synthesis and Properties of Diamino-Substituted Dipyrido [3,2-a: 2′,3′-c]phenazine. Bull Chem Soc Jpn 65:1006-1011.

14. Sullivan BP, Sullivan DJ, Meyer TJ, Inorg Chem, 197817:3334-3341.

15. Tan LF, Zhang S, Liu XH, Chen YD, Liu XW, J Organomet Chem, 2008, 693:3387-3395.

16. Wolfe, A., Shimer, G.H., Meehan, T, Biochemistry, 1987, 26: 6392–6396.

17. J. R. Lakowicz, G. Webber. Biochemistry, 1973, 12: 4161.

18. Chaires, J.B., Dattagupta, N., Crothers, D.M, Biochemistry, 1982, 21: 3927–3932.

19. Satyanarayana S, Dabrowiak JC, Chaires JB, Biochemistry, 1993, 32:2573–2584.

20. T. Mosmann, J. Immunol. Methods, 1983, 65: 55-63.

PRINCIPAL INVESTIGATOR